OPTIMIZATION AND DATA MINING IN HEALTHCARE: PATIENTS CLASSIFICATION AND EPILEPTIC BRAIN STATE TRANSITION STUDY USING DYNAMIC MEASURES, PATTERN RECOGNITION AND NETWORK MODELING

By

JICONG ZHANG

A DISSERTATION PRESENTED TO THE GRADUATE SCHOOL
OF THE UNIVERSITY OF FLORIDA IN PARTIAL FULFILLMENT
OF THE REQUIREMENTS FOR THE DEGREE OF
DOCTOR OF PHILOSOPHY

UNIVERSITY OF FLORIDA

2011

To my parents in China

ACKNOWLEDGMENTS

I would like to thank Dr. Panagote M. Pardalos, Dr. Basim M. Uthman, Dr. Deng-Shan Shiau, Dr. J. Chris Sackellares and Dr. J. Cole Smith for their guidance and support. During the past four and a half years, their energy and enthusiasm have motivated me to become a better researcher. I would also like to thank Dr. William Hager, Dr. Joseph P. Geunes, and Dr. Jean Philippe Richard for serving on my supervisory committee and for their insightful comments and suggestions.

I have been very lucky to have the chance to work with many excellent people in the department of Industrial and Systems Engineering (I.S.E) and Center for Applied Optimization (C.A.O). I would like to thank Dr. Chang-Chia Liu, Dr. Pando G. Georgiev, Dr. Yongpei Guan, Petros Xanthopoulos, Dr. Vladimir Boginski, Dr. Stas Busygin, Dr. Stanislav Uryasev, Dr. Vitaliy Yatsenko, Dr. Ravindra K. Ahuja, Dr. Joseph C. Hartman, Dr. Petar Momcilovic, Dr. Ashwin Arulselvan, Dr. Onur Seref, Dr. Nikita Boyko, Dr. Altannar Chinchuluun, Dr. Michael Bewernitz from B.D.L., Dr. Oleg Shylo, Dr. Alla Kammerdiner, and others in C.A.O for their valuable friendship and kindly assistance.

I thank the staff in the Department of Neurology at the Gainvesville VA Medical Center including Scott Bearden and David Juras for their collaboration in collecting research data. I thank the principal research scientist Dr. Wangcai Liao in Cyberonics Inc. for his sharing of his experience in research and product development of implantable medical devices. I thank Joy Mitchell from North Florida Foundation for Research and Education, Inc. for providing travel support in my research and conference. I acknowledge the financial support provided by College of Engineering and I.S.E department throughout my Ph.D. study. I acknowledge the collaboration of Optima Neuroscience Inc. by providing research data. I acknowledge the financial support

provided by Cyberonics Inc. during my research work there. I also acknowledge the collaboration and financial support provided by VA hospital in Tampa. There are many colleagues I have worked with and many friends I have made at University of Florida, VA hospital or the collaborating companies, who gave me their help and support but were not mentioned here, I would like to take this opportunity to thank all of them for being with me throughout this wonderful journey.

Lastly, I wish to thank my lovely family in my home country China my father Gang Zhang, my mother Dongmei Li, and my grandfather Zhitang Zhang for their selfless sacrifice and constant love.

TABLE OF CONTENTS

page

LIST OF TABLES

LIST OF FIGURES

LIST OF ABBREVIATIONS

AED	Antiepileptic Drug(s)
ApEn	Approximate Entropy
AR	Auto Regression
ARIMA	Auto-Regressive Integrated Moving Average
ARMA	Auto-Regressive Moving Average
BZD	Benzodiazepines
CNS	Central Nervous System
CT	X-ray Computed Tomography
ECG	Electrocardiography
ECoG	Electrocorticography
EEG	Electroencephalogram
FAR	False Alarm Rate
fMRI	Functional Magnetic Resonance Imaging
FMX	Frequency Modulation Extended Range
GC	Granger Causality
LSE	Least Square Estimation (model)
MMSE	Minimum Mean Square Error (model)
MRI	Magnetic Resonance Imaging
NCSE	Nonconvulsive Status Epilepticus
PCA	Principal Component Analysis
PD	Probability of Detection
PMRS	Pattern Match Regularity Score
PPV	Positive Predictivity Value
STD	Standard Deviation

STLmax	the Maximum Short Term Lyapunov exponent
STM	Standard deviation Minimum
STX	Standard deviation Maximum
SVM	Support Vector Machine
TEG	Teager Energy
TLSE	Total Least Square Estimation (model)
TME	Toxic Metabolic Encephalopathy

Abstract of Dissertation Presented to the Graduate School
of the University of Florida in Partial Fulfillment of the
Requirements for the Degree of Doctor of Philosophy

OPTIMIZATION AND DATA MINING IN HEALTHCARE: PATIENTS CLASSIFICATION AND EPILEPTIC BRAIN STATE TRANSITION STUDY USING DYNAMIC MEASURES, PATTERN RECOGNITION AND NETWORK MODELING

By

Jicong Zhang

August 2011

Chair: Panos M. Pardalos
Major: Industrial and Systems Engineering

Epilepsy is the second most common chronic neurological disorder that affected over 50 million people in the world, of which one fifth were never treated. Recurrent unprovoked seizures, which are used to characterize epilepsy, are transient symptoms of abnormal, excessive or synchronous neuronal activities in the brain. Seldom cured with medication or surgery, epilepsy is generally being controlled clinically. Patients with refractory epilepsy may feel stressed or live in depression with the uncertainty of seizure-occurring time in daily lives, since most epileptic seizures come all of a sudden. A seizure detection and/or prediction method can help identify the occurrence of seizures and alleviate the uncertainties, hence improving the quality of life of epileptic patients. In the dissertation, the epileptic brain state transition and epileptic brain network were investigated with dynamic measures, granger causality, network modeling and optimization. With the electroencephalogram (EEG) recordings, epileptic brain network was constructed using dynamic features and dependency or causal functions. The relationship between the change of epileptic brain network and the evolution of epileptic seizure was further investigated and some indications were found for

identifying the preictal and ictal periods. Furthermore, alternative methods using multiple features extraction and classification were applied to investigate the epileptic brain state transition, using principle component analysis, support vector machine, and skeleton methods. In addition, the electrocardiogram (ECG) based seizure detection methods were also investigated. Last but not least, a patient classification method for the fast diagnosis of nonconvulsive status epilepticus from toxic metabolic encephalopathies was presented.

CHAPTER 1
INTRODUCTION OF EPILEPSY

To study an epileptic brain, it is necessary to understand what is epilepsy is and what are the major types of epilepsy.

Definition of Neurological Disorder and Epilepsy

Epilepsy is the second most common chronic neurological disorder that affected over 50 million people or 1% of the world's population, where neurological disorder is the disturbance in structure or function of the central nervous system (CNS) resulting from developmental abnormality, disease, injury or toxin. About one fifth of patients with epilepsy were never treated. Epilepsy can occur at any age of human, but is more likely to occur in young children or people over the age of 65 years. Chronic seizure conditions or recurrent unprovoked seizures, which are used to characterize epilepsy, are transient symptoms of abnormal, excessive or synchronous neuronal activities in the brain. However, epilepsy itself should not be understood as a single disorder, but rather as syndrome with vastly divergent symptoms (all involving episodic abnormal electrical activities) in the brain.

Categorization of Epilepsy

Epilepsy refers to a diverse set of abnormalities, with different causes, different symptoms and clinical expressions, and different treatments. There are many types of epilepsies: some types are subtle that can be easily missed by an observer; and some are dramatic as to be frightening (Engel 1989; Engel & Pedley, 1998).

The epilepsies can be categorized according to the extent of causes into: (1) idiopathic epilepsy, (2) symptomatic epilepsy, and (3) cryptogenic epilepsy, where idiopathic epilepsy has no apparent cause and may have genetic causes; symptomatic

epilepsy has a cause that has been identified; and cryptogenic epilepsy has a likely cause that has not been identified.

Usually, epilepsies are also categorized by clinicians on the basis of the characterization, behavior and associated pattern of brain electrical discharge recorded by the EEG. Although this categorization scheme ignores the underlying bases (molecular and cellular) for the epileptic seizures, it results in a useful and complex system for diagnosis and treatment (Commission on Classification and Terminology of the International League Against Epilepsy 1981, 1989).

According to the areas of the brain of abnormal electrical discharge, epileptic seizures can be categorized into partial seizures and generalized seizures. While the abnormal electrical discharge in partial seizures is limited to a local area of the brain, many parts of the whole brain are involved at once in generalized seizures. It is worth mentioning that some seizures are caused by non-epileptic medical conditions, known as non-epileptic events. For partial seizures, it can further be categorized into complex partial seizures and simple partial seizures: the former type affects consciousness and generally is characterized by automatisms; whereas the latter type do not affect consciousness and may cause sudden, jerking motions of the body and affects vision or hearing. In the category of partial epilepsy, benign focal epilepsy of childhood is idiopathic, and temporal lobe epilepsy and frontal lobe epilepsy are symptomatic or cryptogenic. For generalized seizures, there are major types: absence seizures, tonic-clonic seizures, myoclonic seizures, tonic seizures and atonic seizures. The vast majority of generalized epilepsies are idiopathic. However, some generalized epilepsies, for example west syndrome and Lennox-Gastaut syndrome, are symptomatic or

cryptogenic. In addition, there is a type called secondarily generalized seizures, which starts as a partial seizure in one limited area of the brain, then spreads throughout the brain and becomes generalized. Sometimes the partial seizure phase is so brief that it is hardly noticed. The generalized convulsive phase of these seizures usually lasts no more than a few minutes, the same as primary generalized seizures.

Besides the self-limited seizure types, there are also continuous seizure types, called status epilepticus (SE). Status epilepticus is usually a life threatening condition in which the brain is in a state of persistent seizure. It can be subcategorized into generalized status epilepticus and partial status epilepticus, including generalized tonic-clonic status epilepticus, clonic status epilepticus, absence status epilepticus, tonic status epilepticus, myoclonic status epilepticus, and epilepsia partialis continua of Kojevnikov, Aura continua, limbic status epilepticus, hemiconvulsive status with hemiparesis, respectively.

Furthermore, some seizures are non-epileptic. An example is psychogenic seizures, which are psychological in nature and can happen in people diagnosed with or without epilepsy. Sometimes psychogenic seizures look like true epileptic seizures, but no abnormal electrical activities occur. There are also some medical conditions that have symptoms similar to epileptic seizures, such as narcolepsy, heart stroke, cardiac arrhythmia, and low blood sugar. Epileptic seizures and non-epileptic events can be distinguished by diagnostic tests, typical examples as continuous EEG monitoring, functional MRI and MRI.

CHAPTER 2
CAUSES, DIAGNOSIS AND TREATMENT OF EPILEPSY

Neurobiological Causes of Epilepsy

Because seizures can occur in normal brain reflecting normal responses to injury or stress, occurrence of an isolated single seizure does not necessarily reflect brain pathology. However, repetitive seizures can indicate some chronic pathological condition of the central nervous system. During the time between the seizures, or called interictal period, the brain functions in an apparently normal fashion. For most types of epilepsy, the occurrence of seizure is episodic and apparently unpredictable, which makes it particularly difficult to understand the abnormality of pathological condition.

Rather than categorizing epilepsies on the basis of the characterization behavior during ictal period and the pattern of brain electrical discharges recorded by EEG, it is also possible to categorize many epileptic disorders on the basis of the neurobiological cause, with advances in the understanding of mechanisms of seizures and of the processes by which a chronic seizure state is acquired. A general classification scheme, that covers most types of epilepsy, includes three categories: genetic disorders; developmental disorders; and acquired epilepsies.

Genetic Disorders

It is believed that the mutations of single genes are the causes of a good number of epilepsies (Berkovic & Scheffer, 1999). As is known, many genes code for ion channels or for neurotransmitter receptor proteins, which affect brain excitability. Abnormalities in those proteins can partially explain some seizure discharges. In addition, structural brain abnormalities, in lissencephaly or tuberous sclerosis for example (Spreafico et al., 1999), are causes of other epilepsies which are associated

with single gene mutations. At present, the understanding of abnormalities in the gene products that result in developmental disorders is still at an early stage, and there are functions of the implicated genes that need to be elucidated. More commonly, some epilepsies, such as childhood absence epilepsy (CAE) and juvenile myoclonic epilepsy (JME), are disorders associated with multiple genes. This provides the possibility of applying genetics in the diagnosis of epilepsy, specifically determining seizure susceptibility in the brain. It is worth mentioning that, characterizing and identifying the genes involved in multigenic seizure disorders is a major challenge in this field, because it is critical to understand which genes play a significant role in determining seizure predisposition. Further, gaining an insightful understanding of the cellular pathways through which the genie abnormalities lead to neurophysiologic dysfunction is important. Overall, identifying epilepsy genes is a critical start in developing new drugs or other treatments with specific molecular targets, though there is still a long way to go to completely understand the aberrant central nervous system function.

Developmental Disorders

The genetic and molecular signals in a normal brain have been investigated and understood in the last few decades, benefited from the development in neuroscience research (Sanes & Donoghue, 2000). Neurological disorders, specifically epilepsy, may be caused by any abnormalities in the process of cell proliferation, migration, differentiation and establishment of connections (Schwartzkroin et al., 1995). The incidence of neurological dysfunction is low, given the potential for developmental mistakes. Especially, the percentage of seizure occurrence in the adult population is considerably lower than that in the children, partly due to abnormalities in the brain development (Spreafico et al., 1999), and partly due to the seizure-prone properties of

the immature brain (Nehlig et al., 1992). It is observed that the epilepsy incidence in the children with other developmental disorders is much higher than that in normal children. This reflects some underlying brain pathology. Considering (1) seizure incidence among the children is higher than that among the adults; (2) epilepsies may be caused by abnormalities of genetics or brain development; and (3) the human brain is vulnerable to perinatal trauma; epilepsy is considered primarily as a set of disorders of childhood by a large number of epileptologists. Some phenomena are observed surely not by coincidence: epilepsies are often induced by insults during the young ages, and seizure syndromes are usually highly correlated with developmental brain abnormalities. A commonly accepted explanation to those phenomena is the highly plastic nature of the immature CNS. Overall speaking, the immature CNS is more resilient, compared with the adult CNS where brain trauma may lead to cell death or loss of functions. The immature neurons are not as sensitive as the mature neurons to injurious stimuli. Specifically, the immature brain are capable of producing new neurons to a much greater extent than the adult CNS can, and the immature nerve cells make new connections more readily during the disruption of the normal organization. Although the plasticity of the immature brain helps preserve a large amount of behavioral functions, the new circuits may be established by injured neural elements and may not be entirely normal. Thus, neuronal injury and incorrect connections are considered two major contributors in the development of epileptic electrical discharges during the seizures.

Acquired Epilepsies

Compared with genetic and developmental disorders, the acquired epilepsies are solely induced by some particular insults. The brain was originally normal and would otherwise be normal if the insults had not happened. Such insults could be medical

conditions such as an infection or a tumor, and/or a particular traumatic injury. The hypothesis is that: the injured brain may lose some critical elements which control the electrical excitability of the CNS, and may create inappropriate new connections. However, whether or not some insults will lead to an epileptic state is individual based. A stimulus could be a trigger for epileptogenesis on one subject, and not on another. Subtle factors differences, genetic or environmental, may exist concerning seizure susceptibility and abnormalities of brain development. All those provide a background determining which insults plays out on a subject. For instance, a preexisting injury, though subtle, may make the chance higher that an individual with a serious infection develops epilepsy at a later time. This implies that epilepsy is a progressive disorder (Heinemann et al., 1996), developing with active neuronal processes. And this concept is often discussed in the study of pediatric epilepsies. Thus, any initially subtle insult has the possibility of kindling into a serious and troubling condition over a period of time.

Diagnosis and Treatment of Epilepsy

Accurate diagnosis is a critical first step for the treatment of epilepsy. There are many disorders that have changes in behavior and clinical symptoms similar to those of epilepsy, which makes it difficult to determine if a person is having an epileptic seizure and to diagnose the type of seizure or epilepsy syndrome. One of the most important information that is needed for the diagnosis is: what happened during the seizure occurrence, or the ictal period. Since seizures rarely happen in a doctor’s office, how the patients, the caregivers and other witnesses give the information to the doctor and the healthcare professionals is important. Yet, even with accurate descriptions of events, other records and/or tests are also needed to learn more about the brain: what is causing the events underlyingly and where exactly the problem is located. Typical

records and tools include but are not limited to medical history, blood tests, continuous video EEG monitoring, ECoG monitoring, and brain imaging tests such as functional MRI, CT and MRI. The EEG and ECoG recordings give information about the electrical activity of the brain and the imaging tests can tell in some sense what the brain looks like. Different sources of information, including the individual's feeling, the caregiver's description and the models how seizures may affect the way the brain works, are put together for diagnosis of epilepsy.

After a diagnosis of seizure or epilepsy of sufficient confidence, the best form of treatment need to be selected. Seldom cured with medication or surgery in difficult cases, epilepsy is generally being controlled clinically. The main methods for epileptic seizure control are: (1) the use of antiepileptic drugs (AED); (2) surgical removal of the seizure focus; (3) electrical stimulation. If a continuing tendency to have seizures is diagnosed, a regular use of AED will be prescribed usually. Other methods, including a special diet, brain surgery, or vagus nerve stimulation will be tried if AED's are not effective and successful. Especially, if seizures are localized in one area and is caused by an underlying correctable brain condition, surgery may be able to alleviate the severity of epilepsy or even stop seizures. The goal of epilepsy treatment is to prevent seizures, or reduce the frequency and alleviate the severity, while minimizing the side effect, to increase the quality of life of epileptic patients.

Patients with refractory epilepsy may feel stressed or live in depression with the uncertainty of seizure-occurring time in daily lives, since most epileptic seizures come all of a sudden. An automatic seizure prediction method can help anticipate the

occurrence of forthcoming seizures and alleviate the uncertainties, hence improving the quality of life of epileptic patients.

CHAPTER 3
PATIENTS CLASSIFICATION BETWEEN GENERALIZED NCSE AND TME USING EEG QUANTIFICATION FOR DIAGNOSIS OF STATUS EPILEPSTICUS

Significance

Nonconvulsive status epilepticus (NCSE) is usually defined as an epileptic state lasting 30 minutes or more with some clinically evident change in mental status or behavior (unless comatose) associated with ictal activity on EEG (Brenner, 2002). Nonconvulsive seizures during NCSE do not contain convulsive motor activity and may be repeated discrete seizures or more continuous prolonged seizures.

NCSE is particularly difficult to diagnose in patients presenting with stupor or coma as there are often little or no specific clinical symptoms. Misdiagnosis or delay to diagnosis of adult NCSE may engender morbidity and mortality (Bearden et al., 2008). Often NCSE requires an electroencephalogram (EEG) recording to be examined (Towne et al., 2000; Bearden et al., 2008). An EEG study of 236 patients concluded that 8% of comatose patients without clinical seizure activity had NCSE that would not have been diagnosed without EEG recording (Towne et al., 2000). Nevertheless, even when EEG recordings are performed, diagnosis of NCSE can still be difficult due to the presence of other disorders with similar EEG waveforms (Brenner 2002). In particular, some non-epileptic encephalopathies, such as toxic/metabolic encephalopathy (TME), are indistinguishable by clinical symptoms, and can produce similar EEG patterns as NCSE.

Most EEG patterns of NCSE are generalized epileptiform waves or focal rhythmic ictal transformations that are not difficult to identify as electrographic seizure activity (Geiger & Harner, 1978). Unfortunately, EEG waveforms of generalized triphasic-like waves or diffuse semi-rhythmic delta activity can be seen in patient with either TME or

generalized NCSE (Figure 3-1). Treatment with benzodiazepines (BZDs) can reduce electroencephalographic seizure activity and/or improve clinical state, which may be useful diagnostically. However, the diagnostic utility of BZDs can be limited because BZDs may transiently suppress triphasic waves due strictly to metabolic encephalopathy as well as triphasic-like waves seen during NCSE (Fountain & Waldman, 2001). Furthermore, NCSE and TME can coexist, and at present, combining clinical judgment and experience is the only effective method to diagnose NCSE in equivocal cases (Bearden et al., 2008).

Rapid diagnosis and treatment of NCSE is desirable as untreated NCSE can cause irreversible damage to the brain (Jirsch & Hirsch, 2007). In the past, quantitative EEG analysis has been investigated as an aid in diagnosis of some psychiatric and neurological disorders (Pardalos et al., 2004; Liu, 2008). One approach to expedite diagnosis would be to introduce a fast EEG classification algorithm.

The purpose of this study is to identify EEG characteristics that can distinguish NCSE from non-epileptic encephalopathy. This may assist physicians in making a more rapid diagnosis of NCSE or non-epileptic encephalopathy. In our study, data mining algorithms are applied to extract complex and intrinsic features from large datasets in multi-channel EEG recordings, since the EEG patterns of NCSE can be visually similar to those of non-epileptic encephalopathy.

Approach

Data description: quantitative analysis was performed on EEG recorded from male and female adult patients having been diagnosed with NCSE (generalized or focal) or with a non-epileptic encephalopathy, specifically toxic/metabolic encephalopathy (TME). The clinical diagnosis and EEG interpretation were conducted by a board certified

electroencephalographer. Eleven human subjects were involved in this study, in which six were diagnosed with NCSE, whereas the other five were diagnosed with TME. Length of the recordings for each patient can be seen in Table 3-1.

EEG recordings were acquired using the international 10-20 electrode placement. For each subject, there are 21 recording channels (Fp1, Fp2, F3, F4, C3, C4, A1, A2, P3, P4, O1, O2, F7, F8, T3, T4, T5, T6, Fz, Cz, and Pz).

An effective approach in order to shed light into the underlying non-linear structure of time series, in our case EEG recordings, is analysis in the state space (also known as phase space). In this approach EEG recordings are mapped from the time domain onto an *n* dimensional space of states. In this study, method of delays was used for state space reconstruction (Takens, 1981).

If we consider the time series $x(t)$ (row vector of length *m*) we can construct the *m* by *n* delay matrix $A = [x(t)^T,\ x(t+\tau)^T, \dots, x(t+(n-1)\tau)^T]$ (where τ is the delay parameter and *n* is the embedding dimension). Then, every delay vector in A is a point on the *n* dimensional state space.. In the analysis of dynamic systems the attractor is a very useful visualization tool of the signal because it can reveal structure and patterns that are well hidden in the time domain. In order to quantify state changes and attractor geometrical patterns one can employ several well defined nonlinear dynamic measures.

For the purpose of our study we used three such measures, namely:

- Short term Lyapunov exponents (STLmax): Is a nonlinear state-space based metric that quantifies the instability of a dynamic system. Short term Lyapunov exponents have been used extensively in nonlinear EEG analysis mostly for seizure prediction (Iasemidis et al., 2001, 2004, 2005).
- Phase of the attractor: Also called angular/frequency phase, estimates the rate of change of the stability for a dynamic system. Complementing the Lyapunov

exponents phase is a broadly used nonlinear state space measure that is employed to characterize chaotic systems.

- Approximate entropy (ApEn): Is another phase space statistic that quantifies the complexity of a dynamic system (Pincus, 1991).

In order to analyze the continuous EEG recordings we segmented the whole time series into epochs of a finite time window of 10 seconds at a sample rate of 200 Hz. For each 10-second epoch, values for short term Lyapunov exponents, phase of attractor and approximate entropy were computed. Points were plotted in a three dimensional space (should not be confused with the *n* dimensional embedding space used for calculating the three measures).

Plots for the three nonlinear dynamical measures show very good separation between patients with NCSE and patients with TME. In Figure 3-2, we can see an example 3D scatter plot of the three measures (for one channel of EEG recordings from two different patients). X axis, Y axis and Z axis correspond to approximate entropy (ApEn), phase of attractors (phase/angular frequency), and short term Lyapunov exponents (STL-max) respectively.

The formation of two clearly distinct and well separated clouds of points led us to suggest an automated algorithm for real time detection of NCSE based on the centroids and the mean radius of the clouds, defined by the 3 dimensional scatter plot points. We define as the centroid of N points (x_i , y_i , z_i) i = 1, 2, … , N the point with coordinates:

$$\boldsymbol{c_N} = (\boldsymbol{x_c}, \boldsymbol{y_c}, \boldsymbol{z_c}) = \left(\frac{\mathbf{1}}{\boldsymbol{N}} \sum_{\boldsymbol{i=1}}^{\boldsymbol{N}} \boldsymbol{x_i}, \frac{\mathbf{1}}{\boldsymbol{N}} \sum_{\boldsymbol{i=1}}^{\boldsymbol{N}} \boldsymbol{y_i}, \frac{\mathbf{1}}{\boldsymbol{N}} \sum_{\boldsymbol{i=1}}^{\boldsymbol{N}} \boldsymbol{z_i} \right), \tag{3-1}$$

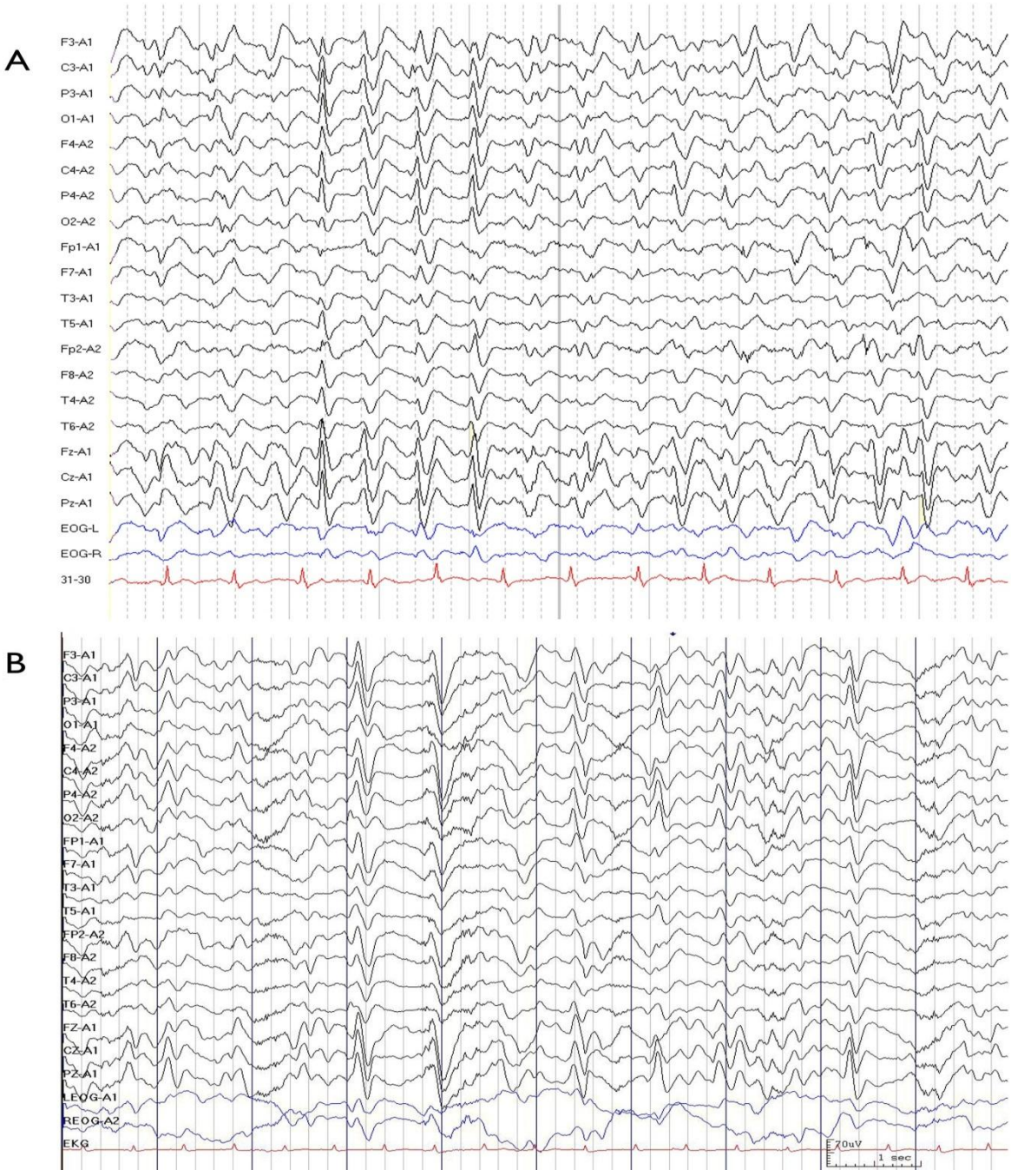

Figure 3-1. 10-second EEG recording of generalized NCSE and TME: A) an equivocal pattern of NCSE (triphasic “like” waves), from a 68-year-old male patient with subdural hematoma, who began having focal NCSE which evolved into generalized NCSE; B) a 10-second EEG recording of triphasic waves in a 56 year old male TME patient with severe acute liver failure. Visual similarities regarding the triphasic waves of TME and triphasic “like” waves of NCSE are profound.

Table 3-1. List of EEG recordings of generalized NCSE and TME patients in this study

Patient ID	1	2	3	4	5	6	7	8	9	10	11
Diagnosis	NCSE	NCSE	NCSE	NCSE	NCSE	NCSE	TME	TME	TME	TME	TME
Recording length(min)	27	33.5	53.5	25	29	63.8	56.16	13	21.66	22.16	25.33

Totally 14 patients were recorded and involved in this study, 6 with generalized NCSE, 5 with TME, and 3 with focal NCSE. Since focal NCSE is not difficult for clinical diagnosis, only the information of the first two types of patients is shown in the table.

The mean Euclidean radius of the N-point cloud is:

$$\overline{d_N} = \frac{1}{N}\sum_{i=1}^{N}\sqrt{(x_c - x_i)^2 + (y_c - y_i)^2 + (z_c - z_i)^2}, \tag{3-2}$$

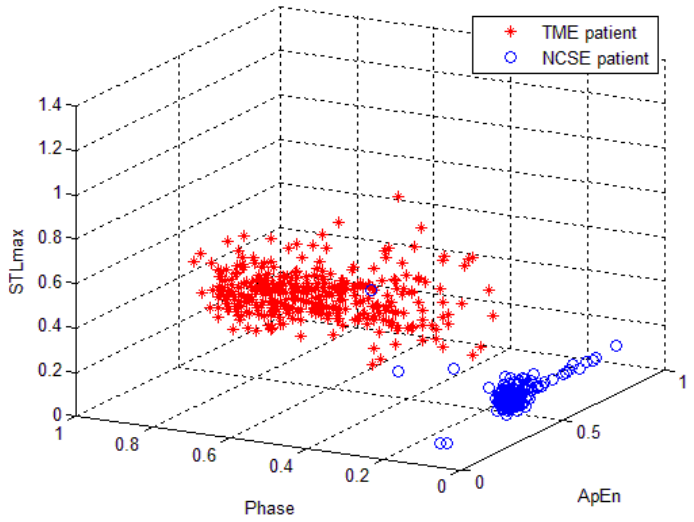

Figure 3-2. Scatter plot of the three nonlinear measures (STL-max, Phase, ApEn) for two different patients. Each circle (NCSE) or star (TME) corresponds to a 10-second EEG epoch. Example shows recordings of a single channel.

In order for each of the features to contribute equally, all three features are normalized in scale [0, 1]. Based on these, the real time algorithm can be described in the following well defined steps:

- Every 10 seconds compute one point on the 3D space spanned by the three nonlinear measures;
- Update the centroid and the mean radius distance using equations 3-1 and 3-2 correspondingly;
- If the centroid coordinates do not change more than a predefined quantity ε, issue diagnosis based on the last centroid coordinates.

Results

Analysis carried out in the whole datasets (11 patients, 21 EEG channels) shows results similar with the preliminary example in Figure 3-2. In Figure 3-3 one can see a

cumulative scattered plot with the three nonlinear dynamical measures for all the 11 patients plotted together, using 21-channel averages in the 3-D feature space. Although the cloud of points is very dense, one can see that there is clear separation between the two classes.

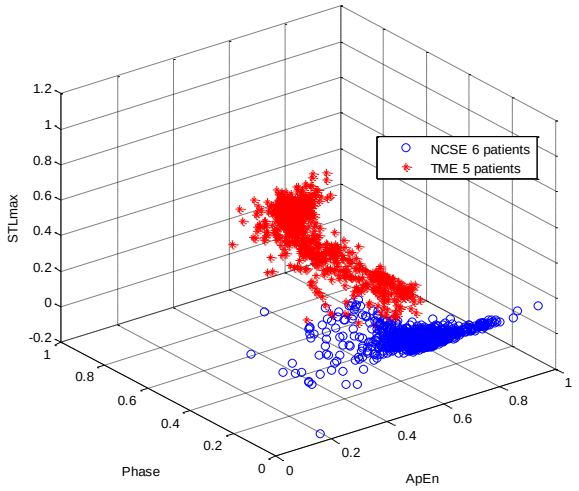

Figure 3-3. Plot of nonlinear dynamical measures (STL-max, Phase, ApEn) for all 11 patients together. Every circle (NCSE) or star (TME) corresponds to a 10-second EEG epoch sample. Plot uses 21-channel average.

We further observed that STLmax and phase of attractor play a major role in this separation, whereas approximate entropy contributes very little. This makes it possible to quantify the subjects' profile by using only two features. We then computed metrics described in Equation 3-1 and Equation 3-2. First, for each patient, we computed the centroids taking into consideration epoch samples generated from all 21 EEG channels. Scatter diagram of the centroids for all 11 patients in 3-D feature space is shown in Figure 3-4 (A).

It is worth mentioning that even if the centroids are projected into two dimensional subspace spanned by STLmax and phase of attractor, there is still clear separation between generalized NCSE and TME patients, as shown in Figure 3-4 (B). Besides, the

centroids of the six NCSE patients are much more concentrated than those of the five TME patients. This indicates that NCSE can be detected with even fewer (two instead of three) dynamical measures and computational effort.

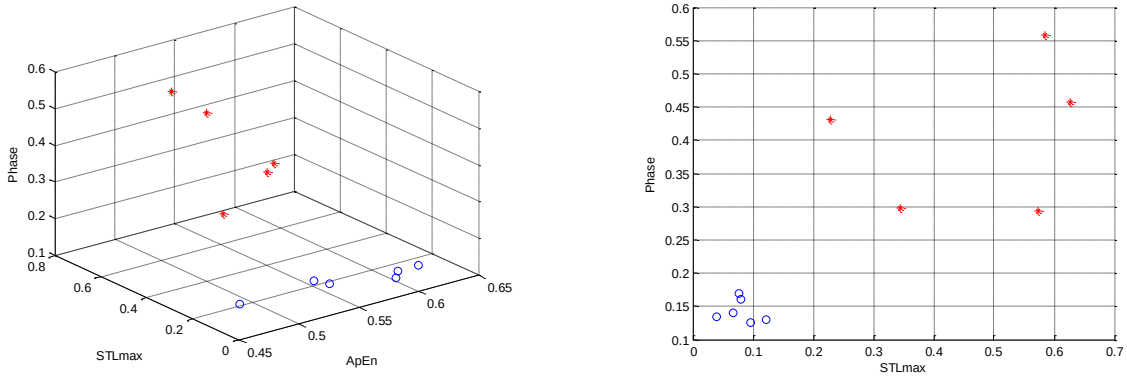

(A) (B)

Figure 3-4. Centroids of each patient (circles correspond to NCSE and stars to TME). We can see that two classes are easily separable either by A) using all three nonlinear dynamical measures, or by B) just using STLmax and phase of attractor. Centroids are computed using the full length of the EEG recording available for each patient.

Next, for each patient, the mean distance from the already-recorded EEG epochs to their centroid in the feature space is computed, as defined by Equation 3-2. In Figure 3-5, for each patient, the evolution curve of the mean distance is plotted. After 20 minutes of EEG recording, the mean distances of the NCSE patients all drop below 0.06, converge and stay there, whereas the mean distances of the TME patients do not converge rapidly and keep above 0.08 after starting EEG recording for a while. This indicates that epoch samples of TME are more scattered than those of NCSE in the feature space. The significant difference can be used as an effective criterion to judge whether a patient should be classified into generalized NCSE or TME.

Numerical results of the experiments are summarized in Table 3-2.

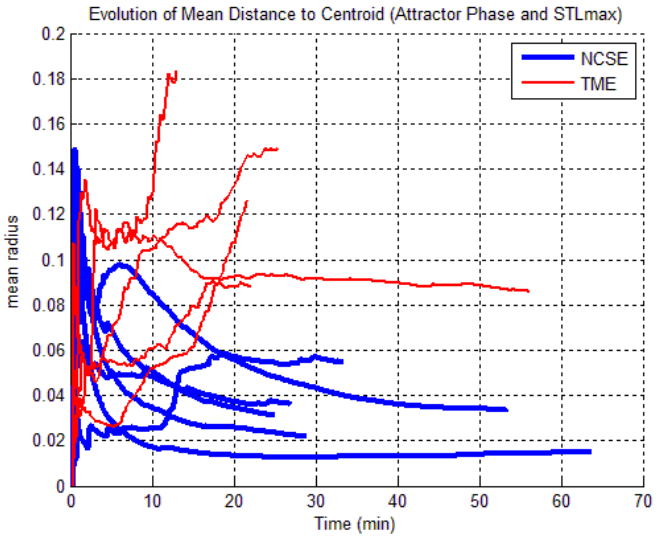

Figure 3-5. Plot of the evolution curve of the mean distances, from EEG samples to the centroid, for 11 patients. Each curve corresponds to one patient (blue thick: NCSE; red thin: TME). The distance is calculated in the two dimensional space spanned by STL-max and phase of attractor. Mean distances of NCSE patients (blue thick) after a time frame of 10-20 minutes all converge to some low value. On the other hand, mean distances of TME patients (red thin) tend to increase or oscillate and does not converge fast.

Table 3-2 and Figure 3-4 already indicate the STLmax and phase of attractors are sufficient to separate those two classes of patients. We then performed a statistical t-test in order to further justify this observation. In Figure 3-6, one can see the results of paired t-tests in each of the 21 EEG channels between every pair of patients using short-term Lyapunov exponent, phase of attractor, and approximate entropy, respectively. In the paired t-test, the minimum length of the EEG recordings of the two patients is used for the comparison. The brightness of each cell in Figure 3-6 represents how many rejections (of null hypotheses) there are out of the 21 EEG channels: the white color corresponds to 21 rejections, and the black to zero. The null hypothesis of the paired t-test is that: two matched sample sets from any two patients, in the vectors X and Y, come from distribution with equal means. X-Y, the difference of X and Y, are assumed to come from a normal distribution with unknown variance. We expect the null

hypothesis will be accepted for patients who belong to the same group and rejected for patients that belong to different groups. Because t-tests between patient pair (A, B) and (B, A) have the same results, all subplots in Figure 3-6 are diagonally symmetric.

Table 3-2. Summary the numerical values of the centroids and the mean distance to centroid of all 11 subjects of the study.

Patient id	diagnosis	x_c (ApEn)	y_c (STLmax)	z_c (Phase)	d_N
1	NCSE	0.53	0.08	0.17	0.05
2	NCSE	0.46	0.08	0.16	0.09
3	NCSE	0.55	0.12	0.13	0.05
4	NCSE	0.61	0.07	0.14	0.07
5	NCSE	0.60	0.09	0.13	0.05
6	NCSE	0.59	0.04	0.13	0.05
7	TME	0.50	0.58	0.56	0.09
8	TME	0.50	0.34	0.30	0.20
9	TME	0.52	0.23	0.43	0.13
10	TME	0.54	0.63	0.46	0.10
11	TME	0.59	0.57	0.29	0.16

In this table, Euclidean distance (norm-2) is used for calculating the mean distance.

For the two nonlinear dynamical measures: short-term Lyapunov exponent and phase of attractor (Figure 3-6, upper left and right), the number of null hypotheses rejections in pairs within the six NCSE patients is very small (colors are dark in the 6 by 6 sub-matrix in upper-left corner); whereas most of the 21 null hypotheses in any patients pair between NCSE and TME are rejected (colors are light in the 5 by 6 sub-matrix in lower-left corner). This reveals the reason why in Figure 3-2 and Figure 3-3 cloud of epochs of the NCSE patients are grouped together and are apart from epochs-cloud of TME.

Furthermore, in pairs within the five TME patients, the number of null hypotheses rejections is larger than that of pairs within the six NCSE patients. This implies the TME patients are more scattered by themselves than the NCSE patients, observed from the

two dimensional feature space spanned by short-term Lyapunov exponent and phase of attractor. This implication is consistent with results in Figure 3-5.

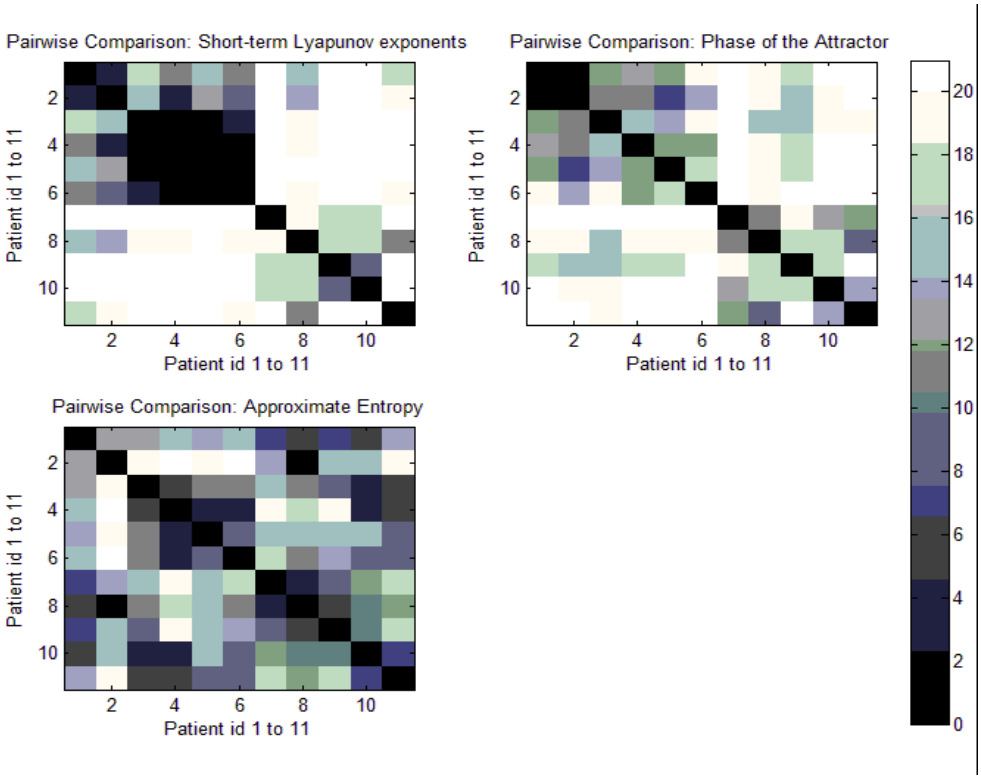

Figure 3-6. Pairwise comparison using nonlinear dynamic measures of all 6 NCSE (Patient id 1~6) and 5 TME (Patient id 7~11) patients. Upper left is STLmax; upper right is phase of attractor; lower left is approximate entropy. For each pair of patient *i* and *j*, t-tests are performed in 21 EEG channels respectively. The value (brightness) of each cell (*i*, *j*) is the number of rejections of null hypothesis, ranging from 0 (darkest black) to 21 (brightest white). The null hypothesis is expected to be accepted for patients who belong to the same group and rejected for patients that belong to different groups.

Patient 8 (TME) and Patient 9 (TME) have EEG recordings of very short length (Table 3-1). As is mentioned before, the minimum length of the EEG recordings of two patients is used for the comparison in the paired t-test. However, when recording time is not long enough, epoch-samples of some NCSE patients may still be scattered in the three-dimensional feature space of nonlinear dynamical measures, and may be close to epoch-samples of TME Patient 8 or 9. This gives an explanation why the t-test in pairs between NCSE Patient (id 1~6) and TME Patient 8 or 9 does not reject the null

hypothesis in some EEG channels. As shown in Figure 3-6, in the upper left and upper right subfigure, some cells in Row 8 or Row 9 (Column 8 or Column 9 accordingly) are slightly dark.

For the third nonlinear dynamic measure: approximate entropy (Figure 3-6, lower left), the t-test indicates that its differentiating effect between NCSE and TME is not optimal.

Discussion and Conclusion

Distinguishing generalized equivocal EEG patterns (semi-rhythmic delta and triphasic-like waves) which can be seen in either NCSE or TME (Toxic/metabolic encephalopathy) is a hard clinical problem. Currently, the only effective method to distinguish generalized NCSE from TME in equivocal cases is combining clinical judgment and experience (Bearden et al., 2008).

From the neuroscience perspective it would be interesting to uncover and model the basic mechanism that underlines the evolution of mental status changes of generalized NCSE patients, though at present the properties of epileptic brain are still not well understood. Nonlinear dynamics have been used in seizure detection and prediction in epilepsy over the last decade. The maximum Lyapunov exponent has been proposed as an indicative metric of the abrupt transient drop in chaoticity in EEG recording before seizure onset. Another example, approximate entropy, which quantifies the unpredictability of fluctuations in a time series, has been proposed for EEG epileptic seizure detection (Srinivasan et al., 2007).

In this study, three nonlinear dynamic measures (STLmax, phase and ApEn) were applied in order to distinguish between generalized NCSE and TME patients. Findings based on a dataset of 11 subjects not only suggest that two of those nonlinear

dynamics, STLmax and phase, could potentially be used as a bed-side assistive tool for generalized NCSE diagnosis in intensive care units; but also provide additional evidence (through application other than seizure prediction or detection) that STLmax and phase of attractors can be useful in quantifying neurophysiological states related to epilepsy. Hopefully, this may trigger fruitful discussion among neurologists, clinicians and scientists about the exact role of nonlinear dynamics in the field of epileptic disorders. Although groups of researchers relating epilepsy with dynamic systems (Milton & Jung, 2003) are active, at present there is no commonly accepted theory, and the mechanism of this connection remains unknown. Based on findings in this study, we suggest that epileptic activity is highly associated and can be modeled using dynamic system analysis.

As mentioned above, STLmax and phase of attractor were found most likely effective for differentiating NCSE patients from TME. In the feature space spanned by those two nonlinear dynamics, for each patient, the mean distance from the centroid to all EEG samples is a useful metric to measure the degree of concentration of EEG epochs. In the 11 subjects in our study, samples of a TME patient were always more scattered than samples of a NCSE patient. Thus, the mean distance can be utilized to assist diagnosis of NCSE.

The paired t-tests help quantify the efficacy of the three nonlinear dynamics (STLmax, phase and ApEn) when differentiating NCSE from TME. The paired t-test verifies that STL-max and phase of attractor can be the base for an automatic machine learning classifier. Such a classifier would use dynamical support vector machine or artificial neural network, and could be trained to do the classification of EEG recordings.

For this purpose a larger training set is needed so that classification error can be minimized.

Though the small number of patients (11) used in this pilot study precludes us from reaching statistically significant conclusions, we are encouraged that the two discriminators we identified were able to accurately distinguish all of our patients. These patients were selected because they had particularly difficult equivocal generalized EEG patterns that experienced electroencephalographers found very difficult to classify as NCSE or TME. We anticipate following this study with a perspective study using larger number of subjects to allow testing for statistically significant results.

This algorithm may be useful during bedside real-time EEG recording or during post-recording analysis. The three dynamics and derivative metrics proposed in this study were computed using an ordinary laptop computer. The computation time is very close to real time computation and the computation can be done simultaneously as the EEG recording is done. This may assist physicians in generating a more rapid, accurate diagnosis of NCSE or non-epileptic encephalopathy (Zhang et al., 2010).

CHAPTER 4
MINIMUM PREDICTION ERROR MODELS

Minimum error prediction is crucial in time series analysis. Especially, prediction based on multiple time series, such as EEG and ECoG, plays an important role, in the application of epileptic patients monitoring, seizure control and treatment.

A prediction is a statement that a particular event will occur in the future, which can refer to the estimation of unknown situations in time series, cross-sectional or longitudinal data. Prediction implies at least two factors: importance and difficulty (Stevenson, Howard, ed., 1998). Risk and uncertainty are crucial to prediction, thus it is important to minimize the prediction errors. There are no specifically assumed statistical distributions in the prediction models in this article.

In the first part of this chapter, two prediction models are discussed: the Least Square Estimation (LSE) model, and the Minimum Mean Square Error (MMSE) model. Both of these two models aim at minimizing the square errors in their respective senses: (1) sum of squares, and (2) mean square. LSE is known as a linear deterministic model that can be used to obtain approximate solutions of over-determined systems. The basic problem is: a limited-length time series {Z (i)} is being predicted from another limited-length time series {X (i)}, which can be generalized to infinite-length time series case. By minimizing the sum of error squares in time series prediction, the principle of orthogonality is obtained as a necessary condition of reaching the global minimum error. It is further shown that: the energy of the observed time series {Z (i)}, is the summation of the energy of the LSE estimation time series $\{Z_{\text{LSE estimation}}(i)\}$ and the energy of the LSE error process time series {e (t)}. Furthermore, another way of understanding the LSE model is exhibited: a linear projection onto the column space of the data matrix *A*,

where the columns of *A* are composed of the time-delay vectors of the time series {X (i)}. In addition, a stochastic model is converted to: MMSE, which is also linear, to minimize the mean square error in prediction. We further show that the MMSE model is a special case of ARMA / ARIMA models.

LSE Model

Basic LSE Model

At the beginning of this article, the Least Squares Error (LSE) model is presented.

In a causal system, consider two time series X (*i*) and Z (*i*) (*i* = 0, 1, 2, 3, ...), where X (*i*), X (*i* - 1), X (*i* - 2), …, X (*i* – *M* + 1) are the unobserved underlying variables and will influence the observed time series *Z* (*i*) in a linear way, expressed as following:

$$\mathrm{Z}(i) \quad = \sum_{k=0}^{M-1} w_k{}' \, \mathrm{X}\,(i-k) + \mathrm{e}'(i), \tag{4-1}$$

where the $\mathrm{w_k}'$ (k = 0, 1, 2, … , M - 1) are parameters of the LSE model and $\mathrm{e}'(\mathrm{i})$ is the model error. The measurement error $\mathrm{e}'(\mathrm{i})$ is unobservable and is used to count the model's inaccuracy.

Let:

$$\mathrm{Y}(i) \quad \triangleq \sum_{k=0}^{M-1} w_k{}' \, \mathrm{X}\,(i-k)\,, \tag{4-2}$$

$$\mathrm{e}'(i) \triangleq \mathrm{Z}\,(i) \; - \; \mathrm{Y}\,(i)\,, \tag{4-3}$$

The measurement error process $\mathrm{e}'(i)$ in the LSE model is assumed white with zero expectation and the same variance:

$$E\big(\mathrm{e}'(i)\big) = 0 \;\; , \;\; \text{for all } i, \tag{4-4}$$

And

$$\mathrm{E}\big(\mathrm{e}'(i)\ \mathrm{e}'(k)\big) = \sigma^2\ \mathrm{I}(i-k), \tag{4-5}$$

where

$$\mathrm{I}(i-k) = \begin{cases} 1 & \text{if } i-k \neq 0 \\ 0 & \text{if } i-k = 0' \end{cases}$$

In the LSE model, given the observed data, we select / design the tap weights $w_k{}'$ (k = 0, 1, 2 …… M-1) to minimize the sum of error squares (viewed as error energy). The objective function is as following:

$$\Theta(w_0{}', w_1{}', \ldots, w_{M-1}{}') \quad = \sum_{i=s}^{t} [\mathrm{e}'(\mathrm{i})]^2, \tag{4-6}$$

where s and t ($s \leq t$) are the index limits at which the error minimization occurs. Once the tap weights $w_k{}'$ (k = 0, 1, 2, …, M-1) are selected, they are fixed as parameters in the interval $s \leq i \leq t$. Not losing generality, suppose index range of the observed data is [1, N], and set $s = M$, $t = N$. Then, we get the observed input data matrix (Makhoul, 1975; Markel and Gray, 1976):

$$\begin{bmatrix} X(M) & X(M+1) & \cdots & X(N) \\ X(M-1) & X(M) & & X(N-1) \\ \vdots & & \ddots & \vdots \\ X(1) & X(2) & \cdots & X(N-M+1) \end{bmatrix}$$

where the arrays above, from the first column (M) to the last column (N), correspond to the unobserved input variable vectors. Hence, the cost function in Equation 4-6 becomes:

$$\Theta(w_0{}', w_1{}', \ldots, w_{M-1}{}') = \sum_{i=M}^{N} [\mathrm{e}'(\mathrm{i})]^2, \tag{4-7}$$

Assume that $\Theta(w_0', w_1', \ldots, w_{M-1}')$ is differentiable, then the necessary condition for minimizing $\Theta(w_0', w_1', \ldots, w_{M-1}')$ is:

$$\nabla\Theta = [0, 0, \ldots, 0]^{\mathrm{T}} \quad (M \text{ dimensional}), \tag{4-8}$$

Apply Equation 4-7 to Equation 4-8, we get:

$$\begin{aligned}[-2\sum_{i=M}^{N} X(i-0)e'_{min}(\mathrm{i}), \qquad -2\sum_{i=M}^{N} X(i-1)e'_{min}(\mathrm{i}),\\ \ldots\ldots, -2\sum_{i=M}^{N} X(i-(M-1))e'_{min}(\mathrm{i})]^{\mathrm{T}}\\ = [0, 0, \ldots, 0]^{\mathrm{T}} \quad (M \text{ dimensional}),\end{aligned} \tag{4-9}$$

Therefore, a necessary condition for $\Theta(w_0', w_1', \ldots, w_{M-1}')$ to reach its global minimum is:

$$\sum_{i=M}^{N} X(i-k)e'_{min}(\mathrm{i}) = 0, \qquad k = 0,1, \ldots, M-1, \tag{4-10}$$

Let the tap weights $w_0', w_1', \ldots\ldots, w_{M-1}'$ that is optimized to operate the LSE condition have the special values $w_0^{min}, w_1^{min}, \ldots\ldots, w_{M-1}^{min}$. Then, we define $\mathrm{Y}^{\min}(\mathrm{i})$ as:

$$\mathrm{Y}^{\min}(\mathrm{i}) \triangleq \sum_{k=0}^{M-1} \mathrm{w}_{\mathrm{k}}^{\min}\, \mathrm{X}\,(\mathrm{i}-\mathrm{k}), \tag{4-11}$$

Multiply both sides of Equation 4-10 by w_k^{min} and then sum the results over the value of index k in the range 0, 1, 2, …, (M - 1), then we get:

$$\sum_{k=0}^{M-1} w_k^{min} \sum_{i=M}^{N} X(i-k)e'_{min}(\mathrm{i}) = 0, \tag{4-12}$$

Interchange the order of summation, we get:

$$\sum_{i=M}^{N}\left[\sum_{k=0}^{M-1} w_k^{min} X(i-k)\right] e'_{min}(\mathrm{i}) = 0, \tag{4-13}$$

Use Equation 4-11 to substitute the inside summation item in Equation 4-13, we get:

$$\sum_{i=M}^{N} Y_i^{min} e'_{min}(\mathrm{i}) = 0, \tag{4-14}$$

Equation 4-14 is a necessary condition for global minimization of $\Theta({w_0}', {w_1}', \dots, {w_{M-1}}')$, which is called the principle of orthogonality. In Equation 4-14, Y_i^{min} (defined in Equation 4-11) is considered the least-square (LS) estimate of the desired (observed) response Z (i). Hence Y_i^{min} can be written as $\hat{Z}^{min}(i\,|X_i, X_{i-1}, \dots, X_{i-M+1})$, then Equation 4-14 can be reformulated as:

$$\sum_{i=M}^{N} \hat{Z}^{min}(i\,|X_i, X_{i-1}, \dots, X_{i-M+1}) e'_{min}(\mathrm{i}) = 0, \tag{4-15}$$

Taking the time average of the left-hand side of Equation 4-15, we find that the cross-correlation of two time series $\hat{Z}^{min}(i\,|X_i, X_{i-1}, \dots, X_{i-M+1})$ and $e^*_{min}(\mathrm{i})$ is 0. So, the LSE estimate of the observed response Z (i) represented by $\hat{Z}^{min}(i\,|X_i, X_{i-1}, \dots, X_{i-M+1})$, and the LSE model error process $e^*_{min}(\mathrm{i})$ are orthogonal over time.

$$\underbrace{Z(i)}_{observed\ response} \tag{4-16}$$

$$= \underbrace{Z^{min}(i\,|X_i, X_{i-1}, \dots, X_{i-M+1})}_{estimate\ of\ observed\ response}$$

$$+ \underbrace{e'_{min}(\mathrm{i})}_{LSE\ model\ estimation\ error},$$

If we define:

$$E_Z = \sum_{i=M}^{N} |Z(i)|^2,$$

$$E_{LSE\ est} = \sum_{i=M}^{N} \left| Z^{min}(i\ |X_i, X_{i-1}, \dots, X_{i-M+1}) \right|^2,$$

$$E_{LSE\ error} = \sum_{i=M}^{N} |e^*_{min}(\mathrm{i})|^2,$$

By using the *principle of orthogonality* (Equation 4-15), we get:

$$E_Z = E_{LSE\ estimation} + E_{LSE\ error}, \tag{4-17}$$

Equation 4-17 tells: The energy of the observed time series Z (i) is the summation of the energy of the LSE estimation time series, and the energy of the LSE error process time series. All the three items in Equation 4-17 are nonnegative.

Another Approach of Understanding the LSE Model

Since Y_i^{min} in Equation 4-11 is also written as $\hat{Z}^{min}(i\ |X_i, X_{i-1}, \dots, X_{i-M+1})$ in Equation 4-16, according to Equation 4-11 and Equation 4-16, we get:

$$e^*_{min}(\mathrm{i}) = \mathrm{Z\ (i)} - \sum_{k=0}^{M-1} w_k^{min}\ \mathrm{X\ (i-k)}, \tag{4-18}$$

Substitute Equation 4-18 into Equation 4-14, we get:

$$\sum_{i=M}^{N} X(i-k) \left[\mathrm{Z\ (i)} - \sum_{h=0}^{M-1} w_h^{min}\ \mathrm{X\ (i-h)} \right] = 0, \tag{4-19}$$

$$k = 0, 1, 2, \dots, M-1,$$

Reorganize we get:

$$\sum_{i=M}^{N} X(i-k)\mathrm{Z}\,(\mathrm{i}) = \sum_{h=0}^{M-1}\left[w_h^{min}\ \sum_{\mathrm{i=M}}^{\mathrm{N}} \mathrm{X}\,(\mathrm{i}-\mathrm{k})\mathrm{X}(\mathrm{i}-\mathrm{h})\right], \quad \mathrm{k} \tag{4-20}$$

$$= 0,1,2,\ldots,\mathrm{M}-1,$$

Here we define:

$$\beta(-k) \triangleq \sum_{i=M}^{N} X(i-k)\mathrm{Z}\,(\mathrm{i}), \qquad 0 \le k \le M-1, \tag{4-21}$$

$$\Phi(h,k) \triangleq \sum_{\mathrm{i=M}}^{\mathrm{N}} \mathrm{X}\,(\mathrm{i}-\mathrm{k})\mathrm{X}(\mathrm{i}-\mathrm{h}), \qquad 0 \le h \le M-1, \tag{4-22}$$

$$0 \le k \le M-1,$$

Then Equation 4-20 can be rewritten as:

$$\beta(-k) = \sum_{h=0}^{M-1}\left[w_h^{min}\ \Phi(\mathrm{h},\mathrm{k})\right], \qquad \mathrm{k} = 0,1,2,\ldots,\mathrm{M}-1, \tag{4-23}$$

Let the M by M matrix $\boldsymbol{\Phi}$ be:

$$\boldsymbol{\Phi} \triangleq \begin{bmatrix} \Phi(0,0) & \Phi(1,0) & \cdots & \Phi(\mathrm{M}-1,0) \\ \Phi(0,1) & \Phi(1,1) & & \Phi(\mathrm{M}-1,1) \\ \vdots & & \ddots & \vdots \\ \Phi(0,\mathrm{M}-1) & \Phi(1,\mathrm{M}-1) & \cdots & \Phi(\mathrm{M}-1,\mathrm{M}-1) \end{bmatrix}, \tag{4-24}$$

Let the vector $\boldsymbol{\beta}$ (M by 1) be:

$$\boldsymbol{\beta} \triangleq [\beta(0) \quad \beta(-1) \quad \ldots \quad \beta(-\mathrm{M}+1)]^T, \tag{4-25}$$

Let the vector $\boldsymbol{w^{min}}$ (M by 1) be:

$$\boldsymbol{w^{min}} \triangleq [\mathrm{w}_0^{\min} \quad \mathrm{w}_1^{\min} \quad \ldots \quad \mathrm{w}_{\mathrm{M}-1}^{\min}]^T, \tag{4-26}$$

Then, Equation 4-23 can be rewritten as:

$$\boldsymbol{\beta} = \boldsymbol{\Phi w^{min}}, \tag{4-27}$$

Assume $\boldsymbol{\Phi}$ is nonsingular, then:

$$\boldsymbol{w^{min}} = \boldsymbol{\Phi^{-1}\beta}, \tag{4-28}$$

Equation 4-28 is the design of a linear least square estimation (LSE), where $\boldsymbol{\Phi^{-1}}$ is the inverse of the time-average cross-correlation matrix and $\boldsymbol{\beta}$ is the cross-correlation vector between unobserved time series $\boldsymbol{X}$ and observed time series $\boldsymbol{Z}$. When noise is assumed to be white Gaussian distributed, its counterpart filter design is the Wiener-Hopf Equation.

According to Equation 4-22 and Equation 4-24, $\boldsymbol{\Phi}$ can be decomposed into:

$$\boldsymbol{\Phi} \triangleq \boldsymbol{A}^{\mathrm{T}}\boldsymbol{A}, \tag{4-29}$$

where

$$\boldsymbol{A} \triangleq \begin{bmatrix} \mathrm{X(M)} & \mathrm{X(M+1)} & \cdots & \mathrm{X(N)} \\ \mathrm{X(M-1)} & \mathrm{X(M)} & & \mathrm{X(N-1)} \\ \vdots & & \ddots & \vdots \\ \mathrm{X(1)} & \mathrm{X(2)} & \cdots & \mathrm{X(N-M+1)} \end{bmatrix}^{T}, \tag{4-30}$$

Let

$$\boldsymbol{Z} \triangleq [\mathrm{Z(M)} \quad \mathrm{Z(M+1)} \quad \ldots \quad \mathrm{Z(N)}]^{T}, \tag{4-31}$$

Then, according to Equation 4-30 and 4-31, and the definition of $\boldsymbol{\beta}$ in Equation 4-25 and 4-21

$$\boldsymbol{\beta} \triangleq \boldsymbol{A}^{\mathrm{T}}\boldsymbol{Z}, \tag{4-32}$$

Equation 4-27 can be rewritten as the following using the decomposition expression in Equation 4-29

$$\boldsymbol{\beta} = \boldsymbol{A^{T}Aw^{min}}, \tag{4-33}$$

Integrating Equation 4-32 and Equation 4-33

$$\boldsymbol{A^{T}Z} = \boldsymbol{A^{T}Aw^{min}}, \tag{4-34}$$

Therefore,

$$\boldsymbol{w^{min}} = (\boldsymbol{A^T A})^{-1}\boldsymbol{A^T Z}, \tag{4-35}$$

Let

$$\boldsymbol{Y} = \widehat{\boldsymbol{Z}}^{\boldsymbol{min}} \triangleq [\hat{Z}^{\min}(\mathrm{M}) \quad \hat{Z}^{\min}(\mathrm{M}+1) \quad \ldots \quad \hat{Z}^{\min}(\mathrm{N})]^T, \tag{4-36}$$

Substitute Equation 4-35 into Equation 4-11, we get:

$$\boldsymbol{Y} = \widehat{\boldsymbol{Z}}^{\boldsymbol{min}} \triangleq \boldsymbol{A}\, \boldsymbol{w^{min}} = \boldsymbol{A}\, (\boldsymbol{A^T A})^{-1}\boldsymbol{A^T Z}, \tag{4-37}$$

Noting that $\boldsymbol{A}\,(\boldsymbol{A^T A})^{-1}\boldsymbol{A^T}$ is the projection operator onto the linear space spanned by the columns of the data matrix ***A***.

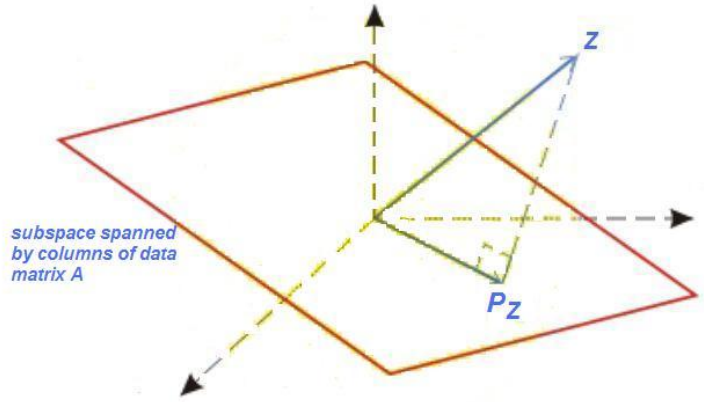

Figure 4-1. The LSE prediction can be considered as the observed variable vector *Z* projected from the (*N*-*M*+1) dimensional whole space onto the *M* dimensional subspace spanned by columns of data matrix ***A***.

Hence, the LSE estimation vector, which is expressed by $\widehat{\boldsymbol{Z}}^{\boldsymbol{min}}$ or $\boldsymbol{Y}$, is the orthogonal projection of observable variable vector $\boldsymbol{Z}$ onto the linear space spanned by the columns of the data matrix ***A***. Suppose M < N – M + 1 (Stewart, 1973) (Figure 4-1). If data matrix ***A*** is full rank, then, its column space is an M dimensional sub-space of the (N-M+1) dimensional full space. Assume that, the data matrix ***A*** is already known with no uncertainty.

In practice, ***A*** could be unknown. In this case, a set of training data with limited length will be used to estimate the LSE parameters. Some further properties of LSE are

investigated by other literatures (Miller, 1974; Goodwin & Payne, 1977; Hanson, 1995; Hayes, 2008). In an alternative way of thinking, X(*t*) can be considered as another time series observed. Then, we interpret the problem as: the present states of time series Z(*t*) can be predicted by the present and previous states of another time series X(*t*), using the LSE model.

MMSE Model Prediction

Next, we introduce the Minimum Mean Square Error (MMSE) prediction, described by the conditional expectation (Hamilton, 1994; Priestley, 1981):

$$\hat{X}_p(q) = E\left[X_{p+q}|X_p, X_{p-1}, \ldots\right], \tag{4-38}$$

If we want a linear-form prediction, $\hat{X}_p(q)$ should have the following form (Whittle, 1983; Priestley, 1981):

$$\hat{X}_p(q) = \sum_{i=0}^{p-1} w_i X_{p-i}, \tag{4-39}$$

Suppose we identify a particular model for a given time series, we need to estimate the model parameters and wish to compute forecasts from the fitted model (M_f), instead of the true model (M), which we do not know. If we use a quadratic loss function, the best way to compute a forecast is to choose $\hat{X}_p(h)$ (h=1, 2 … q-1) to be the conditional expected value of $\hat{X}(p+h)$ on the model, and use information I_N available at time *N*.

$$\hat{X}_p(q) = E\left[X_{p+q}|M_f, I_N\right], \tag{4-40}$$

Then, the MMSE forecast with MA model of possibly infinite order would be (Box et al., 1994):

$$\hat{X}_p(q) = \sum_{i=q}^{\infty} w_i Z_{p+q-i}, \tag{4-41}$$

where the future values are replaced by zero.

More generally, the MMSE forecast from an Auto-Regressive Moving Average (ARMA) model (Shamway, et al., 2000) can be computed by:

$$\hat{X}_p(q) = \sum_{i=1}^{q-1} \Theta_i \hat{X}_{p+q-i} + \sum_{i=q}^{K} \Theta_i X_{p+q-i} + \sum_{i=q}^{J} w_i Z_{p+q-i}, \tag{4-42}$$

where the future value of Z is replaced by zero and the future values of X is replaced by the conditional expectation $\hat{X}$ (Box et al. 1994).

Similarly, if we use the Auto-Regressive Integrated Moving Average (ARIMA) model (Shamway, et al., 2000), then the MMSE forecast would be:

$$\begin{aligned} &\hat{X}_p(q) - \hat{X}_p(q-1) \\ &= \sum_{i=1}^{q-2} \Theta_i \left(\hat{X}_{p+q-i} - \hat{X}_{p+q-1-i}\right) + \Theta_{q-1}\left(\hat{X}_{p+1} - X_p\right) \\ &+ \sum_{j=q}^{K} \Theta_j \left(X_{p+q-j} - X_{p+q-1-j}\right) + \sum_{t=q}^{J} w_t Z_{p+q-t}, \end{aligned} \tag{4-43}$$

where the future value of Z is replaced by zero and the future values of X is replaced by the conditional expectation of $\hat{X}$.

ARMA and ARIMA models can convert to each other, though generally ARMA models are used for accumulative value forecast, while ARIMA models are used for differential value forecast. For special cases, e.g. ARIMA (0, 1, 1), it is a simple exponential smoothing. Recursive calculation is commonly used for the *q*-step MMSE forecast at time *p* using ARMA or ARIMA models.

Other Prediction Methods

To handle non-stationarity and seasonality, the prediction process need to select a suitable model for a given time series. The prediction based on the more general class of ARIMA or Seasonal Auto-Regressive Integrated Moving Average (SARIMA) models is called the Box-Jenkins prediction (Box et al., 1994). The model involves in an iterative procedure with: (1) Formulating, (2) fitting, (3) checking and adjusting.

Depending on how the first few observations are treated, there exist different prediction procedures for fitting ARIMA model (e.g. maximum likelihood and conditional least square). But only for short series (no more than several hundred points), the choice of procedures is important and makes a significant difference. It is shown that, for short series even when asymptotically unbiased, parameter estimates are likely to be biased (Ansley and Newbold, 1980). Furthermore, different software package, using different estimation routines, can produce model parameter estimates with non-trivial differences (Newbold et al., 1994). Hence it is a wise choice to use software which specifies exactly what estimation procedures is adopted.

The way that trend is removed before applying the Box-Jenkins approach can be vital for non-stationary time series. Especially, the order of differencing can be crucial if differencing is applied. Alternative methods of removing trend, prior to fitting an ARIMA model, may lead to better forecasting (Makridakis and Hibon, 1997).

There are other categories of prediction methods not included in this chapter, like the ensemble prediction, simulation methods or the judgmental methods incorporating intuitive judgments, opinions and subjective probability estimates (e.g. composite prediction; Delphi method; Scenario building).

Different models have their respective limitations and advantages in difference scenarios. When selecting the fit prediction models for epileptic seizure prediction, comprises need to be made to tradeoff the robustness, performance, feasibility and complexity (Zhang et al., 2011).

CHAPTER 5
CAUSAL RELATIONS BETWEEN TWO OR MULTIPLE TIME SERIES

The causal relations are useful in the modeling of directed networks of epileptic brain and in the epileptic focus localization for epilepsy surgery. In this chapter, a wide-sense stationary, purely nondeterministic time series is studied, for an issue closely related to prediction: the causal relations between multiple time series. We start from two-variable (time series) and three variable (time series) models. The causal relations in two or multiple time series are discussed in comparison, in statistical senses.

We first discuss (1) the simple causal model, and (2) the instantaneous causal model, between two time series {Xt} and {Yt} (Granger, 1969). We assume that: the time series are wide-sense stationary and purely nondeterministic. In the simple causal model, the previous states of {Xt} and {Yt} are used, to predict the present state of {Xt} and {Yt}, respectively. In the instantaneous causal model, the previous states of {Xt}, as well as the previous and present states of {Yt}, are used to predict the present state of {Xt}; and vice versa. Though this is in stochastic sense, the principle of orthogonality is still kept for minimizing prediction error. Then the three-variable models are discussed briefly in frequency formulation (Granger, 1969). Finally, causal relations between one group of time series and the other group of time series are studied in frequency domain (Geweke 1982). The underlying principle of orthogonality is kept for error minimization.

Two-Variable (Time Series) Models

Let $\mathrm{X_t}$ and $\mathrm{Y_t}$ be two wide-sense stationary, purely nondeterministic time series with zero means. The simple causal model (Granger, 1969) is

$$X_t = \sum_{j=1}^{m} a_j \mathrm{X_{t-j}} + \sum_{j=1}^{m} b_j \mathrm{Y_{t-j}} + \varepsilon_t, \tag{5-1}$$

$$Y_t = \sum_{j=1}^{m} c_j \mathrm{X}_{\mathrm{t-j}} + \sum_{j=1}^{m} d_j \mathrm{Y}_{\mathrm{t-j}} + \eta_t, \tag{5-2}$$

where ε_t and η_t are two zero-mean serially uncorrelated noise process (time series) with $\mathrm{E}(\varepsilon_t, \eta_s) = 0$ for any t and s. Since ε_t is serially uncorrelated, for any p ≠ q, $\mathrm{E}(\varepsilon_p,\ \varepsilon_q) = 0$. Since η_t is serially uncorrelated, for any p ≠ q, $\mathrm{E}(\eta_p,\ \eta_q) = 0$.

In the simple causal model, the previous states of $\{X_t\}$ and $\{Y_t\}$ are used to predict the present state of $\{X_t\}$ and the present state of $\{Y_t\}$, respectively.

A more general model: instantaneous causal model (Granger, 1969), is

$$X_t = \sum_{j=1}^{m} a_j \mathrm{X}_{\mathrm{t-j}} + \sum_{j=0}^{m} b_j \mathrm{Y}_{\mathrm{t-j}} + \varepsilon_t, \tag{5-3}$$

$$Y_t = \sum_{j=0}^{m} c_j \mathrm{X}_{\mathrm{t-j}} + \sum_{j=1}^{m} d_j \mathrm{Y}_{\mathrm{t-j}} + \eta_t, \tag{5-4}$$

In the instantaneous causal model, the previous states of $\{X_t\}$ as well as the previous and present states of $\{Y_t\}$, are used to predict the present state of $\{X_t\}$. Similarly, the previous states of $\{Y_t\}$, as well as the previous and present states of $\{X_t\}$, are used to predict the present state of $\{Y_t\}$.

Comparing Equation 5-1 and Equation 5-3, if the instantaneous causality is occurring ($b_0 \neq 0$), then, knowledge of the present state of $\{Y_t\}$ will improve the prediction for the present state of $\{X_t\}$, and $\mathrm{var}(\varepsilon_t)$ will decrease. Similarly, comparing Equation 5-2 and Equation 5-4, if the instantaneous causality is occurring ($c_0 \neq 0$), then, knowledge of the present state of $\{X_t\}$ will improve the prediction for the present state of $\{Y_t\}$, and $\mathrm{var}(\eta_t)$ will decrease.

To obtain the frequency formulation of the simple causal model, we can rewrite Equation 5-1 and Equation 5-2 by using the time shift (delay) operator U, where $UX_t = X_{t-1}$

$$X_t = a(U)X_t + b(U)Y_t + \varepsilon_t, \tag{5-5}$$

$$Y_t = c(U)X_t + d(U)Y_t + \eta_t, \tag{5-6}$$

where COEF (U) (COEF = a, b, c, d) are power series in U with coefficient of U^0 being zero.

Next, we use Cramer representation of the series to get (Granger, 1969):

$$X_t = \int_{-\pi}^{\pi} e^{it\omega}\, dZ_x(\omega), \tag{5-7}$$

$$Y_t = \int_{-\pi}^{\pi} e^{it\omega}\, dZ_Y(\omega), \tag{5-8}$$

Note: Cramer representation is widely used in spectrum estimation for wide-sense stationary process; similar to the role of Fourier transform in time-frequency analysis in deterministic time series.

Because k units of time shift (delay) (represented by U^k) in the time domain, is equivalent to being multiplied by $e^{-i\omega k}$ in the frequency domain, also noting that Cramer representation is a linear transformation, thus we get:

$$a(U)X_t = \int_{-\pi}^{\pi} e^{it\omega}\, a\left(e^{-i\omega}\right) dZ_x(\omega), \tag{5-9}$$

$$b(U)Y_t = \int_{-\pi}^{\pi} e^{it\omega}\, b\left(e^{-i\omega}\right) dZ_y(\omega), \tag{5-10}$$

$$c(U)X_t = \int_{-\pi}^{\pi} e^{it\omega}\, c\left(e^{-i\omega}\right) dZ_x(\omega), \tag{5-11}$$

$$d(U)Y_t = \int_{-\pi}^{\pi} e^{it\omega}\, d\left(e^{-i\omega}\right) dZ_y(\omega), \tag{5-12}$$

Integrate Equations 5-7 to 5-12 into Equations 5-5 to 5-6, we get (for every t):

$$\int_{-\pi}^{\pi} e^{it\omega} \left[\left(1 - a\left(e^{-i\omega}\right)\right) dZ_x(\omega) - b\left(e^{-i\omega}\right) dZ_y(\omega) - dZ_\varepsilon(\omega)\right] \tag{5-13}$$

$$= 0,$$

$$\int_{-\pi}^{\pi} e^{it\omega} \left[\left(-c\left(e^{-i\omega}\right)\right) dZ_x(\omega) + (1 - d\left(e^{-i\omega}\right)) dZ_y(\omega)\right. \tag{5-14}$$

$$\left. - dZ_\eta(\omega)\right] = 0,$$

Because Equation (5-13) and (5-14) hold for every t, it further implies:

$$A(\omega) \begin{bmatrix} dZ_x(\omega) \\ dZ_y(\omega) \end{bmatrix} = \begin{bmatrix} dZ_\varepsilon(\omega) \\ dZ_\eta(\omega) \end{bmatrix}, \tag{5-15}$$

where $A(\omega) \triangleq \begin{bmatrix} 1 - a(e^{-i\omega}) & -b(e^{-i\omega}) \\ -c(e^{-i\omega}) & 1 - d(e^{-i\omega}) \end{bmatrix}$, for every ω ϵ [-π , π].

Therefore,

$$\begin{bmatrix} dZ_x(\omega) \\ dZ_y(\omega) \end{bmatrix} = A(\omega)^{-1} \begin{bmatrix} dZ_\varepsilon(\omega) \\ dZ_\eta(\omega) \end{bmatrix}, \tag{5-16}$$

Then, we obtain the spectral and cross-spectral matrix:

$$\begin{bmatrix} f_x(\omega) & Cr(\omega) \\ Cr^*(\omega) & f_y(\omega) \end{bmatrix} \triangleq E \begin{bmatrix} dZ_x(\omega) \\ dZ_y(\omega) \end{bmatrix} \begin{bmatrix} \overline{dZ_x(\omega)} & \overline{dZ_y(\omega)} \end{bmatrix} \tag{5-17}$$

$$= A(\omega)^{-1} E\left(\begin{bmatrix} dZ_\varepsilon(\omega) \\ dZ_\eta(\omega) \end{bmatrix} \begin{bmatrix} \overline{dZ_\varepsilon(\omega)} & \overline{dZ_\eta(\omega)} \end{bmatrix}\right) (A(\omega)^{*T})^{-1}$$

$$= A(\omega)^{-1} \begin{bmatrix} \sigma_\varepsilon(\omega)^2 & 0 \\ 0 & \sigma_\eta(\omega)^2 \end{bmatrix} (A(\omega)^{*T})^{-1},$$

where

$$f_x(\omega) = \frac{1}{\Delta(\omega)}\left(\left|1 - d(e^{-i\omega})\right|^2 \sigma_\varepsilon(\omega)^2 + \left|b(e^{-i\omega})\right|^2 \sigma_\eta(\omega)^2\right),$$

$$f_y(\omega) = \frac{1}{\Delta(\omega)}\left(\left|c(e^{-i\omega})\right|^2 \sigma_\varepsilon(\omega)^2 + \left|1 - a(e^{-i\omega})\right|^2 \sigma_\eta(\omega)^2\right),$$

$$Cr(\omega) \triangleq C_1(\omega) + C_2(\omega)$$

$$= \frac{1}{\Delta(\omega)}\left(1 - d(e^{-i\omega})\right)\overline{c(e^{-i\omega})}\sigma_\varepsilon(\omega)^2$$

$$+ \frac{1}{\Delta(\omega)}\left(1 - \overline{a(e^{-i\omega})}\right)b(e^{-i\omega})\sigma_\eta(\omega)^2,$$

$$\Delta(\omega) = \left|\left(1 - a(e^{-i\omega})\right)\left(1 - d(e^{-i\omega})\right) - b(e^{-i\omega})c(e^{-i\omega})\right|^2,$$

When we study the causality between the two time series $\{X_t\}$ and $\{Y_t\}$, if $\{Y_t\}$ is NOT causing $\{X_t\}$, then $b(U) = 0$, $b\left(e^{-i\omega}\right) = 0$ for all ω, thus $C_2(\omega) = 0$; similarly, if $\{X_t\}$ is NOT causing $\{Y_t\}$, then $c(U) = 0$, $c\left(e^{-i\omega}\right) = 0$ for all ω, thus $C_1(\omega) = 0$. Therefore, the cross spectrum $Cr(\omega)$ can be decomposed into $C_1(\omega)$ and $C_2(\omega)$, representing "$\{X_t\}$ causing $\{Y_t\}$" and "$\{Y_t\}$ causing $\{X_t\}$", respectively, saying, $C_1(\omega)$ and $C_2(\omega)$ can be considered as two arms of the feedback mechanism.

In Equation 5-18 and Equation 5-19, two measures of strength of causality are defined: representing "$\{X_t\}$ to $\{Y_t\}$" and "$\{Y_t\}$ to $\{X_t\}$" respectively:

$$C_{\overrightarrow{xy}}(\omega) \triangleq \frac{|C_1(\omega)|^2}{f_x(\omega)f_y(\omega)} = \frac{E_1(\omega)}{E_x(\omega)E_y(\omega)}, \tag{5-18}$$

$$C_{\overrightarrow{yx}}(\omega) \triangleq \frac{|C_2(\omega)|^2}{f_x(\omega)f_y(\omega)} = \frac{E_2(\omega)}{E_x(\omega)E_y(\omega)}, \tag{5-19}$$

where

$$E_1(\omega) \triangleq |1 - d\left(e^{-i\omega}\right)|^2 |c(e^{-i\omega})|^2 \sigma_\varepsilon(\omega)^2$$

$$E_2(\omega) \triangleq \left|1 - a(e^{-i\omega})\right|^2 \left|b(e^{-i\omega})\right|^2 \sigma_\eta(\omega)^2$$

$$E_x(\omega) \triangleq \left|1 - d(e^{-i\omega})\right|^2 \sigma_\varepsilon(\omega)^2 + \left|b(e^{-i\omega})\right|^2 \sigma_\eta(\omega)^2$$

$$E_y(\omega) \triangleq \left|c(e^{-i\omega})\right|^2 \sigma_\varepsilon(\omega)^2 + \left|1 - a(e^{-i\omega})\right|^2 \sigma_\eta(\omega)^2$$

In Equation 5-20 and Equation 5-21, the *causal phase* diagrams are further defined, to study the phase lag against frequency cross spectrum:

$$\Phi_{\overrightarrow{xy}}(\omega) \triangleq phase\ of\ C_1(\omega), \tag{5-20}$$

$$\Phi_{\overrightarrow{yx}}(\omega) \triangleq phase\ of\ C_2(\omega), \tag{5-21}$$

Similar to the frequency formulation of the simple causal model (refer to Equations 5-1 and 5-2), we consider the frequency formulation of the instantaneous causal model (refer to Equations 5-3 and 5-4). A spectral and cross-spectral matrix can be obtained similar to what is given by Equation 5-17, as follow:

$$\begin{bmatrix} f_x(\omega) & Cr(\omega) \\ Cr^*(\omega) & f_y(\omega) \end{bmatrix} \triangleq E \begin{bmatrix} dZ_x(\omega) \\ dZ_y(\omega) \end{bmatrix} \begin{bmatrix} \overline{dZ_x(\omega)} & \overline{dZ_y(\omega)} \end{bmatrix} \tag{5-22}$$

$$= A(\omega)^{-1} E\left(\begin{bmatrix} dZ_\varepsilon(\omega) \\ dZ_\eta(\omega) \end{bmatrix} \begin{bmatrix} \overline{dZ_\varepsilon(\omega)} & \overline{dZ_\eta(\omega)} \end{bmatrix}\right) (A(\omega)^{*T})^{-1}$$

$$= A(\omega)^{-1} \begin{bmatrix} \sigma_\varepsilon(\omega)^2 & 0 \\ 0 & \sigma_\eta(\omega)^2 \end{bmatrix} (A(\omega)^{*T})^{-1},$$

where

$$f_x(\omega) = \frac{1}{\Delta(\omega)} \left(\left|1 - d(e^{-i\omega})\right|^2 \sigma_\varepsilon(\omega)^2 + \left|b(e^{-i\omega})\right|^2 \sigma_\eta(\omega)^2\right),$$

$$f_y(\omega) = \frac{1}{\Delta(\omega)} \left(\left|c(e^{-i\omega})\right|^2 \sigma_\varepsilon(\omega)^2 + \left|1 - a(e^{-i\omega})\right|^2 \sigma_\eta(\omega)^2\right),$$

$$Cr(\omega) \triangleq C_1(\omega) + C_2(\omega)$$

$$= \frac{1}{\Delta(\omega)}\left(1 - d\left(e^{-i\omega}\right)\right)\left(\overline{c(e^{-\iota\omega})} - c_0\right)\sigma_\varepsilon(\omega)^2$$

$$+ \frac{1}{\Delta(\omega)}\left(1 - \overline{a(e^{-\iota\omega})}\right)\left(b\left(e^{-i\omega}\right) - b_0\right)\sigma_\eta(\omega)^2,$$

$$\Delta(\omega) = \left|\left(1 - a\left(e^{-i\omega}\right)\right)\left(1 - d\left(e^{-i\omega}\right)\right)\right.$$

$$\left. - \left(b\left(e^{-i\omega}\right) - b_0\right)\left(c\left(e^{-i\omega}\right) - c_0\right)\right|^2,$$

Note: b_0 and c_0 are the coefficients of instant causality of $\{Y_t\}$ in Equation 5-3 and $\{X_t\}$ in Equation 5-4, respectively.

Summary: the spectral methods can be applied to analyzing causal relations between two time series $\{X_t\}$ and $\{Y_t\}$. Furthermore, the spectral methods in the frequency domain are robust in their interpretation, compared with the equation models in the time domain.

Three-Variable (Time Series) Models

Extend the two-variable model (simple causal model) in Equation 5-5 and 5-6 to three-variable model (Granger, 1969), we get

$$X_t = a_1(U)X_t + b_1(U)Y_t + c_1(U)Z_t + \varepsilon_{1,t}, \quad (5\text{-}23)$$

$$Y_t = a_2(U)X_t + b_2(U)Y_t + c_2(U)Z_t + \varepsilon_{2,t}, \quad (5\text{-}24)$$

$$Z_t = a_3(U)X_t + b_3(U)Y_t + c_3(U)Z_t + \varepsilon_{3,t}, \quad (5\text{-}25)$$

Here we keep using the time shift operator U ($\mathrm{UX_t} = \mathrm{X_{t-1}}$). Since there is no instantaneous causality, the coefficients of U^0 are always zero.

Applying the frequency formulation (using Cramer representation) to the three-variable model, the spectral and cross-spectral matrix is obtained:

$$\begin{bmatrix} f_x(\omega) & C_r^{xy}(\omega) & C_r^{xz}(\omega) \\ C_r^{xy*}(\omega) & f_y(\omega) & C_r^{yz}(\omega) \\ C_r^{xz*}(\omega) & C_r^{yz*}(\omega) & f_z(\omega) \end{bmatrix} \tag{5-26}$$

$$= E\begin{bmatrix} dZ_x(\omega) \\ dZ_y(\omega) \\ dZ_z(\omega) \end{bmatrix}\left[\overline{dZ_x(\omega)} \quad \overline{dZ_y(\omega)} \quad \overline{dZ_z(\omega)}\right]$$

$$= A(\omega)^{-1}E(\begin{bmatrix} dZ_{\varepsilon 1}(\omega) \\ dZ_{\varepsilon 2}(\omega) \\ dZ_{\varepsilon 3}(\omega) \end{bmatrix}[\overline{dZ_{\varepsilon 1}(\omega)} \quad \overline{dZ_{\varepsilon 2}(\omega)} \quad \overline{dZ_{\varepsilon 3}(\omega)}])(A(\omega)^{*T})^{-1}$$

$$= A(\omega)^{-1}\begin{bmatrix} \sigma_1(\omega)^2 & 0 & 0 \\ 0 & \sigma_2(\omega)^2 & 0 \\ 0 & 0 & \sigma_3(\omega)^2 \end{bmatrix}(A(\omega)^{*T})^{-1},$$

where

$$A = \begin{bmatrix} 1 - a_1(e^{-i\omega}) & -b_1(e^{-i\omega}) & -c_1(e^{-i\omega}) \\ -a_2(e^{-i\omega}) & 1 - b_2(e^{-i\omega}) & -c_2(e^{-i\omega}) \\ -a_3(e^{-i\omega}) & -b_3(e^{-i\omega}) & 1 - c_3(e^{-i\omega}) \end{bmatrix},$$

Similar to the calculation in the two-variable model, the power spectrum of X_t, Y_t, and Z_t, as well as the cross spectrum: $C_r^{xy}(\omega)$, $C_r^{xz}(\omega)$, and $C_r^{yz}(\omega)$, can be calculated in the three-variable model.

Further, the Partial cross spectrum between X_t and Y_t given Z_t is defined as $C_r^{xy,\ z}(\omega) \triangleq C_r^{xy}(\omega) - C_r^{xz}(\omega)f_z(\omega)^{-1}C_r^{zy}(\omega)$, where $C_r^{xy}(\omega), C_r^{xz}(\omega), C_r^{zy}(\omega), f_z(\omega)$ are derived from Equation (5-26). When partial cross spectrum is considered, more useful results arise.

$$C_r^{xy,\ z}(\omega) = -\frac{1}{\Delta_Z(\omega)}\sigma_1^2\sigma_2^2 b_3\left(e^{-i\omega}\right)a_3\left(e^{-i\omega}\right) \tag{5-27}$$

$$-\frac{1}{\Delta_Z(\omega)}\sigma_1^2\sigma_2^2\left(b_2\left(e^{-i\omega}\right)-1\right)a_2\left(e^{-i\omega}\right)$$

$$-\frac{1}{\Delta_Z(\omega)}\sigma_2^2\sigma_3^2 b_1\left(e^{-i\omega}\right)\left(a_1\left(e^{-i\omega}\right)-1\right)$$

$$\triangleq C_{r1}^{xy,\ z}(\omega) + C_{r2}^{xy,\ z}(\omega) + C_{r3}^{xy,\ z}(\omega)$$

where

$$\Delta_Z(\omega) = \sigma_1^2\Big|\left(b_2\left(e^{-i\omega}\right)-1\right)\left(c_3\left(e^{-i\omega}\right)-1\right)$$

$$-c_2\left(e^{-i\omega}\right)b_3\left(e^{-i\omega}\right)\Big|^2$$

$$+\sigma_2^2\Big|c_1\left(e^{-i\omega}\right)b_3\left(e^{-i\omega}\right)$$

$$-b_1\left(e^{-i\omega}\right)\left(c_3\left(e^{-i\omega}\right)-1\right)\Big|^2$$

$$+\sigma_3^2\Big|b_1\left(e^{-i\omega}\right)c_2\left(e^{-i\omega}\right)$$

$$-c_1\left(e^{-i\omega}\right)\left(b_2\left(e^{-i\omega}\right)-1\right)\Big|^2,$$

As shown in Equation 5-27, the partial cross spectrum between X_t and Y_t can be decomposed into $C_{r1}^{xy,\ z}(\omega)$, $C_{r2}^{xy,\ z}(\omega)$, and $C_{r3}^{xy,\ z}(\omega)$, where the first component represents the relations of X_t and Y_t through Z_t, and the second and third components together represent generalizations of the causal cross spectra (between X_t and Y_t) which come from the two variable case.

Multiple-Variable Models

Generalizing the two- and three-variable causal relation models to multiple-variable models brings in-depth insights into the causal relation and feedback problem (Geweke, 1982). In this sub-section, causal relations between one group of time series

and another group of time series are studied. The discussion in this sub-section is still based on wide-sense stationary, purely nondeterministic time series.

Let $\vec{V}_t: m\ by\ 1$ be a zero-mean wide-sense stationary, purely nondeterministic multiple time series. And suppose that, $\vec{V}_t$ has been partitioned into two sub-vectors: $\vec{V}_t^T = \left[\vec{X}_t^T,\ \ \vec{Y}_t^T\right],\ \vec{X}_t: k\ by\ 1\ \ and\ \ \vec{Y}_t: l\ by\ 1,\ \ m = k + l$. We try to find out the causal relations as well as the measurement of linear dependence and feedback between $\vec{X}_t: k\ by\ 1$ and $\vec{Y}_t: l\ by\ 1$.

By assuming the existence of the spectral density matrix $\boldsymbol{S}_{\vec{V}}(\omega)$ at all frequencies $\omega \in [-\pi, \pi]$, we have a corresponding partition of the spectral density matrix $\boldsymbol{S}_{\vec{V}}(\omega)$

$$\boldsymbol{S}_{\vec{V}}(\omega) = \begin{bmatrix} \boldsymbol{S}_{\vec{X}}(\omega) & \boldsymbol{S}_{\vec{X}\vec{Y}}(\omega) \\ \boldsymbol{S}_{\vec{Y}\vec{X}}(\omega) & \boldsymbol{S}_{\vec{Y}}(\omega) \end{bmatrix} \tag{5-28}$$

We assume there is a moving average representation of $\vec{V}_t: m\ by\ 1$ as follow:

$$\vec{V}_t = \sum_{r=0}^{\infty} \boldsymbol{A_r}\vec{\varepsilon}_{t-r}\,,\ \ E(\vec{\varepsilon}_t) = 0, var(\vec{\varepsilon}_t) = \boldsymbol{\gamma} \tag{5-29}$$

In which, $\vec{\varepsilon}_{t-r}$ is serially uncorrelated; for any $\sum_{r=0}^{\infty} \boldsymbol{A_r}\vec{z}^r = 0,\ |\vec{z}| \geq 1$ holds; and $\sum_{r=0}^{\infty} ||\boldsymbol{A_r}||^2 < \infty$. ($\left||P|\right|$ is the square root of the largest eigenvalue of $P'P$; $|P|$ is the square root of the determinant of $P'P$.) The existence of moving average representation is equivalent to the existence of the spectral density matrix $\boldsymbol{S}_{\vec{V}}(\omega)$ at almost all frequencies $\omega \in [-\pi, \pi]$ (Doob, 1953). Furthermore, a lower bound on the mean squared error of one-step-ahead minimum mean $\boldsymbol{\gamma}$ is given by using $\boldsymbol{S}_{\vec{V}}(\omega)$:

$$\ln|\boldsymbol{\gamma}| = \frac{1}{2\pi}\int_{-\pi}^{\pi} \ln|\boldsymbol{S}_{\vec{V}}(\omega)|d\omega \tag{5-30}$$

If there exists a constant $CONST \geq 1$ such that for almost all $\omega \in [-\pi, \pi]$ we have (Rozanov, 1967):

$$CONST^{-1}\, \boldsymbol{I_n} \preccurlyeq \boldsymbol{S}_{\vec{V}}(\omega) \preccurlyeq CONST\, \boldsymbol{I_n} \tag{5-31}$$

Which means both $(CONST\, \boldsymbol{I_n} - \boldsymbol{S}_{\vec{V}}(\omega))$ and $(\boldsymbol{S}_{\vec{V}}(\omega) - CONST^{-1}\, \boldsymbol{I_n})$ are positive semi-definite, and that the spectral density matrix is bounded uniformly away from zero almost everywhere in $[-\pi, \pi]$, which is weaker than the condition that, $\vec{V}_t$ is an autoregressive moving average (ARMA) process of finite orders with invertible AR and MA parts.

Then, the relationship in Equation 5-27 can be inverted so that $\vec{V}_t$ become a function of $\{\vec{V}_{t-r},\ r \geq 1\}$ and $\vec{\varepsilon}_t$.

$$\vec{V}_t = \sum_{r=1}^{\infty} \boldsymbol{B_r} \vec{V}_{t-r} + \vec{\varepsilon}_t, \quad E(\vec{\varepsilon}_t) = 0, var(\vec{\varepsilon}_t) = \boldsymbol{\gamma} \tag{5-32}$$

Predict from the Past of Itself

Considering $\vec{V}_t$ has been partitioned into two sub-vectors $\vec{V}_t^T = \left[\vec{X}_t^T, \quad \vec{Y}_t^T\right]$, if the condition in Equation 5-30 holds, then, $\vec{X}_t$ and $\vec{Y}_t$ each has an autoregressive (AR) representation, denoted by

$$\vec{X}_t = \sum_{r=1}^{\infty} \boldsymbol{E1_r}\, \vec{X}_{t-r} + \overrightarrow{\eta 1}_t\ , \quad E\left(\overrightarrow{\eta 1}_t\right) = 0, var\left(\overrightarrow{\eta 1}_t\right) = \boldsymbol{\Gamma 1} \tag{5-33}$$

$$\vec{Y}_t = \sum_{r=1}^{\infty} \boldsymbol{G1_r}\ \vec{Y}_{t-r} + \overrightarrow{\sigma 1}_t, \qquad E\left(\overrightarrow{\sigma 1}_t\right) = 0, var\left(\overrightarrow{\sigma 1}_t\right) = \boldsymbol{\Xi 1} \tag{5-34}$$

where $\overrightarrow{\eta 1}_t$ is one-step-ahead error when $\vec{X}_t$ is predicted from its own past $\{\vec{X}_{t-r},\ r \geq 1\}$; similarly $\overrightarrow{\sigma 1}_t$ is one-step-ahead error when $\vec{Y}_t$ is predicted from its own past $\{\vec{Y}_{t-r},$

$r \geq 1\}$. Recall Equations 4-15, 4-16 and 4-17 (the Principle of Orthogonality) in the LSE model in the previous chapter. By generalizing the Principle of Orthogonality to infinite orders, to minimize the one-step prediction error, $\overrightarrow{\eta 1_t}$ is orthogonal (uncorrelated) to $\sum_{r=1}^{\infty} \boldsymbol{E1_r}\, \vec{X}_{t-r}$ (the projection of $\vec{X}_t$ on its own past), and $\overrightarrow{\sigma 1_t}$ is orthogonal (uncorrelated) to $\sum_{r=1}^{\infty} \boldsymbol{G1_r}\, \vec{Y}_{t-r}$ (the projection of $\vec{Y}_t$ on its own past). Thus, $\overrightarrow{\eta 1_t}$ is by itself serially uncorrelated, and $\overrightarrow{\sigma 1_t}$ is by itself serially uncorrelated. But $\overrightarrow{\eta 1_t}$ and $\overrightarrow{\sigma 1_t}$ may be correlated with each other contemporaneously and at various leads and lags.

Predict from the Past of Itself and the Past of Others

A further step to take is the projection of $\vec{X}_t$ on its own past and the past of $\vec{Y}_t$, and the projection of $\vec{Y}_t$ on its own past and the past of $\vec{X}_t$, as follow

$$\vec{X}_t = \sum_{r=1}^{\infty} \boldsymbol{E2_r}\, \vec{X}_{t-r} + \sum_{r=1}^{\infty} \boldsymbol{F2_r}\, \vec{Y}_{t-r} + \overrightarrow{\eta 2}_t \;, \quad E\left(\overrightarrow{\eta 2}_t\right) = 0, var\left(\overrightarrow{\eta 2}_t\right) = \boldsymbol{\Gamma 2} \tag{5-35}$$

$$\vec{Y}_t = \sum_{r=1}^{\infty} \boldsymbol{H2_r}\; \vec{X}_{t-r} + \sum_{r=1}^{\infty} \boldsymbol{G2_r}\; \vec{Y}_{t-r} + \overrightarrow{\sigma 2}_t, \quad E\left(\overrightarrow{\sigma 2}_t\right) = 0, var\left(\overrightarrow{\sigma 2}_t\right) = \boldsymbol{\Xi 2} \tag{5-36}$$

By generalizing the Principle of Orthogonality in the LSE model to infinite orders, $\overrightarrow{\eta 2}_t$ is orthogonal (uncorrelated) to $\sum_{r=1}^{\infty} \boldsymbol{E2_r}\, \vec{X}_{t-r} + \sum_{r=1}^{\infty} \boldsymbol{F2_r}\, \vec{Y}_{t-r}$ (the projection of $\vec{X}_t$ on $\left\{\vec{X}_{t-r},\ r \geq 1\right\}$ and $\left\{\vec{Y}_{t-r},\ r \geq 1\right\}$), and $\overrightarrow{\sigma 2}_t$ is orthogonal (uncorrelated) to $\sum_{r=1}^{\infty} \boldsymbol{G2_r}\; \vec{Y}_{t-r} + \sum_{r=1}^{\infty} \boldsymbol{H2_r}\; \vec{Y}_{t-r}$ (the projection of $\vec{Y}_t$ on $\left\{\vec{X}_{t-r},\ r \geq 1\right\}$ and $\left\{\vec{Y}_{t-r},\ r \geq 1\right\}$), to minimize the one-step prediction error. Thus, $\overrightarrow{\eta 2}_t$ is by itself serially uncorrelated, and $\overrightarrow{\sigma 2}_t$ is by itself

serially uncorrelated. It is worth mentioning that $\overrightarrow{\eta 2_t}$ and $\overrightarrow{\sigma 2_t}$ may be correlated with each other contemporaneously and at various leads and lags.

The linear prediction model in Equation 5-34 and 5-35 is another expression of the linear prediction model in Equation 5-31. The two expressions are the same intrinsically, considering $\vec{V}_t^T = \left[\vec{X}_t^T, \quad \vec{Y}_t^T\right]$.

Therefore, $\vec{\varepsilon}_t{}^T = \left[\overrightarrow{\eta 2}_t{}^T, \quad \overrightarrow{\sigma 2}_t{}^T\right]$ and we have the partition of $\boldsymbol{\gamma}$ as follow

$$\boldsymbol{\gamma} = var(\vec{\varepsilon}_t) = var\begin{pmatrix}\overrightarrow{\eta 2}_t \\ \overrightarrow{\sigma 2}_t\end{pmatrix} = \begin{bmatrix}\boldsymbol{\Gamma 2} & \boldsymbol{Cov_{xy}} \\ \boldsymbol{Cov_{xy}}' & \boldsymbol{\Xi 2}\end{bmatrix} \tag{5-37}$$

Predict from the Past of Itself and the Present State and the Past of Others

A third step to take is to pre-multiply the following matrix on Equation 5-34 and Equation 5-35

$$\begin{bmatrix}\boldsymbol{I_k} & \boldsymbol{-Cov_{xy}\Xi 2^{-1}} \\ \boldsymbol{-Cov_{xy}'\Gamma 2^{-1}} & \boldsymbol{I_l}\end{bmatrix}$$

Then, the first k equations can be considered as a new linear system of $\vec{X}_t$, projected on $\{\vec{X}_{t-r},\ r \geq 1\}$ and $\{\vec{Y}_{t-r},\ r \geq 0\}$; similarly, the next l equations can be considered a new linear system of $\vec{Y}_t$, projected on $\{\vec{X}_{t-r},\ r \geq 0\}$ and $\{\vec{Y}_{t-r},\ r \geq 1\}$, as follow

$$\vec{X}_t = \sum_{r=1}^{\infty} \boldsymbol{E3_r}\, \vec{X}_{t-r} + \sum_{r=0}^{\infty} \boldsymbol{F3_r}\, \vec{Y}_{t-r} + \overrightarrow{\eta 3}_t \ , \quad E\left(\overrightarrow{\eta 3}_t\right) \tag{5-38}$$

$$= 0, var\left(\overrightarrow{\eta 3}_t\right) = \boldsymbol{\Gamma 3}$$

$$\vec{Y}_t = \sum_{r=0}^{\infty} \boldsymbol{H3_r}\ \vec{X}_{t-r} + \sum_{r=1}^{\infty} \boldsymbol{G3_r}\ \vec{Y}_{t-r} + \overrightarrow{\sigma 3}_t, \quad E\left(\overrightarrow{\sigma 3}_t\right) \tag{5-39}$$

$$= 0, var\left(\overrightarrow{\sigma 3}_t\right) = \boldsymbol{\Xi 3}$$

where

$$\overrightarrow{\eta 3}_t = \overrightarrow{\eta 2}_t - \boldsymbol{Cov_{xy}\Xi 2^{-1}}\overrightarrow{\sigma 2}_t \tag{5-40}$$

$$\overrightarrow{\sigma 3}_t = \overrightarrow{\sigma 2}_t - \boldsymbol{Cov_{xy}}'\boldsymbol{\Gamma 2^{-1}}\overrightarrow{\eta 2}_t \tag{5-41}$$

Hence $E(\overrightarrow{\eta 3}_t) = E\left(\overrightarrow{\eta 2}_t\right) - \boldsymbol{Cov_{xy}\Xi 2^{-1}}E(\overrightarrow{\sigma 2}_t) = 0 - \boldsymbol{Cov_{xy}\Xi 2^{-1}}\ 0 = 0$, and similarly can prove $E\left(\overrightarrow{\sigma 3}_t\right) = 0$.

Note that: each of $\overrightarrow{\eta 2}_t$ and $\overrightarrow{\sigma 2}_t$ is uncorrelated (orthogonal) to both $\left\{\vec{X}_{t-r},\ r \geq 1\right\}$ and $\left\{\vec{Y}_{t-r},\ r \geq 1\right\}$, as already discussed above. According to Equations 5-39 and 5-40, each of $\overrightarrow{\eta 3}_t$ and $\overrightarrow{\sigma 3}_t$ is uncorrelated to both $\left\{\vec{X}_{t-r},\ r \geq 1\right\}$ and $\left\{\vec{Y}_{t-r},\ r \geq 1\right\}$.

According to Equation 5-39, $\overrightarrow{\eta 3}_t$ is also uncorrelated to $\overrightarrow{\sigma 2}_t$:

$$cov(\overrightarrow{\eta 3}_t, \overrightarrow{\sigma 2}_t) = E(\overrightarrow{\eta 3}_t \overrightarrow{\sigma 2}_t{}^T)$$

$$= E\left(\left(\overrightarrow{\eta 2}_t - \boldsymbol{Cov_{xy}\Xi 2^{-1}}\overrightarrow{\sigma 2}_t\right)\overrightarrow{\sigma 2}_t{}^T\right)$$

$$= \boldsymbol{Cov_{xy} - Cov_{xy}\Xi 2^{-1}\Xi 2 = 0}$$

Hence, $\overrightarrow{\eta 3}_t$ is uncorrelated to all $\overrightarrow{\sigma 2}_t$, $\left\{\vec{X}_{t-r},\ r \geq 1\right\}$ and $\left\{\vec{Y}_{t-r},\ r \geq 1\right\}$. According to Equation 5-35, $\overrightarrow{\eta 3}_t$ is uncorrelated to $\vec{Y}_t$. Thus, $\overrightarrow{\eta 3}_t$ is uncorrelated to $\left\{\vec{X}_{t-r},\ r \geq 1\right\}$ and $\left\{\vec{Y}_{t-r},\ r \geq 0\right\}$. Therefore, Equation 5-37 is a linear (orthogonal) projection of $\vec{X}_t$ on $\left\{\vec{X}_{t-r},\ r \geq 1\right\}$ and $\left\{\vec{Y}_{t-r},\ r \geq 0\right\}$.

Similarly, according to Equation 5-40, $\overrightarrow{\sigma 3}_t$ is also uncorrelated to $\overrightarrow{\eta 2}_t$:

$$cov(\overrightarrow{\sigma 3_t}, \overrightarrow{\eta 2_t}) = E(\overrightarrow{\sigma 3_t}\overrightarrow{\eta 2_t}^T)$$

$$= E\left(\left(\overrightarrow{\sigma 2_t} - \boldsymbol{Cov_{xy}}'\boldsymbol{\Gamma 2^{-1}}\overrightarrow{\eta 2_t}\right)\overrightarrow{\eta 2_t}^T\right)$$

$$= \boldsymbol{Cov_{xy}}' - \boldsymbol{Cov_{xy}}'\boldsymbol{\Gamma 2^{-1}\Gamma 2} = \mathbf{0}$$

Hence, $\overrightarrow{\sigma 3_t}$ is uncorrelated to all $\overrightarrow{\eta 2_t}$, $\{\vec{X}_{t-r},\ r \geq 1\}$ and $\{\vec{Y}_{t-r},\ r \geq 1\}$. According to Equation 5-34, $\overrightarrow{\eta 3_t}$ is uncorrelated to $\vec{X}_t$. Thus, $\overrightarrow{\sigma 3_t}$ is uncorrelated to $\{\vec{X}_{t-r},\ r \geq 0\}$ and $\{\vec{Y}_{t-r},\ r \geq 1\}$. Therefore, Equation 5-38 is a linear (orthogonal) projection of $\vec{Y}_t$ on $\{\vec{X}_{t-r},\ r \geq 0\}$ and $\{\vec{Y}_{t-r},\ r \geq 1\}$.

Predict from the Past of Itself and the Temporally Complete Information of Others

A final step is to consider the linear projection of $\vec{X}_t$ on $\{\vec{X}_{t-r},\ r \geq 1\}$ and $\{\vec{Y}_{t-r},$ integer $r \in (-\infty, \infty)\}$, and the linear projection of $\vec{Y}_t$ on $\{\vec{X}_{t-r},\ integer\ r \in (-\infty, \infty)\}$ and $\{\vec{Y}_{t-r},\ r \geq 1\}$.

Recall the partition of the spectral density matrix $\boldsymbol{S}_{\vec{Y}}(\omega)$ in Equation 5-27. Let

$$\tilde{\boldsymbol{L}}(\omega) = \boldsymbol{S}_{\vec{X}\vec{Y}}(\omega)\boldsymbol{S}_{\vec{Y}}(\omega)^{-1} \qquad for\ all\ \omega \in [-\pi, \pi] \tag{5-42}$$

Note: assume equation 5-30 is true, then, the spectral density matrix exits and is bounded uniformly away from zero almost everywhere in $[-\pi, \pi]$)

Use inverse Fourier transform of $\tilde{\boldsymbol{L}}(\omega)$:

$$\boldsymbol{L}_{\mathrm{r}} = \frac{1}{2\pi}\int_{-\pi}^{\pi} \tilde{\boldsymbol{L}}(\omega)e^{-i\omega r}d\omega \tag{5-43}$$

Let

$$\overrightarrow{W_{\mathrm{t}}} = \vec{X}_{\mathrm{t}} - \sum_{r=-\infty}^{\infty} \boldsymbol{L}_{\mathrm{r}}\,\vec{Y}_{\mathrm{t-r}} \tag{5-44}$$

Then, from the spectral representation of $\vec{V}$ (Equation 5-27), it is be proven that $\overrightarrow{W_t}$ is uncorrelated (orthogonal) with all $\{\vec{Y}_r,\ integer\ r \in (-\infty, \infty)\}$.

Therefore, if we rewrite Equation 5-43 in $\vec{X}_t = \sum_{r=-\infty}^{\infty} \boldsymbol{L}_r \vec{Y}_{t-r} + \overrightarrow{W_t}$, then, Equation 5-43 can be considered as an expression of the linear projection of $\vec{X}_t$ on $\{\vec{Y}_r,\ integer\ r \in (-\infty, \infty)\}$.

From Equation 5-27 and 5-43, it can be further shown that:

$$\boldsymbol{S}_{\overrightarrow{W}}(\omega) = \boldsymbol{S}_{\vec{X}}(\omega) - \boldsymbol{S}_{\vec{X}\vec{Y}}(\omega)\boldsymbol{S}_{\vec{Y}}(\omega)^{-1}\boldsymbol{S}_{\vec{Y}\vec{X}}(\omega) \quad for\ all\ \omega \in [-\pi, \pi] \tag{5-45}$$

Considering the assumption in Equation 5-30: because $\boldsymbol{S}_{\overrightarrow{W}}(\omega)$ consists of the first *k* rows and columns of $\boldsymbol{S}_{\vec{V}}(\omega)$, and Equation 5-30 holds, we also have

$$CONST^{-1}\ \boldsymbol{I_k} \preccurlyeq \boldsymbol{S}_{\overrightarrow{W}}(\omega) \preccurlyeq CONST\ \boldsymbol{I_k} \tag{5-46}$$

Note: for some constant $CONST$ and for all $\omega \in [-\pi, \pi]$ in above.

Therefore, $\overrightarrow{W_t}$ has an autoregressive representation, as follow

$$\overrightarrow{W_t} = \sum_{r=1}^{\infty} \boldsymbol{D_r}\overrightarrow{W_{t-r}} + \overrightarrow{\eta 4_t},\quad E\left(\overrightarrow{\eta 4_t}\right) = 0, var\left(\overrightarrow{\eta 4_t}\right) = \boldsymbol{\Gamma 4} \tag{5-47}$$

where $\overrightarrow{\eta 4_t}$ is uncorrelated (orthogonal) with $\{W_{t-r},\ r \geq 1\}$.

Use $\vec{X}_t = \sum_{r=-\infty}^{\infty} \boldsymbol{L}_r \vec{Y}_{t-r} + \overrightarrow{W_t}$ from Equation 5-43 to substitute all $\{W_{t-r},\ r \geq 0\}$ in Equation 5-46, after re-organizing, we get

$$\vec{X}_t = \sum_{r=1}^{\infty} \boldsymbol{E4_r}\,\vec{X}_{t-r} + \sum_{r=-\infty}^{\infty} \boldsymbol{F4_r}\,\vec{Y}_{t-r} + \overrightarrow{\eta 4_t}\ ,\quad E\left(\overrightarrow{\eta 4_t}\right) = 0, var\left(\overrightarrow{\eta 4_t}\right) = \boldsymbol{\Gamma 4} \tag{5-48}$$

By Equation 5-46, $\overrightarrow{\eta 4_t}$ is a linear function of $\{W_{t-r},\ r \geq 0\}$, and since any $\{\overrightarrow{W_r},\ integer\ r \in (-\infty, \infty)\}$ is uncorrelated (orthogonal) with all $\{\vec{Y}_r,\ integer\ r \in (-\infty, \infty)\}$, therefore, $\overrightarrow{\eta 4_t}$ is uncorrelated with all $\{\vec{Y}_r,\ integer\ r \in (-\infty, \infty)\}$.

According to Equation 5-43, $\vec{X}_s$ is a linear function of $\{\vec{Y}_r,\ integer\ r \in (-\infty, \infty)\}$ and $\overrightarrow{W_s}$ for any $integer\ s$. Also, $\overrightarrow{\eta 4_t}$ is uncorrelated (orthogonal) with $\{W_{t-r},\ r \geq 1\}$, as already discussed above. Therefore, $\overrightarrow{\eta 4_t}$ is uncorrelated with $\{\vec{X}_{\mathrm{t-r}},\ r \geq 1\}$.

Hence, Equation 5-47 is the linear projection of $\vec{X}_{\mathrm{t}}$ on $\{\vec{X}_{\mathrm{t-r}},\ r \geq 1\}$ and $\{\vec{Y}_r,\ integer\ r \in (-\infty, \infty)\}$.

Similarly (symmetrically), Equation 5-48 is the linear projection of $\vec{Y}_{\mathrm{t}}$ on $\{\vec{Y}_{\mathrm{t-r}},\ r \geq 1\}$ and $\{\vec{X}_r,\ integer\ r \in (-\infty, \infty)\}$.

$$\vec{Y}_t = \sum_{r=-\infty}^{\infty} \boldsymbol{H4_r}\ \vec{X}_{t-r} + \sum_{r=1}^{\infty} \boldsymbol{G4_r}\ \vec{Y}_{t-r} + \overrightarrow{\sigma 4_t}, \quad E\left(\overrightarrow{\sigma 4_t}\right) = 0, var\left(\overrightarrow{\sigma 4_t}\right) = \boldsymbol{\Xi 4} \tag{5-49}$$

It is worth mentioning that: all the prediction models in this chapter are based on the assumption that the time series analyzed are a zero-mean wide-sense stationary, and purely nondeterministic. The analysis could be extended to some non-stationary and purely nondeterministic time series, and similar autoregressive representations can be obtained (Zhang et al., 2011).

CHAPTER 6
EPILEPTIC BRAIN NETWORK MODELING AND BRAIN STATE TRANSITION STUDY

Network Modeling of Brains

In the last decade, the study of complex networks has dramatically expanded across diverse scientific fields, including the study and investigation of the brain. There is a tendency that science is concerned more about the structure, behavior, and evolution of the brain, which is an extremely complex system, using modern network approach. A brain includes a huge number of components: molecules, cells, neurons, functional regions and systems. To understand the brain, not only the knowledge of elementary components is required, but also the knowledge of the ways in which those components interact with each other and the corresponding emergent properties. Generally, normal brains display organized and characteristic diverse patterns, due to the highly structured and selective coupling between the components, for example cells, neurons, or functional brain regions. The connectivity also has many different types, such as molecular interactions, coupling between neurons, and the driving force between different brain zones in nervous systems or other biological systems.

Brain networks span multiple spatial scales, from micro scale of individual cells, neurons, and synapses, to the macro scale of cognitive systems, embodied organisms and brain functional regions. It is impossible to fully understand brain functions as an integrated system unless the brain is approached on all of those multiple scales and knowledge of the network interactions on and across multiple scales of organization is obtained. It is worth mentioning that none of the scales in the hierarchy is privileged over any others. Through multiple scale network interactions, molecules and cells give

rise to behavior and cognition. The quantitative study of brain networks requires sophisticated mathematical and statistical techniques.

The network modeling and analytics of brains have opened new experimental and theoretical directions in many areas of neuroscience. It plays a significant role in neuro-anatomy, neurodevelopment, electrophysiology, functional brain imaging, and the neural basis of cognition. Especially, the analysis of network connectivity, topology and architecture illuminates many problems that concern diagnosis and treatment of brain disorders, the brain state transition study, and integrative brain functions: investigation of the brain network interactions among groups of a number of nerve cells between brain functional regions or connected in local brain circuits; quantitatively study of the brain network to shape brain anatomy for architectural principles, such as localize the focal areas of an epilepsy; Trace the extent and location of structural brain network damage for biomarkers to measure the nature and severity of insults like brain trauma, brain traumatic injury, and/or other cognitive dysfunctions.

Neocortical Epilepsy and Its Clinical Challenges

Neocortical epilepsy is a type of seizure disorder that can be either partial (focal) or generalized, in which the seizures originate in the neocortex, part of the external surface layer of the brain. Seizures caused by neocortical epilepsy do not respond well to medication, and therefore epilepsy surgery is often one of the very few options that patients with neocortical epilepsy have. Unfortunately, surgery for neocortical epilepsy does not have the same success rates as that for other kinds of epilepsy. In patients with other forms of epilepsy, such as mesial temporal lobe epilepsy (MTLE), in which the lesion that causes the seizure is clearly defined, surgery can provide seizure freedom in 70 to 80 percent of cases. On the other hand, patients with neocortical

epilepsy see lower success rates. This could be because (1) it may be difficult to isolate the region that is causing the seizures with the currently available technologies; (2) there may be multiple initiation points; or (3) the initiation points may be related to important functional sites in the brain. Because of the complications, patients with neocortical epilepsy often need individually tailored surgeries. A recent study (Lee et al., 2005) in 89 patients with nonlesional neocortical epilepsy showed that, based on the epileptogenic focus location, only 47% of the patients were seizure-free (Engel Class I) after the surgery, and additional 7% experienced a significant reduction in seizure frequency (Engel Class II). Therefore, a successful development of a more reliable method that can be used to identify suitable epilepsy surgery candidates with high confidence for patients with neocortical epilepsy would be a major contribution to advance the care for those patients.

Existing Solutions in Clinical Applications

High-resolution magnetic resonance imaging (MRI) is the most important diagnostic technique for epilepsy surgery in neocortical epilepsy. It offers a high predictive value for surgical outcomes (Cascino et al., 1993). However, MRI is ineffective in 29% of patients with partial epilepsy (Semah et al., 1998), and many patients referred to epilepsy centers for surgery have normal MRI results. Previous studies report that surgical outcome is poor for patients with neocortical epilepsy with normal MRI, but these conclusions were based on limited numbers of patients (Cascino, 2004). Intracranial EEG monitoring is indispensable for neocortical epilepsy with normal MRI. Depth and subdural EEG monitoring could provide accurate localization of the region of seizure onset. However, sampling error can lead to false or missed localization. False and missed localization during intracranial EEG monitoring is

particular common with extratemporal seizure origin (Williamson et al., 1992a; 1992b). Nevertheless, several studies have demonstrated the usefulness of focus localization in neocortical epilepsy with quantitative intracranial EEG analyses. Worrell described the finding, in six patients with neocortical epilepsy, of high-frequency (60-100 Hz) epileptiform oscillations are highly localized in the seizure onset zone (Worrell et al., 2004). They further reported that focal neocortical seizures often occur during periods of increased high-frequency activity in the seizure onset zone, indicating that high-frequency activities are involved in neocortical ictogenesis. Ochi also reported high-frequency oscillations (HFOs) were observed in 78 out of 79 seizures studied (Ochi et al., 2007). In addition, in four postoperatively seizure-free patients, more electrodes recorded higher-frequency HFOs inside the resection area than outside before and after clinical seizure onset, while in five patients with residual seizures, electrodes recorded more HFOs that were of higher or equal frequency outside the surgical area than inside after clinical onset. Based on a “focus index” measure, Roopun et al. used few examples to demonstrate that basic dynamic changes in focal epilepsy of neocortical origin may be useful in localizing the origin of seizures. The findings of these studies and many others support the hypothesis that the dynamics of intracranial EEGs are associated with the behavior of epileptogenic focus in neocortical epilepsy.

Epileptic Brain Network Modeling for Neocortical Epilepsy

Recent observations in humans with MTLE and in the animal models for this condition (Spencer and Spencer, 1994; Bertram, 1997) suggest multifocal seizure onset (i.e. seizures that begin focally within different limbic structures with each seizure) as well as synchronized regional seizure onset (i.e. presumed simultaneous seizure initiation). These observations, together with multifocal physiological and anatomical

changes in the animal models, have raised the possibility of a widely distributed neural network (e.g., specific cortical and subcortical networks) in the gensis and expression of partial- and generalized-onset seizures. Spencer defined a network to be “a functionally and anatomically connected, bilaterally represented, set of cortical and subcortical brain structures and regions in which activity in any one part affects activity in all the others” (Spencer, 2002). One central observation on which this definition is based is that vulnerability to seizure activity in any one part of the network is influenced by activity everywhere else in the network, and that the network as a whole is responsible for the clinical and electrographic phenomenon that we associate with human seizures. She further distinguishes between the network and the "seizure onset zone". The seizure onset zone for neocortical seizures is defined by the ictal EEG. It is the area where the seizure discharge is first seen on ECoG (subdural electrodes). It may involve one to many electrode sites. In some patients, seizures (based on clinical manifestations) can start with EEG discharges beginning in different "onset zones" and spreading along different routes as the seizure progresses.

At least three human epilepsy networks have been reported based on the extensive observations on epilepsy patients (Spencer, 2002). The first one is the medial temporal/limbic network which includes the hippocampi, the amygdalae, the entorhinal cortices, lateral temporal neocortices, and extratemporal components of the medial thalamus and the inferior frontal lobes. The other two networks are less commonly identified, even in their component parts: the medial occipital/lateral temporal network and the superior parietal/medial frontal network. These lines of evidence based on clinical observations, intracranial EEG, functional neuroimaging, anatomic observations,

and the response of seizures to specific invasive treatments, support the existence and importance of the networks in the genesis of human epilepsy, and further suggest that the network structures are essential to the development of the seizure and thus the existence and maintenance of the epileptic disorder.

Although much of the evidence of epileptic network has been most consistent in MTLE, extratemporal epilepsy also is associated with multifocal, sometimes extensive, reductions in metabolism demonstrated on interictal PET studies, but this has not been as reproducible or as well documented as that in the medial temporal / limbic syndrome (Juhasz et al., 2000). Interestingly, despite high sensitivity to extratemporal regions of epileptogenicity, which show hypometabolism on interictal studies, PET scans are not sensitive to initial areas of seizure propagation in extratemporal epilepsy, another demonstration of the nonequivalence of network and propagation areas (Juhasz et al., 2000).

The existence of epileptic network can also be supported by the responses to the invasive therapy. If human epilepsy is the expression of specific, abnormally active, intrinsically defined and connected cortical/subcortical/bilateral networks, then one could theoretically alter seizure expression by intervening in any part of the specific network. Published reports document 60–90% excellent response, meaning cessation of seizures, after *any kind* or extent of temporal lobe resection in patients identified as having medial temporal lobe epilepsy. Operations involving anterior temporal lobe, medial structures only, lateral structures only, or more or less extensive lateral temporal resection can cure this disorder. Procedures with no anatomic overlap are similarly successful. This cannot be explained unless the multiple areas are all critical in the

production of the intractable seizures of this disorder. Then interruption of the network in any one of those areas would be (and apparently is) sufficient to alter the seizures. The similarly excellent response with cessation of seizures after temporal lobe resection in well-selected patients who have bilateral independent medial temporal lobe origin of seizures is another example of the existence of a network, interference with which at any site alters the expression of the intractable seizures (Hirsch et al., 1991a; 1991b).

Based on the above observations, it may be pertinent to consider study of other kinds of phenomena in individual patients, which may define the network in better terms than we have sought in the past because of our single-minded attention to defining regions of so-called seizure onset. For example, quantitative intracranial EEG analysis, background patterns, sleep effects on interictal and ictal activity, and other types of functional assessments may contribute considerably to our understanding of the role of networks in the expression of the epilepsies. Studying broad regions of brain structures related by the presence of such networks, using quantitative EEG analyses and sophisticated approaches, may detect alterations in the behavior of the network before the more traditional “seizure discharge” is seen, and allow prediction of seizures before manifestation clinically or on traditional EEG.

EEG Analysis on Networks in Epileptic Brains

Compared with scalp EEGs, intracranial EEGs or ECoGs generally have higher signal-to-noise ratio and/or signal-to-artifacts ratio and are of higher recording quality. Intracranial EEGs exhibit the most significant observations that support the network hypotheses (Spencer, 2002). Because the entire network participates in the expression of the seizure activity and can be entrained from any of its various parts, initial electrical events (at “seizure onset”) may vary in their specific location of expression and

occurrence within the network. The initial area of apparent seizure involvement is not really an onset area, because “onset” could be expressed any place in the network, and might even vary from seizure to seizure in a given patient. This locational variability may produce different morphologies of “seizure onset” when EEG recording is performed in only one part of the network (Spencer and Spencer, 1994). This may be the main reason why, with the surgery candidates and the resection brain region determined by the current focus localization techniques, the chance of a patient with neocortical epilepsy becoming seizure free after an invasive brain surgery is still less than 50%. A reliable quantitative method based on intracranial EEGs for determining the spatial distribution of the focal region(s) and their possible network may assist epileptologists to more accurately identify surgery candidates that will result in better surgery outcomes for patients with neocortical epilepsy.

Monto studied epileptic brain networks by quantifying the long-range temporal correlation (LRTC) in subdural human EEG recordings (Monto et al., 2007). Their observations on the spread of abnormally large LRTCs suggested that the epileptic focus is associated with significant changes in network behavior even in the cortical areas immediately surrounding the clinically determined focus. By applying synchronization and graph analysis to intracranial EEG recordings, Ponten investigated the hypothesis that functional neuronal networks during temporal lobe seizures change in configuration before and during seizures (Ponten et al. 2007). The study found that the functional brain networks change from a more random configuration during an interictal recording period to a more ordered configuration during seizures, especially during seizure spreading. The authors further suggested that the findings supported the

theory that a random network (during interictal periods) even had a stronger tendency to synchronize (Netoff et al., 2004), which could cause seizures. More recently, Zaveri calculated a magnitude squared coherence (MSC) on background intracranial EEG as a measure of functional connectivity to investigate the network effects within and outside the seizure onset area. The analysis demonstrated an inverse relationship between the connectivity strength and the distance from the seizure onset area (especially during the β frequency band) (Zaveri et al., 2009). Another similar work by Ortega et al. (2008) showed the presence of clusters of increased synchronization in different locations on the lateral temporal cortex in patients with temporal lobe epilepsy. Although remain unproven, it is possible that increased connectivity (as can be defined by coherence, synchronization clusters, or nonzero functional connectivity) helps initiate seizures. If increased brain connectivity or alteration in network topology helps initiate seizures, then network nodes and pathways could serve as targets for resective or disconnective surgery, implantable devices, and investigations of seizure anticipation.

To use EEGs to explore the role of the cortex (e.g. frontal cortex) in the epileptic brain network in a quantitative way is a more promising approach compared with traditional ways to identify areas of the cortex involved in an epilepsy network by looking for areas that demonstrate interictal spikes. It is generally accepted that the areas that show interictal spikes do not consistently correspond to the seizure onset zone. Nevertheless, it is very likely that areas with interictal spikes and the seizure onset zone are both within the same epileptic brain network. One important issue is to identify the most critical nodes or critical regions within the network that are responsible for the epileptogenic process.

CHAPTER 7
BRAIN STATE TRANSITION STUDY FOR SEIZURE DETECTION AND PREDICTION, USING MULTIPLE FEATURE EXTRACTION, PRINCIPAL COMPONENT ANALYSIS AND CLASSIFICATION

Purpose and Scope

In epileptic seizure prediction, a question needs to be answered: whether a consistent trend and quantitative measure can be discovered, from inter-ictal period to ictal period, based on the EEG recording from epileptic patients. Technically, it is an epileptic brain state transition study, which has the potential to be applied to real time epileptic seizure detection and seizure prediction.

Epileptic patients as subjects get involved for continuous EEG recording in several days. For each subject, several hours of inter-ictal recording, and at least three seizures of ictal recording and the corresponding pre-ictal recording (mostly start from one hour before the onset of seizure), will be included. The whole recording will be divided into few-seconds epochs for feature extraction, principal component analysis, and SVM learning and testing. A quantitative score will be applied to each epoch for classification, depending on (1) the type of applications (e.g. seizure prediction, seizure detection); and (2) specifications (e.g. seizure prediction horizon).

Procedure Design and Performance Evaluation Criteria

In order to serve as a real-time seizure detection and seizure prediction (warning) system or as a part of an epileptic brain state transition study, the experiment on the algorithm will need to demonstrate its capability of classifying the inter-ictal, pre-ictal, and ictal states of the epileptic brain and differentiating through continuous EEG recording. The usefulness of the algorithm is dependent on the quality of EEG recordings (signal-to-noise ratio, type and strength of artifacts) and the specification of

application. The task of investigating and demonstrating (if useful) this capability with patients of epilepsy will be undertaken in three steps:

- Step 1, Epileptic Brain State Transition Study Using Multiple Features Extraction on Different Lengths and Overlap of Data Epochs
- Step 2, Preprocess and Feature Space Dimensionality Reduction
- Step 3, Classification Algorithm Using Different Types of Support Vector Machines: Training (Learning), Testing and Performance Evaluation

Consistent separation of the inter-ictal, pre-ictal, and ictal states of the epileptic brain is the key of usefulness of this algorithm. For this reason, a considerable sized database (10-15 subjects) need be setup for testing the algorithm. The dataset in this study is mainly from BIH-MIT database of scalp EEG recordings, most of which are with 23 channels. The algorithm is patient-specific and need to be trained by a segment of continuous EEG recording including inter-ictal, pre-ictal, and ictal periods.

Some definitions are put as in the following:

- SENSITIVITY (SE). Percentage of events correctly identified by the algorithm in relation to the events actually marked by the subject.
- FALSE ALARM RATE (FAR). Frequency of events incorrectly detected by the algorithm per hour.
- POSITIVE PREDICTIVITY VALUE (PPV). The proportion of true positives on the total of true positives and false positives, which reflects the probability of a positive test.
- FEATURE EXTRACTION (FE). A special form of dimensionality reduction in classification and pattern recognition.
- PRINCIPAL COMPONENT ANALYSIS (PCA). A mathematical procedure that transforms a number of possibly correlated variables into a smaller number of uncorrelated variables.

Some criteria and design inputs are applied to evaluate the performance of the algorithm, such as SE, FAR and PPV, as in the following:

- Consistency of EEG recording: each subject needs to be in a consistent state (e.g. sleeping / awake) during inter-ictal, pre-ictal and ictal periods for each recording.
- Ambulatory Artifacts: EEG segments that include very strong artifacts (the amplitude is one order higher than the background EEG) need to be annotated in one or more channels.
- Prediction horizon: better between 3 min and 50 min
- Sensitivity (Se): milestone sets Se at >75%
- False Alarm Rate (FAR): milestone sets FAR better at < 1 / hour, also depending on the seizure occurrence frequency and the prediction horizon.

Subjects each include at least three seizures in EEG recording through inter- ictal, pre-ictal and ictal periods. For each subject, a randomly selected one third of seizures are included in the training dataset, and the other two thirds of seizures are included in the testing dataset. For each seizure, the pre-ictal period better starts from one hour before the onset or earlier. The sensitivity and positive predictive value also depend on the level of artifacts and the consistency of state (e.g. sleep / awake; sit / intensive movement) of the subjects being recorded.

There are a great number of types of epileptic seizures. Three major types of epileptic seizures need be included: Tonic chronic epileptic seizures, Absence epileptic seizures, and Simple or complex partial seizures.

The performance of the algorithm needs to be evaluated. Improvement can be made either by parameter tuning / optimization, or by introducing innovative / supplementary methodology. Further, the efficacy of the algorithm can be re-assessed after the tuning phase.

Brain State Classification of Different Epileptic Stages

Conjecture

The epileptic seizures occur after continuous and gradual brain state changes, which are generally difficult to be noted by the behavior of the patients, but can be recognized and identified by EEG recordings.

Methods

Scalp EEGs are recorded during daily life (in ambulatory environment) of epileptic patients. Seven measures (features) (1.STLmax, 2.PMRS, 3.FMX, 4.STM, 5.STX, 6.TEG, 7.STD) are calculated on the epoch samples in each of the EEG channels to evaluate brain state in different epileptic stages (inter-ictal, pre-ictal, and ictal) and help real time detect and/or predict epileptic seizures. For each of the seven measures (features), principal component analysis (PCA) is applied to extract the largest component from feature values of all the channels and to reduce the number of dimensions from the number of total recording channels to one (generally the largest component has more than 90% energy of all the eigenvalues). Then, using only the largest component of all the channels, principal component analysis (PCA) is applied a second time to extract the three largest components (as three indices) from the seven measures (features), so as to further reduce the number of dimensions from seven to three, and to visualize the results. Finally, kernel support vector machine (Kernel SVM) is applied to the three (or two) indices to design a non-linear classifier to separate / distinguish pre-ictal and inter-ictal periods so as to provide indications of different kinds of forthcoming epileptic seizures.

Results and Conclusion

The algorithm was preliminarily tested on epileptic patients. Each of them had three hours' inter-ictal recording, one hour's pre-ictal recording and recording in the ictal period, with the patient awake in both stages. 8% of the total recordings were randomly selected for SVM training and the remaining 92% recordings were used as testing samples in SVM classification. In one of the patients, we had very excellent results in the separation of pre-ictal and inter-ictal stages, whereas in the other two patients, we had good and acceptable results in the classification of different epileptic stages.

By twice applying PCA respectively on all the recording channels and on the seven measures (features) of the scalp EEGs, some effective quantitative indices can be found to help recognize and identify the gradual brain-status changes in different epileptic stages. Furthermore, those indices can be used to help design a classifier of pre-ictal and inter-ictal stages to support the accurate prediction of epileptic seizures.

In Figure 7-1 to Figure 7-6, the plot of the two largest PCA components and the three largest PCA components of Patient 48, 51, 52 are shown each from the interictal period to the ictal period, respectively. In Figure 7-7 to Figure 7-12, the plot of the classification effects based on kernel methods are shown, in which Figure 7-7 to Figure 7-9 use polynomial kernels, and Figure 7-10 to Figure 7-12 use quadratic kernels.

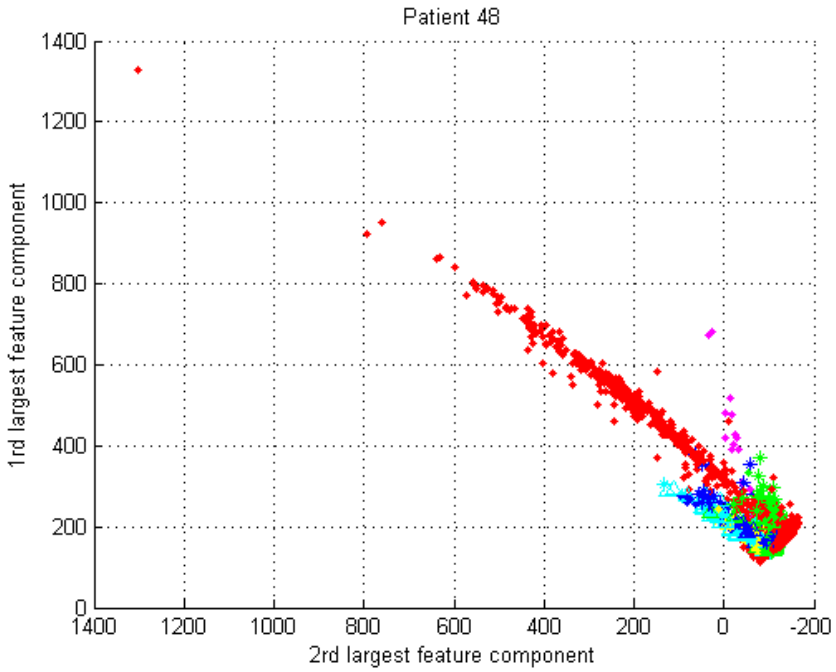

Figure 7-1. Plot of the two largest components of patient 48 from interictal to ictal period: Interictal in red color; preictal period are divided into consecutive 5min segments and are plotted in different colors and shapes.

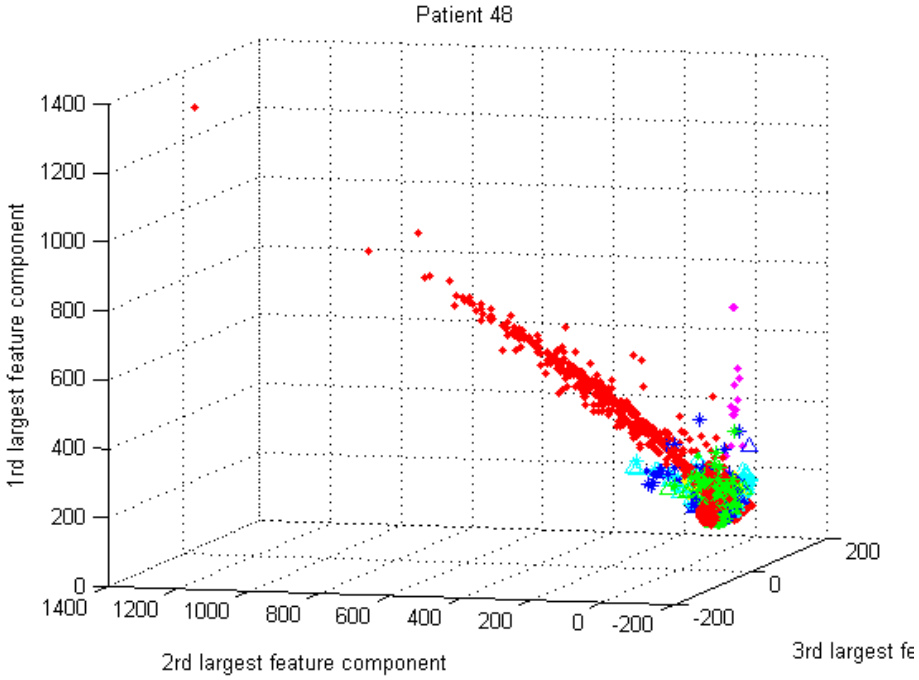

Figure 7-2. Plot of the three largest components of patient 48 from interictal to ictal period: Interictal in red color; preictal period are divided into consecutive 5min segments and are plotted in different colors and shapes.

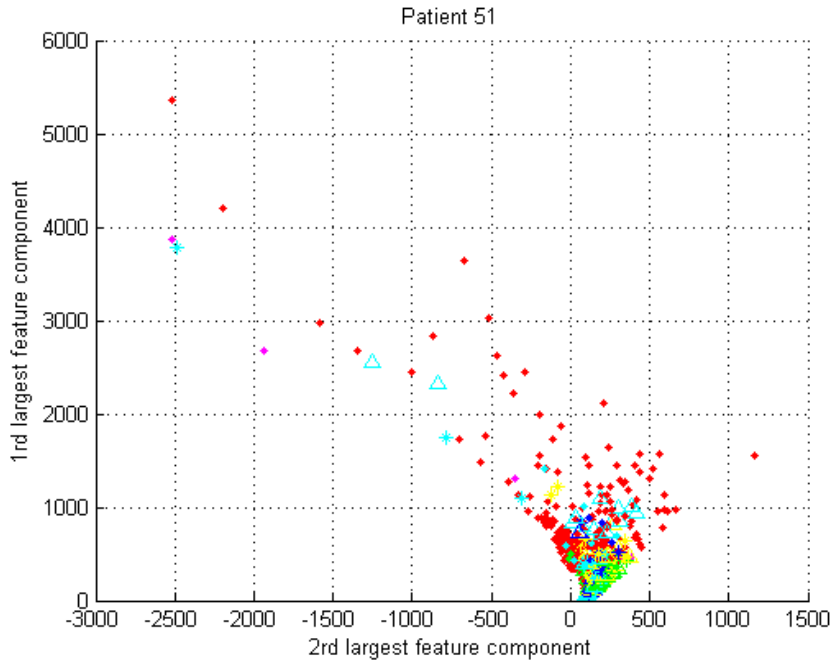

Figure 7-3. Plot of the two largest components of patient 51 from interictal to ictal period: Interictal in red color; preictal period are divided into consecutive 5min segments and are plotted in different colors and shapes.

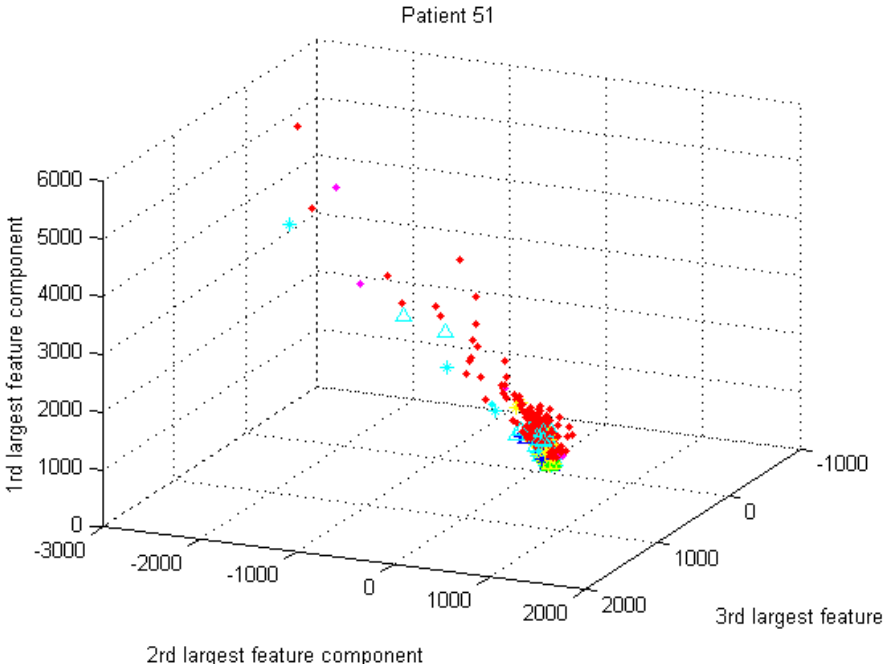

Figure 7-4. Plot of the three largest components of patient 51 from interictal to ictal period: Interictal in red color; preictal period are divided into consecutive 5min segments and are plotted in different colors and shapes.

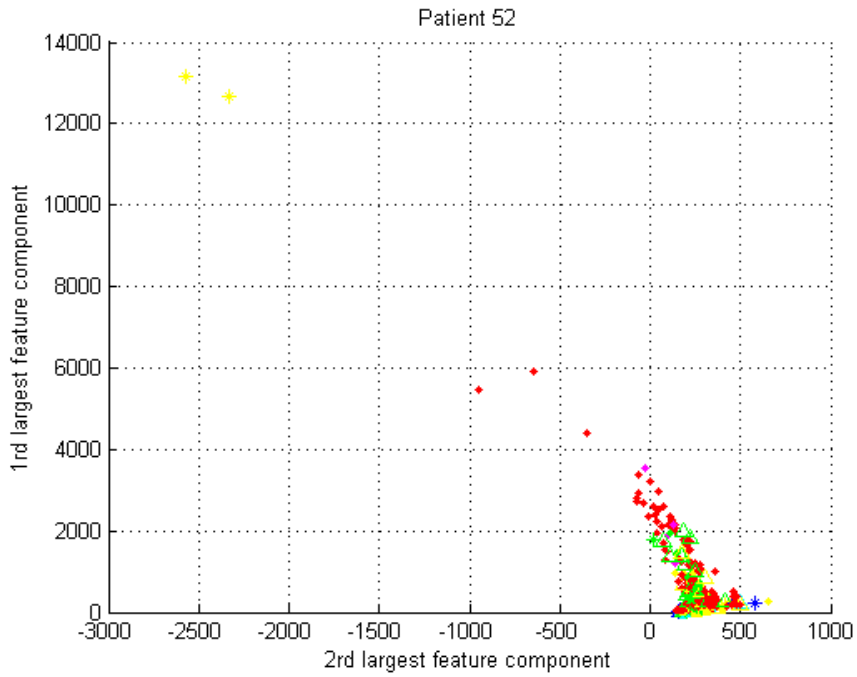

Figure 7-5. Plot of the two largest components of patient 52 from interictal to ictal period: Interictal in red color; preictal period are divided into consecutive 5min segments and are plotted in different colors and shapes.

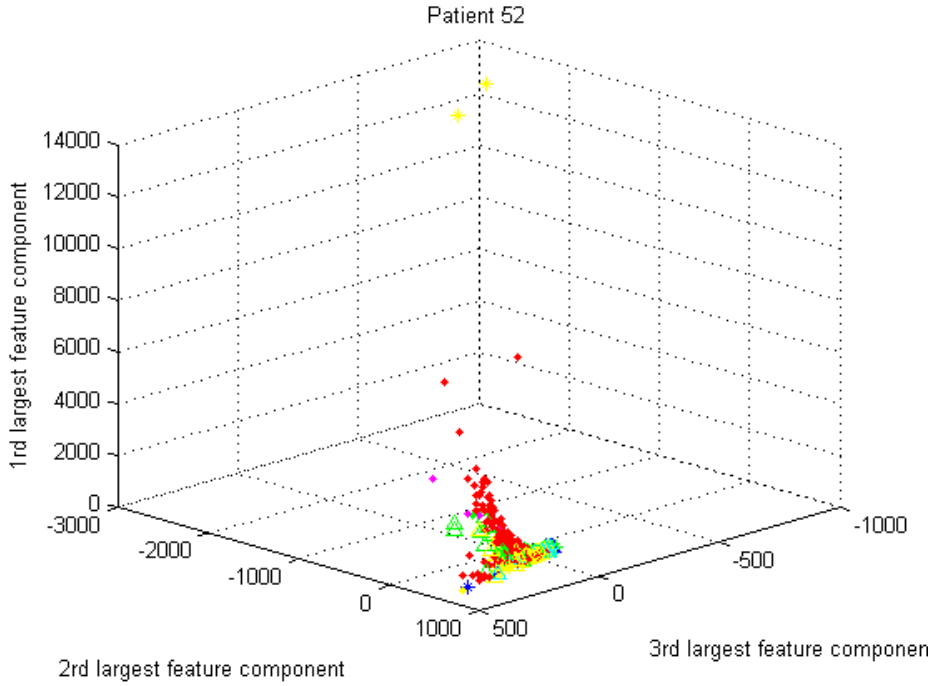

Figure 7-6. Plot of the three largest components of patient 52 from interictal to ictal period: Interictal in red color; preictal period are divided into consecutive 5min segments and are plotted in different colors and shapes.

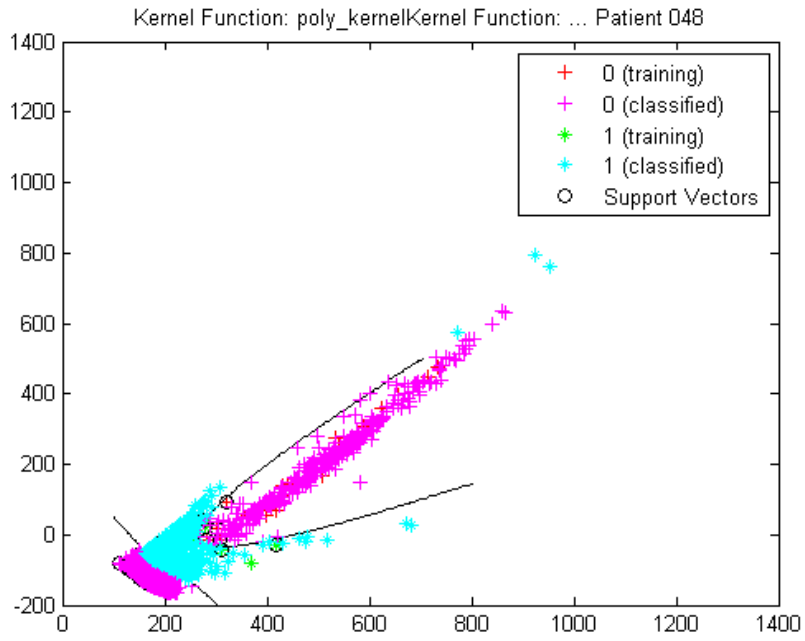

Figure 7-7. Plot of kernel classification effect between interictal period and preictal period, using polynomial kernel, of Patient 48: interictal in magenta color; preictal in cyan color.

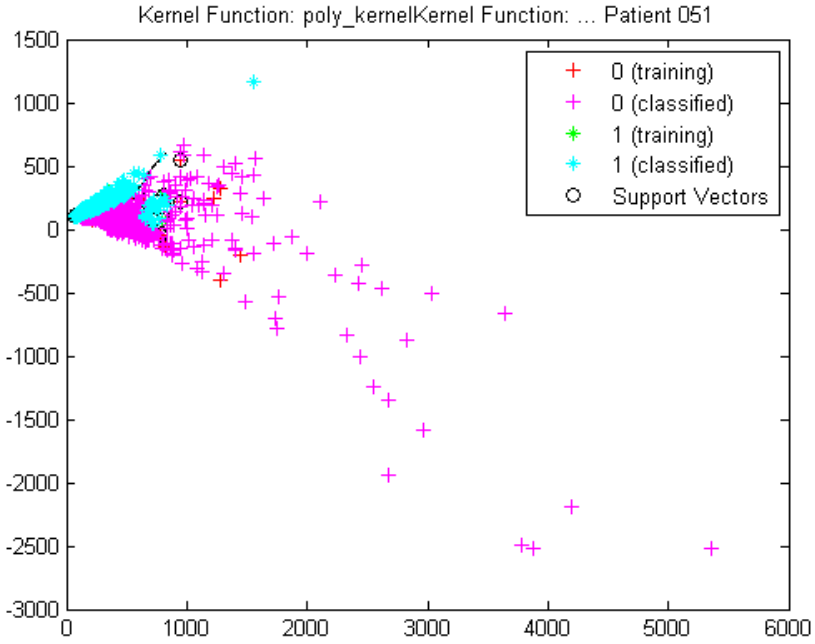

Figure 7-8. Plot of kernel classification effect between interictal period and preictal period, using polynomial kernel, of Patient 51: interictal in magenta color; preictal in cyan color.

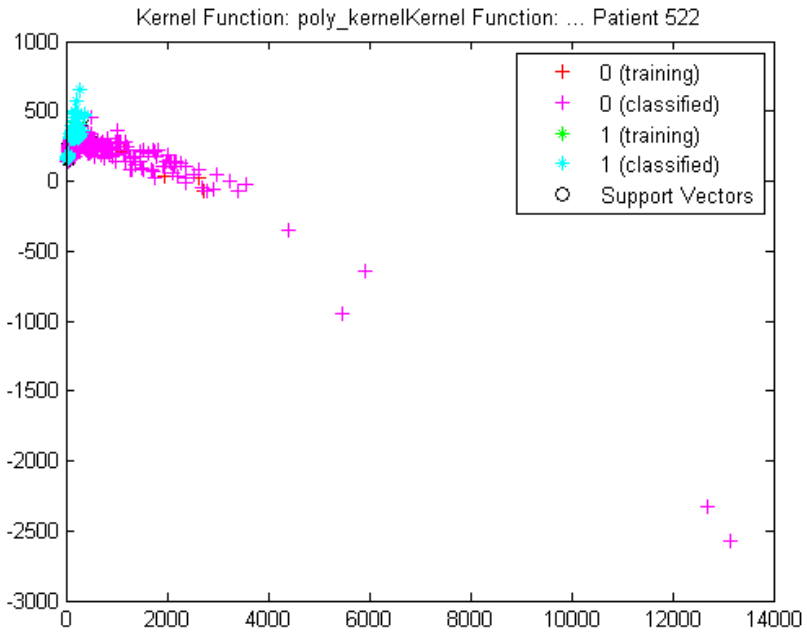

Figure 7-9. Plot of kernel classification effect between interictal period and preictal period, using polynomial kernel, of Patient 52: interictal in magenta color; preictal in cyan color.

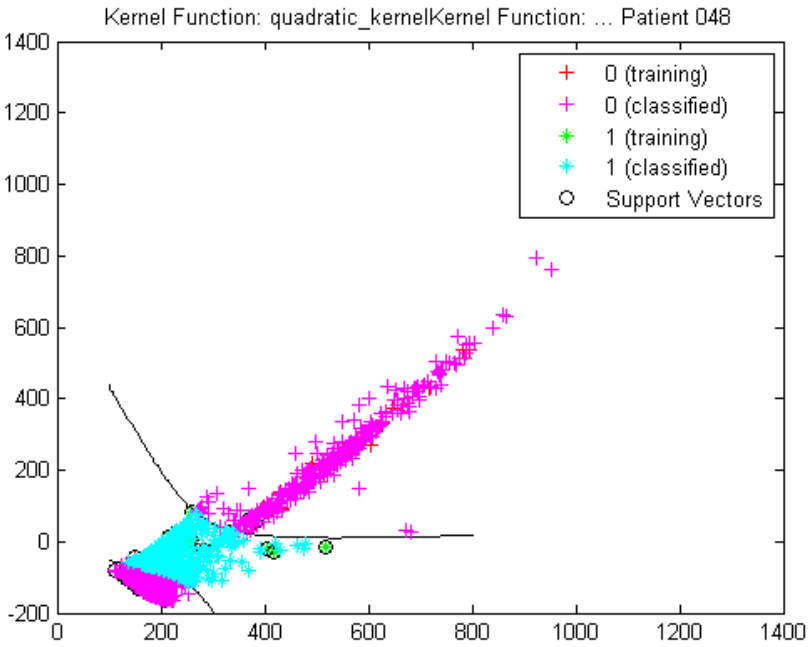

Figure 7-10. Plot of kernel classification effect between interictal period and preictal period, using quadratic kernel, of Patient 48: interictal in magenta color; preictal in cyan color.

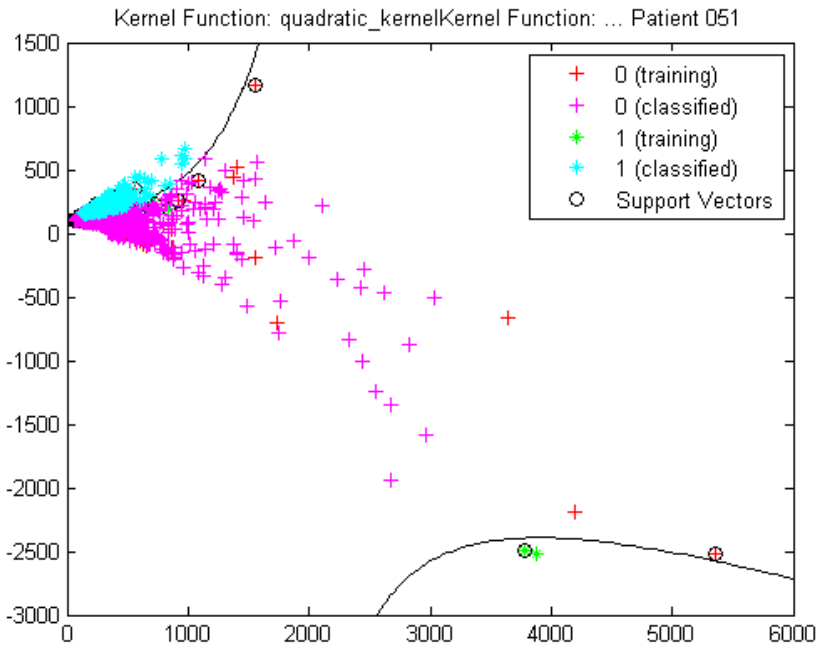

Figure 7-11. Plot of kernel classification effect between interictal period and preictal period, using quadratic kernel, of Patient 51: interictal in magenta color; preictal in cyan color.

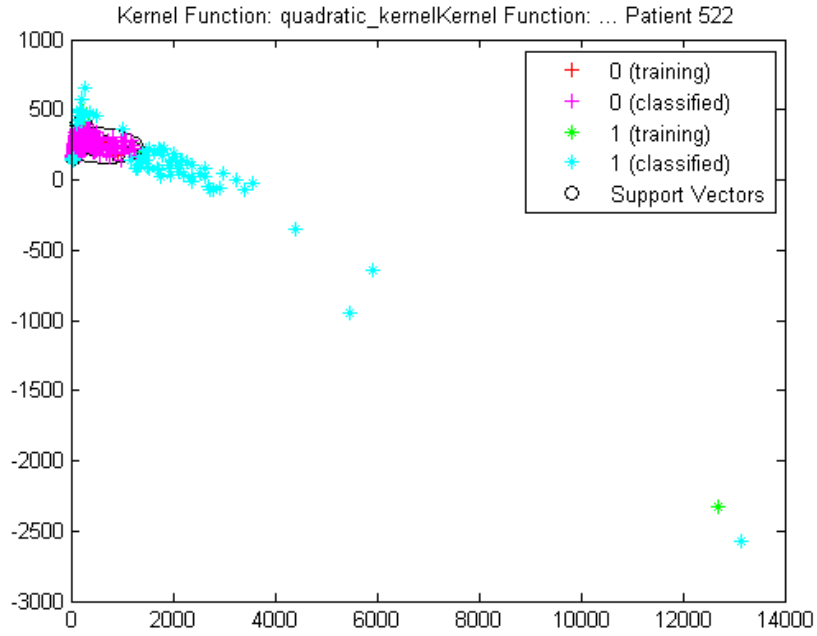

Figure 7-12. Plot of kernel classification effect between interictal period and preictal period, using quadratic kernel, of Patient 52: interictal in magenta color; preictal in cyan color.

Events Detection Using Sub-Bands Division, Multiple Feature Extraction, and Classification in High Dimensional Space on Ambulatory EEG

In an experimental protocol for supplemental materials for NIH fast track application entitled: seizure mitigation through continuous EEG with responsive Vagus nerve stimulation. Types of Events being detected are: (1) Eye Close; (2) Eye Flutter; and (3) Eat and Chewing.

Subjects being recorded are: (1) Subject 1 with 282 min EEG record for test; and (2) Subject 2 with 243 min EEG record for test. The electrode placement of EEG recording is: a subset of International 10-20 electrodes, Fp1, Fz, Pz, Fp2, C3, O1, F3, C4, O2, F4, Cz (Use P4 as reference). And the sample rate is: 240 Hz.

Event Type: Eye Close

Set threshold of classification score at 1.00.

For Subject 1, the Probability of Detection (PD) is 100% (detect 5 out of 5), and the False Alarm Rate (FAR) is 0 per hour. For Subject 2, the Probability of Detection (PD) is 100% (detect 5 out of 5), and the False Alarms Rate (FAR) is 0 per hour.

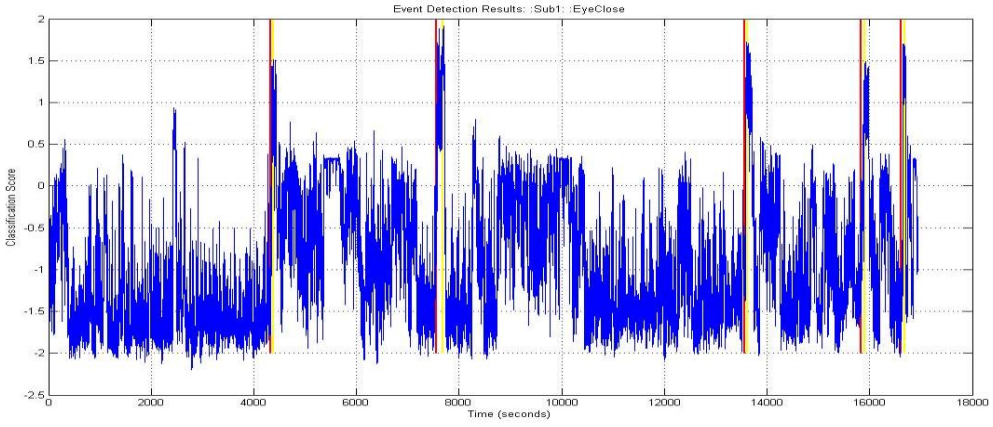

Figure 7-13. Eye Close Detection Results of Subject 1. (Blue: Classification Score of each 2-sec epoch (with 1-sec overlap); Red: reference annotation of onset of eye close; Yellow: reference annotation of offset of eye close)

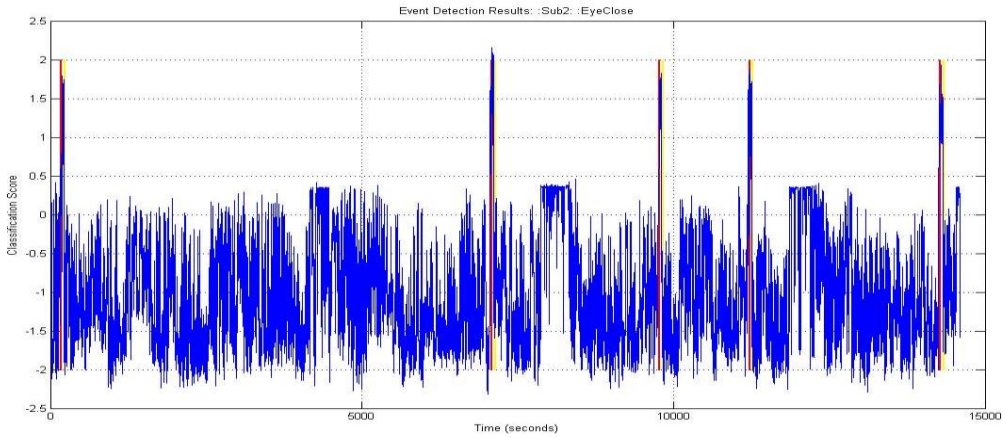

Figure 7-14. Eye Close Detection Results of Subject 2. (Blue: Classification Score of each 2-sec epoch (with 1-sec overlap); Red: reference annotation of onset of eye close; Yellow: reference annotation of offset of eye close)

Event Type: Eye Flutter

Set threshold of classification score at 1.25.

For Subject 1, the Probability of Detection (PD) is 75% (detect 3 out of 4), and the False Alarm Rate (FAR) is 0.638 per hour (detect 3 false positives in 282-min record for test). For Subject 2, the Probability of Detection (PD) is 100% (detect 4 out of 4), and the False Alarms Rate (FAR) is 0.741 per hour (detect 3 false positives in 243-min record for test).

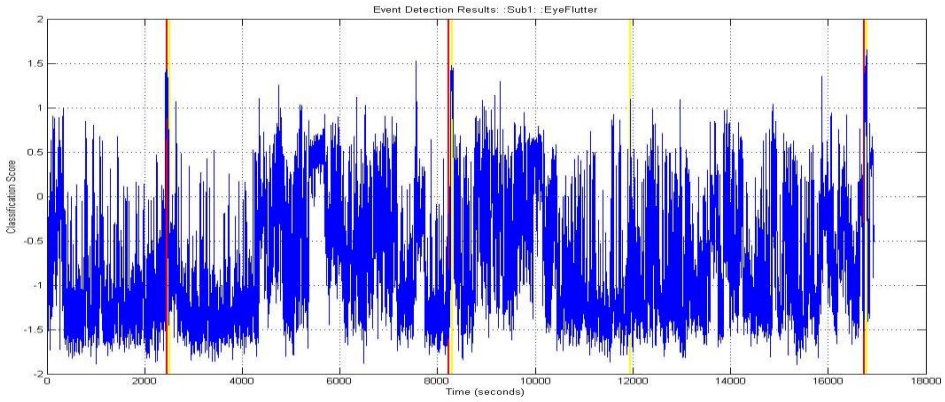

Figure 7-15. Eye Flutter Detection Results of Subject 1. (Blue: Classification Score of each 2-sec epoch (with 1-sec overlap); Red: reference annotation of onset of eye flutter; Yellow: reference annotation of offset of eye flutter)

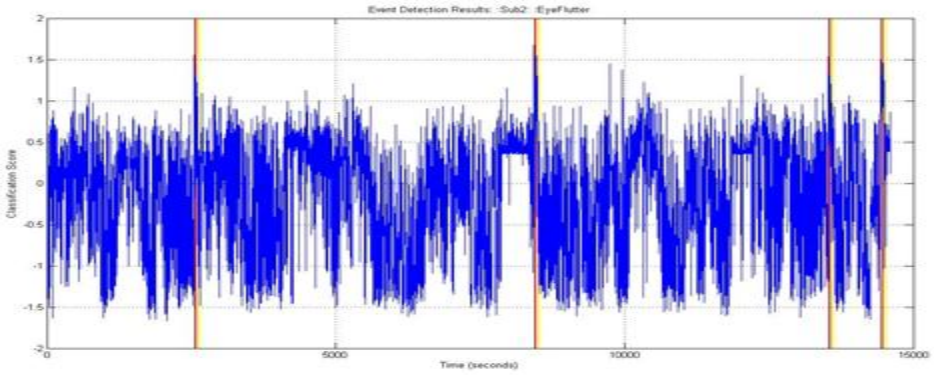

Figure 7-16. Eye Flutter Detection Results of Subject 2. (Blue: Classification Score of each 2-sec epoch (with 1-sec overlap); Red: reference annotation of onset of eye flutter; Yellow: reference annotation of offset of eye flutter)

Event Type: Eat & Chewing

Set threshold of classification score at 1.08.

For Subject 1, the Probability of Detection (PD) is 100% (detect 3 out of 3), and the False Alarm Rate (FAR) is 0.213 per hour (detect 1 false positive in 282-min record for test). For Subject 2, the Probability of Detection (PD) is 57.14% (detect 4 out of 7), and the False Alarm Rate (FAR) is 0.494 per hour (detect 2 false positives in 243-min record for test).

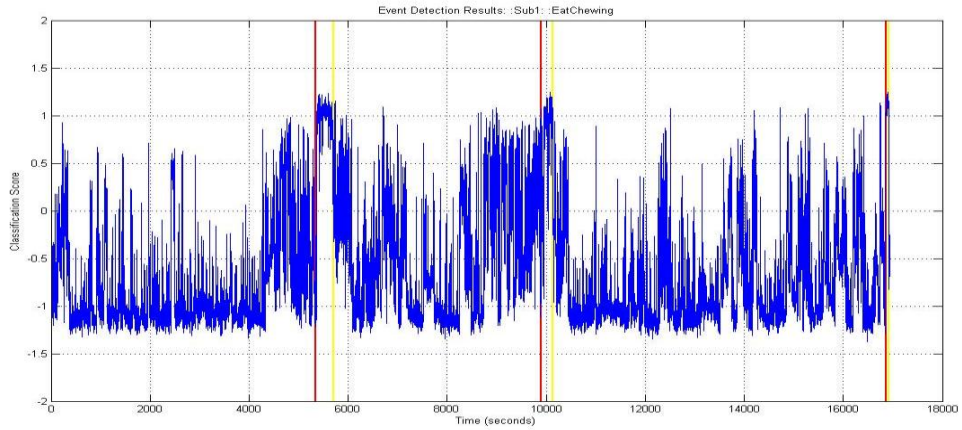

Figure 7-17. Eat & Chewing Detection Results of Subject 1. (Blue: Classification Score of each 2-sec epoch (with 1-sec overlap); Red: reference annotation of onset of eat & chewing; Yellow: reference annotation of offset of eat & chewing)

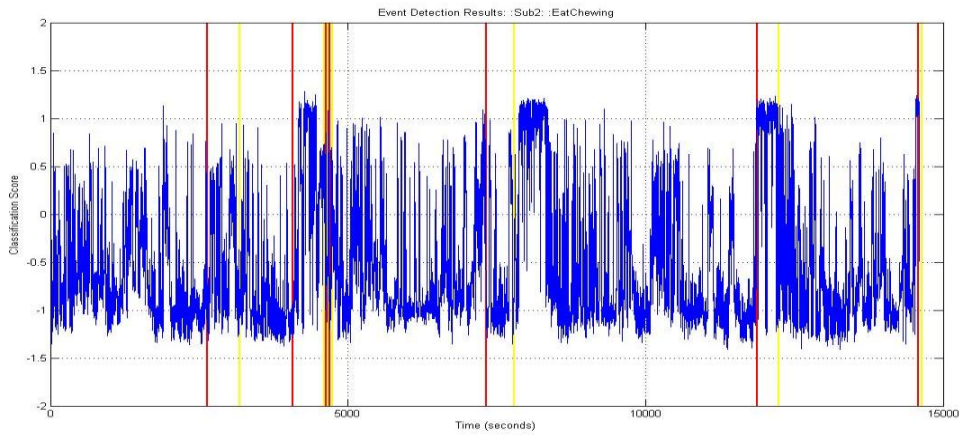

Figure 7-18. Eat & Chewing Detection Results of Subject 2. (Blue: Classification Score of each 2-sec epoch (with 1-sec overlap); Red: reference annotation of onset of eat & chewing; Yellow: reference annotation of offset of eat & chewing)

Patient-Specific Detection of Intractable Seizures Using Sub-Bands Division, Feature Extraction, and Classification in High-Dimensional Space on Scalp EEG Recorded from Pediatric Subjects

Database and Background

The CHB-MIT database, collected at the Children's Hospital Boston, consists of EEG recordings from pediatric subjects with intractable seizures. Subjects were monitored for up to several days following withdrawal of anti-seizure medication in order to characterize their seizures and assess their candidacy for surgical intervention. (Goldberger et al., 2000)

Recordings, grouped into 23 cases, were collected from 22 subjects (5 males, ages 3-22; and 17 females, ages 1.5-19). (Case chb21 was obtained 1.5 years after case chb01, from the same female subject.).

Each case contains between 9 and 42 continuous .edf (European Data Format) files from a single subject. In most cases, the .edf files contain exactly one hour of digitized EEG signals, although those belonging to case chb10 are two hours long, and

those belonging to cases chb04, chb06, chb07, chb09, and chb23 are four hours long; occasionally, files in which seizures are recorded are shorter.

All signals were sampled at 256 samples per second with 16-bit resolution. Most files contain 23 EEG signals (24 or 26 in a few cases). The International 10-20 system of EEG electrode positions and nomenclature was used for these recordings. In a few records, other signals are also recorded, such as an ECG signal in the last 36 files belonging to case chb04 and a vagal nerve stimulus (VNS) signal in the last 18 files belonging to case chb09. In all, these records include 198 seizures (182 in the original set of 23 cases).

Results of Case 1 as An Example

Take case 1 as an example. There are seven *.edf (European Data Format) file has one seizure. All the other 39 files are seizure free. Three randomly selected seizure events are included in the training dataset on this patient. Apply SVM supervised learning, and run the SVM to classify and detect seizures on the remaining part of recording, which includes all the other seizures.

As shown in Figure 7-19 to Figure 7-22, 100% sensitivity and 0 / hr false alarm rate, if set threshold of classification score at 0.5 for this patient. The patient-specific seizure detection results of other cases are also very good with high sensitivity approaching to 100% and very low false alarm rate. It indicates that, for the design of patient-specific automatic seizure detection algorithm, high performance is expectable, though a machine training session needs to be designed for real-world practical use (Shoeb, 2010).

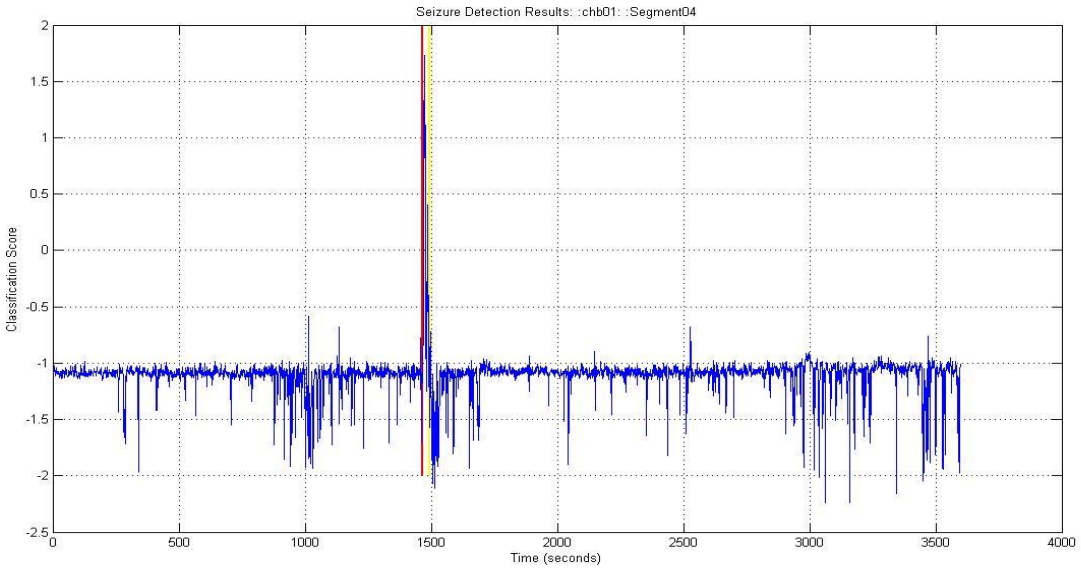

Figure 7-19. Detection Result of Intractable Epileptic Seizure in chb01_04.edf. (Blue: Classification Score of each 2-sec epoch (with 1-sec overlap); Red: reference annotation of seizure onset; Yellow: reference annotation of seizure offset)

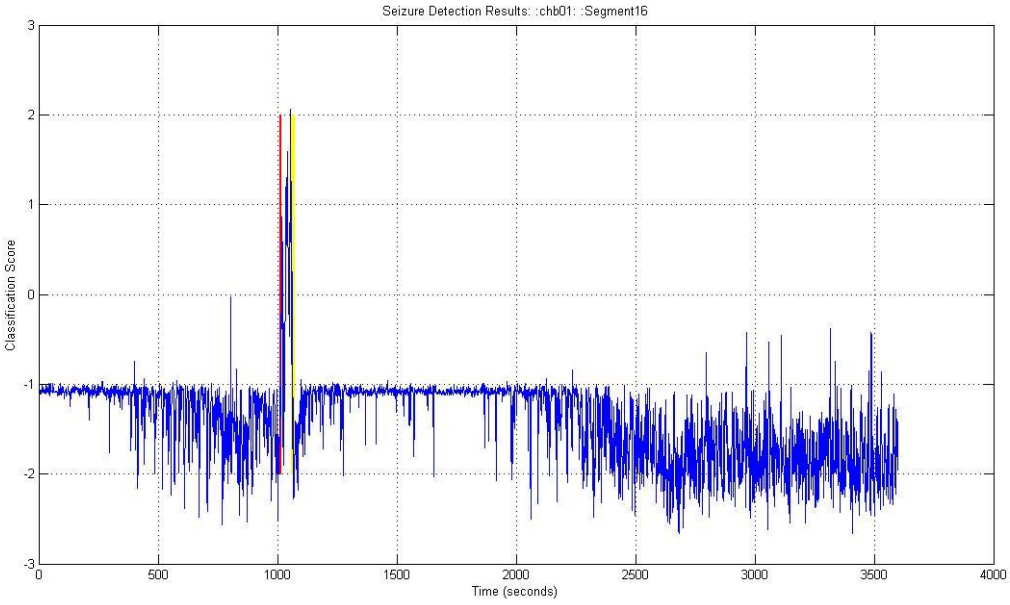

Figure 7-20. Detection Result of Intractable Epileptic Seizure in chb01_16.edf. (Blue: Classification Score of each 2-sec epoch (with 1-sec overlap); Red: reference annotation of seizure onset; Yellow: reference annotation of seizure offset)

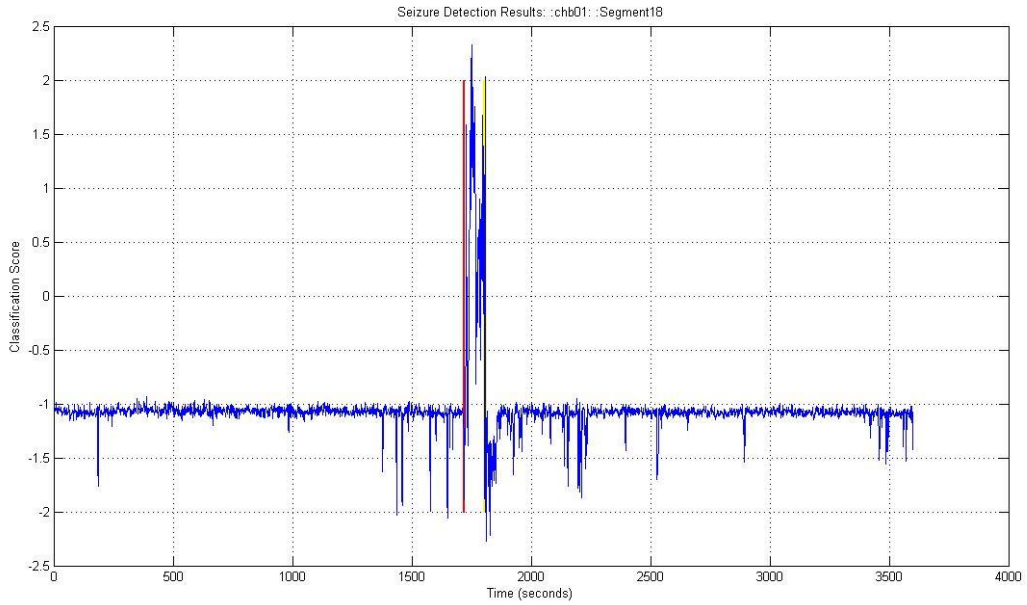

Figure 7-21. Detection Result of Intractable Epileptic Seizure in chb01_18.edf. (Blue: Classification Score of each 2-sec epoch (with 1-sec overlap); Red: reference annotation of seizure onset; Yellow: reference annotation of seizure offset)

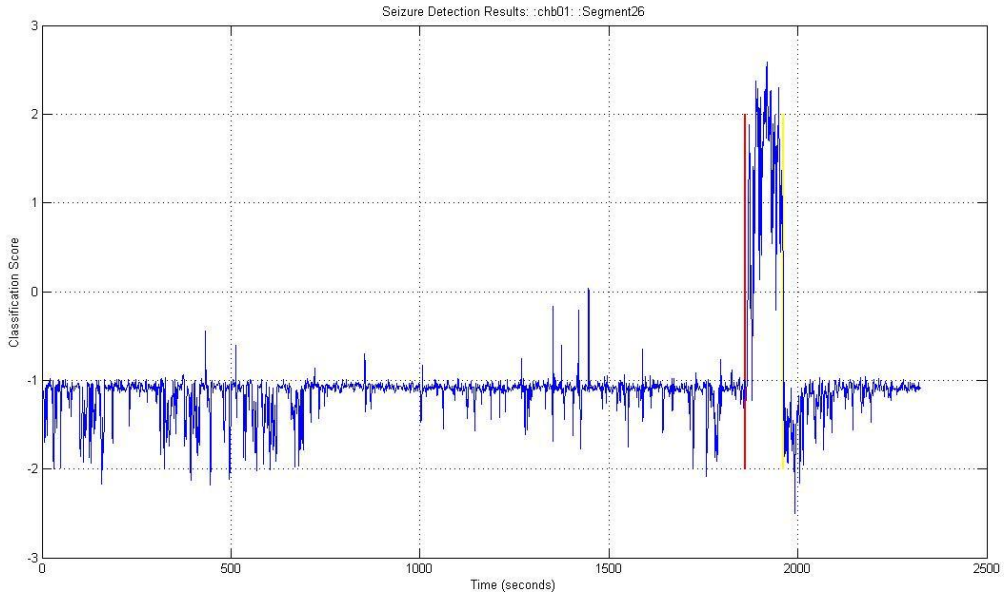

Figure 7-22. Detection Result of Intractable Epileptic Seizure in chb01_26.edf. (Blue: Classification Score of each 2-sec epoch (with 1-sec overlap); Red: reference annotation of seizure onset; Yellow: reference annotation of seizure offset)

CHAPTER 8
R-WAVE/BEAT DETECTION FROM SURFACE ECG WITH MUSCLE ARTIFACTS FOR CARDIAC-BASED SEIZURE DETECTION

Background and Purposes

For some types of partial epileptic seizures, such as temporal lobe epilepsy, the phenomenon of an accompaniment of ictal tachycardia exists in a high percentage of seizure events, partly because the epileptic discharges may influence portions of the central automatic network during the seizure occurrence. Thus the cardiac alterations at the transition from the preictal state to the ictal state can be used to assist the automatic seizure detection, by identifying the changes in heart rate and cardiac arrhythmias. Since the long term ambulatory ECG monitoring is technically feasible and common compared with the long term ambulatory EEG, it would be beneficial if a reliable R-wave (heart beat) detection algorithm can be developed to monitor the heart rate and cardiac arrhythmias accurately for further partial epileptic seizure detection.

In the real application in the neuromodulation industry, an accurate instantaneous heart rate may need to be detected based on ECG for ambulatory use. Furthermore, the ECG electrode placement may be on surface of the skin and may not use the typically used lead-2 which has a very favorable signal-to-noise ratio. As is known, the heart beat detection algorithm using lead-2 ECG has been well developed in the last few decades. However, in applications where the recording electrode placement is not using the lead-2 and is on surface of the skin, the design of a reliable R-wave (heart beat) detection algorithm is much more challenging.

A major challenge is that, the skeletal muscle artifacts are so strong sometimes (e.g. in body movements, exercises, or falls) that its amplitude could be one order higher than the desired ECG signal. Furthermore, the muscle artifacts generally are not

separable from ECG signal in frequency domain or other commonly used transform domains.

Another challenge is that: when a surface ECG recording system is not using lead-2 electrode placement, instead using a patch on the chest for example, the recorded ECG signal from heart would be much weaker than that of using lead-2. Hence, the signal-to-noise ratio is low, even without very strong muscle artifacts.

One of the projects I have been enrolled in a neuromodulation company is designing a product aiming to log seizure events automatically detected by an algorithm built in the product. The seizure detection algorithm therein is based on the changes of heart rate and heart rate variability, both necessitates heart beat detection from acquired ECG with adequate accuracy.

A new beat detection algorithm is designed, developed and implemented to overcome those challenges and has been verified and tested that it has satisfactory results. Compared with some open-source algorithms and another beat detection algorithm (referred to as IMEC) designed and developed in a large group in Belgium, Europe, the proposed beat detection algorithm is superior on standard testing performance and is more robust in extreme cases. The new algorithm meets the performance requirements defined by various standards established by ANSI/AAMI.

I am the major contributor (more than 80% of ideas and work) to the design and development of the proposed algorithm.

Design Features of the Proposed Beat Detection Algorithm

The proposed beat detection algorithm has taken the role of the originally used IMEC algorithm for ECG based beat detection and heart rate monitoring. It is an improved and successful algorithm of R-wave detection under strong noises, including

muscle artifacts, impedance noise, power line noise, and baseline wandering noise. It has many features embedded in the architecture of design and in different modules. Those features have helped improve the performance of the algorithm, such as detection accuracy, sensitivity, false positive rate and positive predictivity value (PPV). Some of the features are described selectively in this section.

The flow chart of the algorithm is shown as in Figure 8-1. Multiple features are extracted from the filtered and preprocessed ECG input, such as the shape and waveform of R-wave, the morphology of QRS complex, the first and second order differential values, the innovative sharpness feature, etc. Among those, features are extracted from the time domain, the frequency domain, and other transformed domains. All the features interact with each other, and are infused for a decision which would generate a pool of heart beat candidates in a given time window. Meanwhile, an individualized likelihood score is generated for each of the heart beat candidates.

In a given time window, the heart beat candidates are then put together for further screening and selection in order to output the true heart beats.

In the selection process, individualized neighborhood widths are partly determined by the likelihood score of each heart beat candidate, as in Figure 8-2.

In addition, the individualized neighborhood widths in a given time window are multiplied by a scaling factor based on previous heart rate statistics, as in Figure 8-3.

For each heart beat candidate, the likelihood score is a measure of the likelihood that it is a true heart beat; meanwhile, the likelihood score is inversely related with the value of the individualized neighborhood width.

The previous heart rate statistics can influence the selection of true heart beats from heart beat candidates pool, dynamically. Generally, the higher the previous heart rate, the better chance the heart beat candidates in the current time window are to be selected. The method of calculating the previous heart rate from previous heart beat data needs to be designed according to the actual application in real world, though not unique. Figure 8-4 is an example.

In feature extraction process, new features are explored and designed for reducing the false positive rate of the beat detector. An example is the sharpness feature, which can assist distinguishing some types of false heart beats from the true heart beats, as in Figure 8-5.

Performance and Standard Testing Results of the Proposed Algorithm

The Testing is designed to characterize the performance of the new and the proposed beat detection algorithm in processing not only Human ECGs from MIT-BIH Databases of Arrhythmia with or without stressed noise, which are widely used as testing ECGs, but also the simulated ECG with major ECG features, such as heart rate, R-wave amplitude, QRS duration, and T-wave amplitude, vary within their normal dynamic ranges.

Since ECG recordings with limited period of time and from limited number of patients can not cover the broad dynamic ranges of major ECG parameters, such as heart rate, R-wave amplitude, QRS duration, and T-wave amplitude, FDA requires that a beat detection algorithm be tested not only with human ECGs but also with simulated ECG with various ECG parameters.

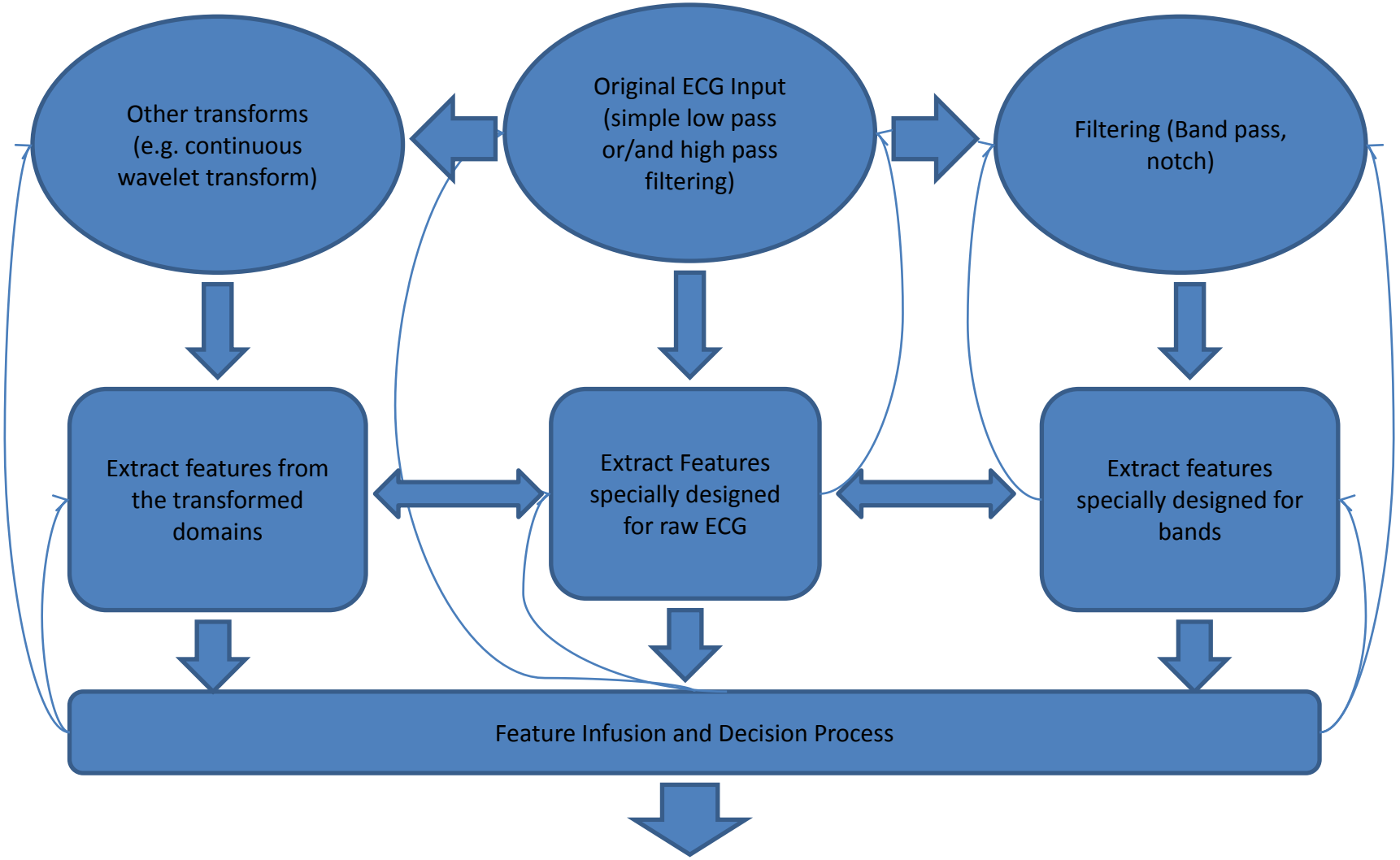

Figure 8-1. Flow chart of multiple features extraction in time domain, frequency domain and other transformed domains and feature infusion

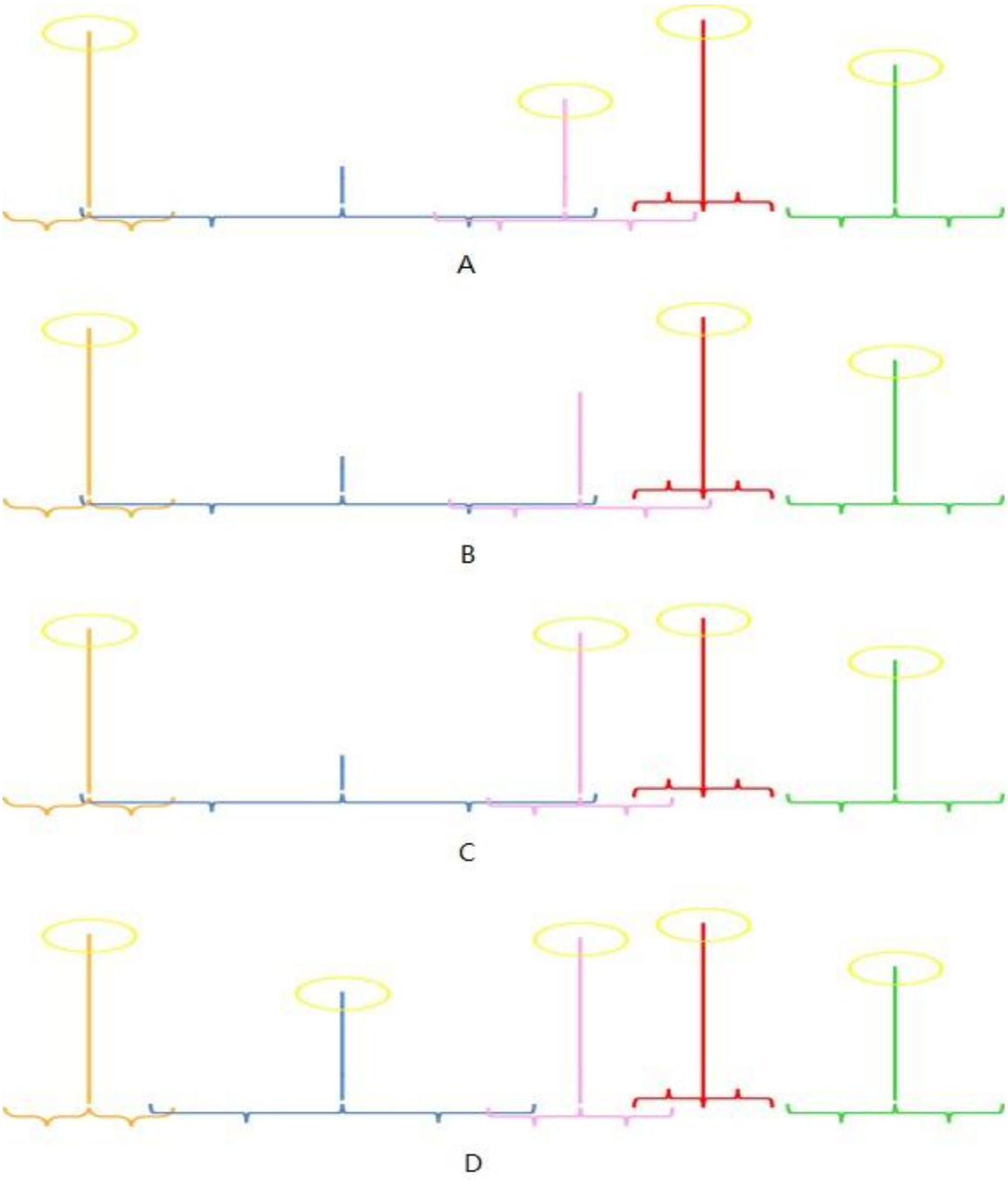

Figure 8-2. Plot of the selection process that individualized neighborhood widths are partly determined by the likelihood score of each candidate heartbeat, in a given time window. A), B), C), D) are four cases. In each case, five heart beat candidates are competing with each other on axis of time within a given time window. Different colors represent different candidates. Each candidate has a likelihood score (the height) and a corresponding individualized neighborhood width (the width). For a candidate, the width of the neighborhood is inversely related to likelihood score. If a candidate has the highest likelihood score within its own neighborhood, then it can be selected (with a yellow ring).

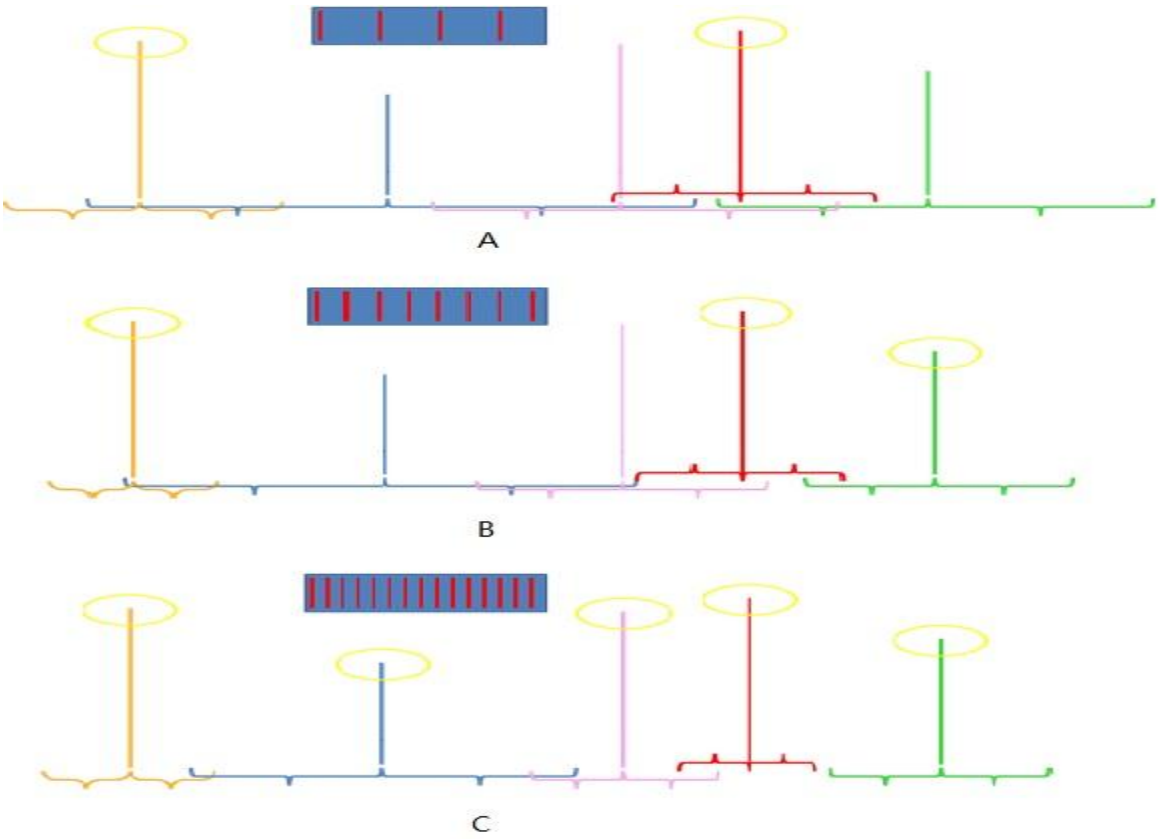

Figure 8-3. Plot of dynamical scaling of the neighborhood widths according to previous heart rate statistics, in a given time window. A), B), C) are three cases with five heart beat candidates competing on the axis of time. Each candidate has a likelihood score (the height) and an individualized neighborhood width (the width). The neighborhood width is partly determined by the likelihood score, and is later on multiplied by a positive scalar from the previous heart rate data. The value of the scalar is the same for all candidates in a given time window, and is inversely related to the previous heart rate. If a candidate has the highest likelihood score within its own neighborhood, then it can be selected.

Some documents applicable to the design, development and testing of the proposed algorithm are as in the following:

- ANSI/AAMI EC13, 2002, Cardiac Monitors, Heart Rate.
- ANSI/AAMI EC38, 2007, Ambulatory electrocardiographs.
- ANSI/AAMI EC57, 1998, Testing and reporting performance results of cardiac rhythm and ST-segment measurement algorithms.
- EN 60601-2-25, 1996, Medical electrical equipment. Particular requirements for safety. Specification for electrocardiographs.

- EN 60601-2-27, 1995, Medical electrical equipment. Particular requirements for safety. Specification for electrocardiographic monitoring equipment.

- EN 60601-2-49, 2001, Medical Electrical Equipment - Part 2-49: Particular Requirements for the Safety of Multifunction Patient Monitoring Equipment.

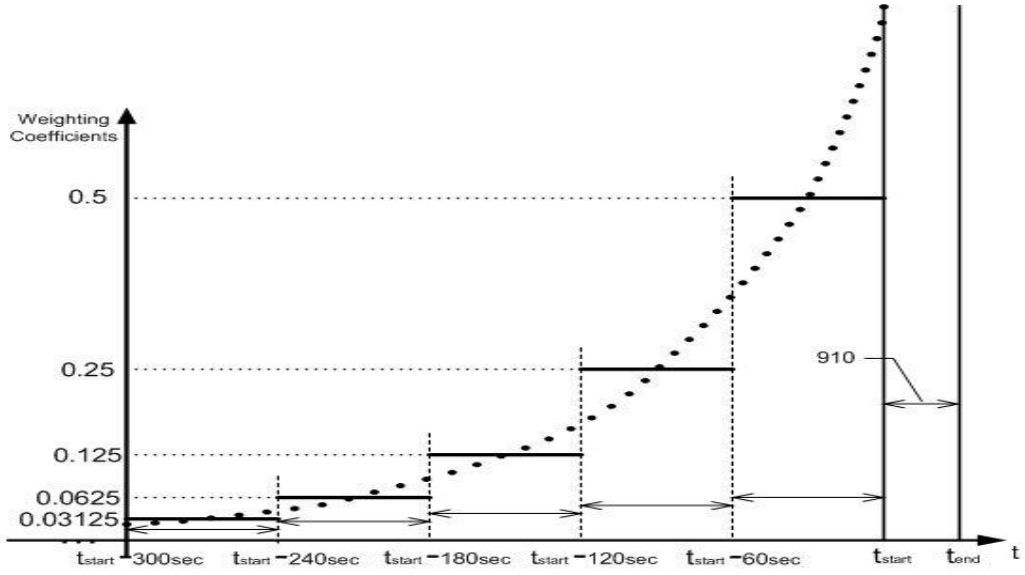

Figure 8-4. Plot of calculating previous heart rate statistics using exponentially decreasing weighting (an example), for a given time window.

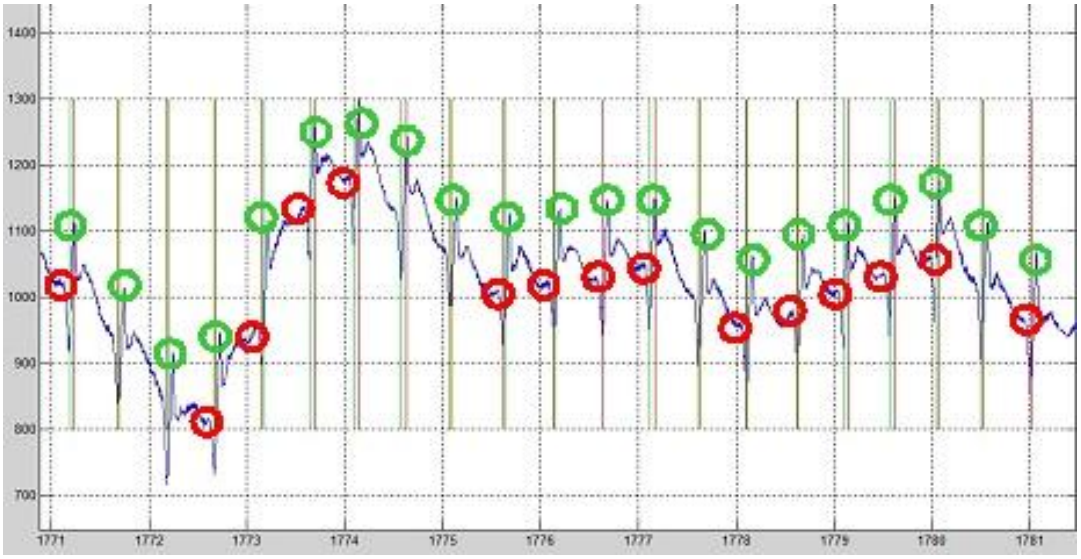

Figure 8-5. Plot of a new feature built into the proposed beat detection algorithm that can help distinguish the true heart beats from a class of false ones. Cyan-colored circles are true heart beats, according to reference annotations; while the red colored circles are false heart beats that are ruled out by the sharpness feature design in the algorithm.

Test: Beat Detection Accuracy with Human ECG

According to EC57 3.1.1 General description of available databases, the MIT-BIH Arrhythmia ECG database with beat annotation is used to test the accuracy of beat detector. Performance of beat detector with match window of 5-, 10-, 20-, 50-, 100-, 150-millisecond were calculated. The results of the test were presented in Table 8-1.

Table 8-1. Results of the proposed beat detection accuracy with human ECG from MIT-BIH Arrhythmia Database

Test Condition	Total Beats	Total True Positive	Total False Negative	Total False Positive	Sensitivity (%)	Positive Predictivity (%)
As for Fiducial Point	109494	13057	96437	96110	11.92	11.96
As for Fiducial Point ± 5 ms		94657	14837	14510	86.45	86.71
As for Fiducial Point ± 10 ms		104176	5318	4991	95.14	95.43
As for Fiducial Point ± 20 ms		106378	3116	2789	97.15	97.45
As for Fiducial Point ± 30 ms		107601	1893	1566	98.27	98.57
As for Fiducial Point ± 50 ms		108498	996	669	99.09	99.39
As for Fiducial Point ± 150 ms		109040	454	127	99.59	99.88

Considering the inaccuracy of the reference annotations (the majority is within two samples from the R-wave or ±5.6 ms) of MIT-BIH arrhythmia database, 20-ms match window is selected. The testing results showed that the proposed beat detection algorithm has adequate performance in detecting the beat of the ECG database, with sensitivity of 97.15% and positive predictivity of 97.45% with 20-ms match window. It has significant improvement in beat detection accuracy compared to IMEC algorithm. In an application where the displayed heart rate is the average heart rate of the most recent beats (but not real instantaneous heart rate), the proposed beat detection algorithm can work very well in most cases. In the application, where heart rate

variability (HRV) may need be used, it is better to have both the sensitivity and positive predictivity above 98% with 20-ms match window on MIT-BIH arrhythmia database.

Test : Beat Detection Accuracy with Noise Stressed Human ECG

According to EC57 3.1.1 General description of available databases, the MIT-BIH noise stressed Arrhythmia ECG data set with beat annotation is used to test the accuracy of the beat detection. Performance of beat detection by comparing the detection with annotated fiducial points of 20-millisecond as match window is calculated.

Table 8-2. Results of the proposed beat detection algorithm (20-ms match window)

Recording	Total	TP	FN	FP	Sensitivity (%)	PPV value (%)
118e24	2278	2276	2	2	99.91	99.91
118e18		2273	5	10	99.78	99.56
118e12		2255	23	119	98.99	94.99
118e06		2100	178	501	92.19	80.74
118e00		1745	533	927	76.60	65.31
118e_6		1490	788	1127	65.41	56.94
119e24	1987	1958	29	23	98.54	98.84
119e18		1952	35	31	98.24	98.44
119e12		1933	54	124	97.28	93.97
119e06		1881	106	413	94.67	82.00
119e00		1629	358	867	81.98	65.26
119e_6		1336	651	1120	67.24	54.40
Total	Beats:	25590				
Total	TP:	22828				
Total	FN:	2762				
Total	FP:	5264				
	TOTAL	Sensitivity (%)	PPV value (%)			
Average	25590	89.24	82.52			
Gross	25590	89.21	81.26			

The testing results showed that the proposed beat detection algorithm has significant improvement in beat detection performance in noise stressed ECG data set, compared to IMEC algorithm. In the application, the artifacts (including noises) may be stronger and SNR may be lower than -6 db.

Table 8-3. Results of the proposed beat detection algorithm (5-ms match window)

Recording	Total	TP	FN	FP	Sensitivity (%)	PPV value (%)
118e24	2278	838	1440	1440	36.79	36.79
118e18		836	1442	1447	36.70	36.62
118e12		833	1445	1541	36.57	35.09
118e06		785	1493	1816	34.46	30.18
118e00		652	1626	2020	28.62	24.40
118e_6		561	1717	2056	24.63	21.44
119e24	1987	1778	209	203	89.48	89.75
119e18		1775	212	208	89.33	89.51
119e12		1768	219	289	88.98	85.95
119e06		1709	278	585	86.01	74.50
119e00		1461	526	1035	73.53	58.53
119e_6		1169	818	1278	58.83	47.60

Total	Beats:	25590
Total	TP:	14165
Total	FN:	11425
Total	FP:	13927

	TOTAL	Sensitivity (%)	PPV value (%)
Average	25590	56.99	52.53
Gross	25590	55.35	50.42

Table 8-4. Results of IMEC beat detection algorithm (5-ms match window)

Recording	Total	TP	FN	FP	Sensitivity (%)	PPV value (%)
118e24	2278	113	2165	2762	4.96	3.93
118e18		124	2154	2635	5.44	4.49
118e12		123	2155	2400	5.4	4.88
118e06		117	2161	2193	5.14	5.06
118e00		118	2160	2159	5.18	5.18
118e_6		103	2175	2717	4.52	3.65
119e24	1987	779	1208	1880	39.2	29.3
119e18		888	1099	1552	44.69	36.39
119e12		889	1098	1270	44.74	41.18
119e06		867	1120	1131	43.63	43.39
119e00		867	1120	1119	43.63	43.66
119e_6		644	1343	2011	32.41	24.26

Total	Beats:	25590
Total	TP:	5632
Total	FN:	19958
Total	FP:	23829

	TOTAL	Sensitivity (%)	PPV value (%)
Average	25590	23.25	20.45
Gross	25590	22.01	19.12

Furthermore, in the application, the QRS complex in ECG recording may have biphasic morphology, instead of the QRS morphology of normal ECGs. Therefore, for the proposed algorithm, the performance in detecting heart beats from the noise stressed ECG recordings need be further improved. The noise-stressed testing results of the proposed beat detection algorithm on the two ECG recordings (#118, #119) are ACCEPTABLE basically.

Test: Beat Detection on Range and Accuracy of Heart Rate with Simulated ECG

According to EC13 Section 4.2.7 Range and accuracy of heart rate meter, “The minimum allowable heart rate meter range shall be 30 to 200 BPM, with an allowable readout error of no greater than ± 10 percent of the input rate or ± 5 BPM, whichever is greater. Cardiac monitors labeled for use with neonatal/pediatric patients shall have an extended heart rate range of at least 250 BPM. In addition, input ECG signals at rates less than the disclosed lower limit of the rate meter range shall not cause the meter to indicate a rate greater than this lower limit. Input signals at rates above the disclosed upper limit of the rate meter range, up to 300 BPM (350 BPM for monitors labeled for use with neonatal/pediatric patients), shall not cause the meter to indicate a rate lower than this upper limit.

To test the performance of the beat detection algorithm, a simulated AAMI NSR signal of 1-millivolt (mV) as the amplitude of R-wave and 25% of the R-wave’s amplitude as the amplitude of T-wave is used to test the range and accuracy of heart rate. For the rate of the simulated signal from 30BPM to 180BPM, the simulated signal is of 100-millisecond (ms) as QRS duration, 180ms as the T-wave duration (d_T), and 350ms as the QT interval (d_{QT}); for the rate from 200BPM to 300BPM, the corresponding parameters are 40ms, 60ms and 150ms, respectively. QRS amplitude is

defined as $a_r + a_{s,}$ as described in EC13. The sample rate of the simulated ECG is 250 Hz.

The testing results showed that the proposed algorithm can detect heart rate correctly when the heart rate ranges at 30, 40, 50, 60, 80, 120, 160, 200, 240, 260, 280, 290 and 300 BPM of the simulated ECG. The error of detected heart rate by the proposed is very small (<0.1%). The proposed algorithm passed the test.

On the other hand, except when the heart rate of simulated ECG ranges at 50, 60, 80, 100, 120, 160 and 200 BPM, the IMEC beat detection algorithm exhibits much bigger errors than the application allows in both ends of low and high heart rates. The IMEC algorithm failed the test.

Table 8-5. Results of the test of the proposed beat detection algorithm on range and accuracy of heart rate with simulated ECG

Simulated Rate (BPM)	30	40	50	60	80	120	160	200	240	260	280	290	300
Measured Rate (BPM)	30	40	50	60	80	120	160	200	240	260	280	290	300
Error (Simulated – Measured) (BPM)	0	0	0	0	0	0	0	0	0	0	0	0	0

Table 8-6. Results of the test of IMEC beat detection algorithm on range and accuracy of heart rate with simulated ECG

Simulated Rate (BPM)	30	40	50	60	80	120	160	200	240	260	280	290	300
Measured Rate (BPM)	69	51	50	60	80	120	160	200	120	102	125	131	127
Error (Simulated – Measured) (BPM)	–39	–11	0	0	0	0	0	0	120	158	155	159	173

Test: Beat Detection on Range of R-Wave Amplitude and QRS Duration with Simulated ECG

According to EC13 Section 4.2.6.1, range of QRS wave amplitude and duration, for a continuous train of simulated ECG pulses, the device shall meet the heart rate range and accuracy requirements of 4.2.7. The minimum range of QRS amplitude (a_r + a_s) is 0.5 to 5.0 mV, and the duration of the QRS wave is between 70 and 120 ms (40 and 120 ms for neonatal/pediatric monitors). For monitors set for adult patients, the heart rate meter shall not respond to signals having a QRS amplitude of 0.15 mV or less, or a duration of 10 ms or less with an amplitude of 1 mV. Response to either or both of these types of signals is permitted in monitors set for neonatal/pediatric patients."

Table 8-7. Results of the test of the proposed beat detection algorithm on range of R-wave amplitude and range of QRS duration with simulated ECG

R-wave Amplitude (mV) \ QRS Duration (ms)	20	30	40	50	60	80	100	120	140
0.15	80.001	80.001	80.001	80.001	80.001	80.001	80.001	80.001	80.001
0.17	80.001	80.001	80.001	80.001	80.001	80.001	80.001	80.001	80.001
0.20	80.001	80.001	80.001	80.001	80.001	80.001	80.001	80.001	80.001
0.25	80.001	80.001	80.001	80.001	80.001	80.001	80.001	80.001	80.001
0.30	80.001	80.001	80.001	80.001	80.001	80.001	80.001	80.001	80.001
0.35	80.001	80.001	80.001	80.001	80.001	80.001	80.001	80.001	80.001
0.40	80.001	80.001	80.001	80.001	80.001	80.001	80.001	80.001	80.001
0.45	80.001	80.001	80.001	80.001	80.001	80.001	80.001	80.001	80.001
0.50	80.001	80.001	80.001	80.001	80.001	80.001	80.001	80.001	80.001
0.60	80.001	80.001	80.001	80.001	80.001	80.001	80.001	80.001	80.001
0.70	80.001	80.001	80.001	80.001	80.001	80.001	80.001	80.001	80.001
0.80	80.001	80.001	80.001	80.001	80.001	80.001	80.001	80.001	80.001
0.90	80.001	80.001	80.001	80.001	80.001	80.001	80.001	80.001	80.001
1.0	80.001	80.001	80.001	80.001	80.001	80.001	80.001	80.001	80.001
2.0	80.001	80.001	80.001	80.001	80.001	80.001	80.001	80.001	80.001
3.0	80.001	80.001	80.001	80.001	80.001	80.001	80.001	80.001	80.001
4.0	80.001	80.001	80.001	80.001	80.001	80.001	80.001	80.001	80.001
5.0	80.001	80.001	80.001	80.001	80.001	80.001	80.001	80.001	80.001

To test the range of R-wave amplitude and QRS duration, the simulated AAMI NSR signal of minimum range of R-wave amplitude from 0.15 to 5.0 mV, and of the

duration of the QRS complex between 10 and 140 ms is used. The heart rate meter should not respond to signals having QRS amplitude of 0.15 mV or less, or duration of 10 ms or less with amplitude of 1mV. The amplitude of the T-wave is 25% of the QRS amplitude, and the rate of the AAMI NSR signal is 80 BPM. The sample rate of the simulated ECG is 250 Hz.

The testing results showed that both the proposed and IMEC beat detection algorithms presented consistent accurate measurement of the heart rate of the simulated ECG. Both the proposed and IMEC algorithms passed the test.

Table 8-8. Results of the test of IMEC beat detection algorithm on range of R-wave amplitude and range of QRS duration with simulated ECG

R-wave Amplitude (mV) \ QRS Duration (ms)	20	30	40	50	60	80	100	120	140
0.15	80.000	80.000	80.000	80.000	80.001	80.001	80.001	80.001	80.001
0.17	80.000	80.000	80.000	80.000	80.001	80.001	80.001	80.001	80.001
0.20	80.000	80.000	80.000	80.000	80.001	80.001	80.001	80.001	80.001
0.25	80.000	80.000	80.000	80.000	80.001	80.001	80.001	80.001	80.001
0.30	80.000	80.000	80.000	80.000	80.001	80.001	80.001	80.001	80.001
0.35	80.000	80.000	80.000	80.000	80.001	80.001	80.001	80.001	80.001
0.40	80.000	80.000	80.000	80.000	80.001	80.001	80.001	80.001	80.001
0.45	80.000	80.000	80.000	80.000	80.001	80.001	80.001	80.001	80.001
0.50	80.000	80.000	80.000	80.000	80.001	80.001	80.001	80.001	80.001
0.60	80.000	80.000	80.000	80.000	80.001	80.001	80.001	80.001	80.001
0.70	80.000	80.000	80.000	80.000	80.001	80.001	80.001	80.001	80.001
0.80	80.000	80.000	80.000	80.000	80.001	80.001	80.001	80.001	80.001
0.90	80.000	80.000	80.000	80.000	80.001	80.001	80.001	80.001	80.001
1.0	80.000	80.000	80.000	80.000	80.001	80.001	80.001	80.001	80.001
2.0	80.000	80.000	80.000	80.000	80.001	80.001	80.001	80.001	80.001
3.0	80.000	80.000	80.000	80.000	80.001	80.001	80.001	80.001	80.001
4.0	80.000	80.000	80.000	80.000	80.001	80.001	80.001	80.001	80.001
5.0	80.000	80.000	80.000	80.000	80.001	80.001	80.001	80.001	80.001

Test: Beat Detection on Tall T-Wave Rejection Capability with Simulated ECG

According to EC13 Section 4.1.2.1 Disclosure of performance specifications, c) Tall T-wave rejection capability “Disclosure shall be made of the maximum T-wave amplitude (a_T) for which heart rate indication is within the error limits specified in 4.2.7. A QRS test signal of 1-millivolt (mV) amplitude and 100-millisecond (ms) duration, with

a heart rate of 80 beats per minute (BPM), shall be used; the T-wave duration (d_T) shall be 180 ms, and the QT interval (d_{QT}) shall be 350 ms. QRS amplitude is defined as a_r + a_s in EC13. A 20-second (sec) monitor stabilization period shall be allowed before testing. The sample rate of the simulated ECG is 250 Hz.

The testing results showed that the proposed beat detection algorithm can detect the heart rate correctly, and passed the test. On the other hand, except for the small T-wave amplitude (50% and below of that of R-wave) of the simulated ECG, the IMEC algorithm presented double detections (detection of both R-wave and T-wave) for tall T-wave ECGs. Thus, the IMEC algorithm has no adequate tall T-wave rejection capability, and failed the test.

Table 8-9. Results of the test of the proposed beat detection algorithm on tall T-wave rejection capability with simulated ECG

Amplitude of T-wave (mV)	0.3	0.5	0.6	0.7	0.8	0.9	1.0	1.1	1.2	1.3	1.4	1.5
Simulated Rate (BPM)	80	80	80	80	80	80	80	80	80	80	80	80
Measured Rate (BPM)	80	80	80	80	80	80	80	80	80	80	80	80
Error (Simulated – Measured) (BPM)	0	0	0	0	0	0	0	0	0	0	0	0

Table 8-10. Results of the test of IMEC beat detection algorithm on tall T-wave rejection capability with simulated ECG

Amplitude of T-wave (mV)	0.3	0.5	0.6	0.7	0.8	0.9	1.0	1.1	1.2	1.3	1.4	1.5
Simulated Rate (BPM)	80	80	80	80	80	80	80	80	80	80	80	80
Measured Rate (BPM)	80	80	167	167	167	167	167	167	167	167	167	167
Error (Simulated – Measured) (BPM)	0	0	-87	-87	-87	-87	-87	-87	-87	-87	-87	-87

LIST OF REFERENCES

Ansley CF, Newbold P (1980). Finite sample properties of estimators for autoregressive moving average models. *J. Econometrics*, 13: 159-183.

Bearden S, Eisenschenk S, Uthman B (2008) Diagnosis of nonconvulsive status epilepticus (NCSE) in adults with altered mental status: clinic - electroencephalographic considerations. *Am J Electroneurodiagnostic Technol*. 48:11-37

Berkovic SF, Scheffer IE (1999) Genetics of the epilepsies. *Curr Opin Neurol* 12:177-182

Bertram EH (1997) Functional anatomy of spontaneous seizures in a rat model of epilepsy. *Epilepsia* 38: 95-105

Box GP, Jenkins GM, Reinsel GC (1994). Book: Time series analysis, forecasting and control, 3rd edn. Englewood Cliffs, NJ: Prentice-Hall. [Chapter 1-5, 7, 8]

Brenner RP (2002) Is it status? *Epilepsia*. 43 (Suppl 3):103-113.

Cascino GD, Jack CR, Parisi JE, Sharbrough FW, Schreiber CP, Kelly PJ, Trenerry MR (1993) Operative strategy in patients with MRI-identified dual pathology and temporal lobe epilepsy. *Epilepsy Research*. February, Vol. 14, Issue 2: 175-182.

Cascino GD (2004) Surgical treatment for epilepsy. *Epilepsy Research*. July, Vol. 60, Issue 2: 179-186.

Chaovalitwongse WA, Prokopyev OA, Pardalos PM (2006) Electroencephalogram (EEG) time series classification: applications in epilepsy. *Annals of Operations Research*. 148(1):227-250.

Charles LL, Richard JH (1995) Solving least squares problems, SIAM publishing, Philadelphia, PA. [Chapter 2, 3, 4]

Chris C (2001). Book: Time-series forecasting, Chapman &Hall / CRC Press, New York, NY. [Chapter 4, 5]

Doob J (1953). Book: stochastic process, John Wiley, New York. [Chapter 3, 4]

Engel JJ (1989). Book: Seizures and epilepsy, F.A. Davis, Philadelphia, PA.

Engel JJ, Pedley TA (1998) Book: Epilepsy: a comprehensive textbook, Lippincott-Raven publishing, Philadelphia, PA.

Fountain NB, Waldman WA (2001) Effects of Benzodiazepines on triphasic waves. *J Clin Neurophysiol*. 18(4):345-352.

Geiger LR, Harner RN (1978) EEG patterns at the time of focal seizure onset. *AMA Arch Neurol*. 35:276-286.

Geweke J (1982), Measurement of linear dependence and feedback between multiple time series. *J. American Statistical Association*, June, Vol. 77, No. 378: 304-313.

Goldberger AL, Amaral LAN, Glass L, Hausdorff JM, Ivanov PCh, Mark RG, Mietus JE, Moody GB, Peng CK, Stanley HE (2000) PhysioBank, PhysioToolkit, and PhysioNet: components of a new research resource for complex physiologic signals. *Circulation* 101(23): e215-e220.

Goodwin, GC, Payne RL (1977). Book: Dynamic system identification: experiment design and data analysis, Academic Press, New York.

Granger CW (1969), Investigating causal relations by econometric models and cross-spectral methods. *Econometrica*, Vol. 37, No. 3, Jul.: 424-438.

Hamilton, JD (1994). Book: Time series analysis. Princeton Univ. Press, Princeton, NJ, [1.5, 3.1, 3.4, 4.1, 5.2, 5.4]

Hayes, MH (2008). Book: Statistical digital signal processing and modeling, John Wiley & Sons Inc., New York, NY

Heinemann SH; Rettig J; Graack HR, Und Pongs O (1996) Functional characterization of KV channel beta-subunits from rat brain, *J. Physiol. Lond.* 493 (Pt 3) Jun. 15: 625-33.

Hirsch LJ, Spencer SS, Williamson PD, Spencer DD, Mattson RH (1991a) Comparison of bitemporal and unitemporal epilepsy defined by depth electroencephalography. *Ann Neurol*. 30:340–346.

Hirsch LJ, Spencer SS, Spencer DD, Williamson PD, Mattson RH (1991b) Temporal lobectomy in patients with bitemporal epilepsy defined by depth electroencephalography. *Ann Neurol*. 30:347–356.

Iasemidis LD (1991) On the dynamics of human brain in temporal lobe epilepsy. Doctor of Philosophy Dissertation, University of Michigan.

Iasemidis LD, Barreto A, Gilmore RL, Uthman BM, Roper S, Sackellares JC (1993) Spatio-temporal evolution of dynamical measures precedes onset of mesial temporal lobe seizures. *Epilepsia* 35S (suppl 8): 133.

Iasemidis LD, Pardalos PM, Shiau DS, Chaovalitwongse WA, Narayanan K, Prasad A, Tsakalis K, Carney PR, Sackellares JC (2005) Long term prospective on-line real-time seizure prediction. *J Clin Neurophysiol*. 116(3):532-544.

Iasemidis LD, Principe JC, Czaplewski JM, Gilman RL, Roper SN, Sackellares JC (1997) Spatiotemporal transition to epileptic seizures: a nonlinear dynamical analysis of scalp and intracranial EEG recordings. Book: In Silva FL, Principe JC, and Almeida LB, editors, *Spatiotemporal Models in Biological and Artificial Systems*. 81-88. IOS press publishing, Amsterdam, Netherland.

Iasemidis LD, Principe JC, Sackellares JC (2000) Measurement and quantification of spatiotemporal dynamics of human epileptic seizures. Book: wwIn Akay M, editor, *Nonlinear biomedical signal processing*. 2:294-318. Wiley-IEEE press Publishing, New York, NY.

Iasemidis LD, Sackellares JC (1991) The temporal evolution of the largest Lyapunov exponent on the human epileptic cortex. Book: Measuring Chaos in the Human Brain. Singapore: 49-82, World Scientific Publishing, Hackensack, NJ.

Iasemidis LD, Sackellares JC, Zaveri HP, Williams WJ (1990) Phase space topography of the electrocorticogram and the Lyapunov exponent in partial seizures. *Brain Topogr*. 2: 187-201.

Iasemidis LD, Shiau DS, Pardalos PM, Sackellares JC (2001) Phase entrainment and predictability of epileptic seizures. Book: In Pardalos PM and Principe JC, editors, Biocomputing. 59-84. Kluwer Academic Publishers, Dordrecht, Netherland.

Iasemidis LD, Shiau DS, Sackellares JC, Pardalos PM, Prasad A (2004) Dynamical resetting of the human brain at epileptic seizures: application of nonlinear dynamics and global optimization tecniques. *IEEE Trans Biomed Eng*. 51(3):493-506.

International League Against Epilepsy (1993) Guidelines for epidemiologic studies on epilepsy: commission on epidemiology and prognosis. *Epilepsia*. 34(4):592-596.

Jirsch J, Hirsch LJ. (2007) Nonconculsive seizures: developing a rational approach to the diagnosis and management in the critical ill population. *Clin Neurophysiol*. 118(8):1660-1670

Juhasz C, Chugani DC, Muzik O, Watson C, Shah J, Shah A, Chugani HT (2000) Relationship between EEG and position emission tomography abnormalities in clinical epilepsy. *Journal of Clinical Neurophysiology*. January, Vol. 17, Issue 1: 29-42.

Kaplan DT, Furman MI, Pincus SM, Ryan SM, Lipsitz LA, Goldberger AL (1991) Aging and the complexity of cardiovascular dynamics. *Biophys J*. 59:945-949.

Kluger Y, Basri R, Chang JT, Gerstein M (2003) Spectral biclustering of microarray data: coclustering genes and conditions. *Genome Res*. 13(4):703-716.

Kolmogorov AN (1958) A new metric invariant of transient dynamical systems and automorphisms in lebesgue space. *Dokl Akad Nauk SSSR*. 119:861-864.

Lebedev MA, Nicolelis MA (2006) Brain-machine interfaces: past, present and future. *Trends Neurosci.* 29(9):536-546.

Lee SK, Lee SY, Kim KK, Hong KS, Lee DS, Chung CK (2005) Surgical outcome and prognostic factors of cryptogenic neocortical epilepsy. *Annals of Neurology*, Vol. 58, Issue 4: 525-532

Liu CC (2008) Brain dynamics, system control and optimization techniques with application in epilepsy. Doctor of Philosophy Dissertation, University of Florida.

Makhoul J (1975). "Linear prediction: A tutorial review", *Proc. IEEE*, vol. 63, pp. 561-580.

Makhoul J (1977). "Stable and efficient lattice methods for linear prediction" *IEEE Trans. Acoust. Speech Signal Process*, vol. ASSP-25, pp. 423-428.

Makridakis S, Hibon M (1997). ARMA models and the Box-Jenkins methodology. *J. Forecasting*. 16, 147-163.

Markel JD, Gray JR (1976). Book: Linear Prediction of Speech, Springer-Verlag, New York, NY.

Miller KS (1974) Book: Complex Stochastic Processes: An Introduction to Theory and Application, Addison-Wesley, Reading, MA.

Milton J, Jung P (2003) Book: Epilepsy as a Dynamic Disease, Springer Publishing, New York, NY.

Monto S, Vanhatalo S, Holmes MD, Palva JM (2007) Epileptogenic neocortical networks are revealed by abnormal temporal dynamics in seizure-free subdural EEG. *Oxford Journals: Cerebral Cortex*. Vol. 17, Issue 6: 1386-1393.

Nehlig A, Daval J, Debry G (1992) Caffeine and the central nervous system: mechanisms of action, biochemical, metabolic and psychostimulant effects. *Brain Res Rev*, 17: 139-170.

Netoff TI, Clewley R, Arno S, Keck T, White JA (2004) Epilepsy in small-world networks. *The journal of neuroscience*. September, 24(37): 8075-8083.

Newbold P, Agiakloglou C, Miller J (1994) Adventures with ARIMA software. Int. J. Forecasting, 10, 573-581.

Ochi A, Otsubo H, Donner EJ, Elliott I, Iwata R, Funaki T, Akizuki Y, Akiyama T, Imai K, Rutka JT, Snead OC (2007) Dynamic changes of ictal high-frequency oscillations in neocortical epilepsy: using multiple band frequency analysis. *Epilepsia* 48:286–296.

Ortega GJ, Prida LM, Sola RG, Pastor J (2008) Synchronization clusters of interictal activity in the lateral temporal cortex of epileptic patients: intraoperative electrocorticographic analysis. Epilepsia. September, Vol. 49, Issue 2: 269-280.

Pardalos PM, Sackellares JC, Carney PR, Lasemidis LD (2004) Book: Quantitative Neuroscience. Kluwer Academic Publishers, New York, NY.

Pincus SM (1991) Approximate entropy as a measure of system complexity. *Proceedings of the National Academy of Sciences of the United States of America 1991*: 2297-2301.

Pincus SM (1995) Approximate entropy (apen) as a complexity measure. *CHAOS*. 5 (1):110–117.

Ponten SC, Bartolomei F, Stam CJ (2007) Small-world networks and epilepsy: graph theoretical analysis of intracerebrally recorded mesial temporal lobe seizure. Clinical Neurophysiology. April, Vol. 118, Issue 4: 918-927.

Priestley MB (1981). Spectral Analysis and Time Series, Vols. 1 and 2. Academic Press, London. [Chapter 1-5, 10]

Rafael CG, Richard EW (2007) Book: Digital Image Processing, Prentice Hall publishing, New Jersey. [Chapter 5].

Sanes JN, Donoghue JP (2000) Plasticity and Primary Motor Cortex, *Annual Review of Neuroscience*. Vol. 23: 393-415

Schwartzkroin PA, Moshe SL, Noebels JL, Swann JW (1995) Book: Brain Development and Epilepsy, Oxford University Press, New York, NY.

Semah F, Picot MC, Adam C, Broglin D, Arzimanoglou A, Bazin B (1998) Is the underlying cause of epilepsy a major prognostic factor for recurrence? *Neurology*, 51: 1256–62

Shoeb A (2009) Application of machine learning to epileptic seizure onset detection and treatment. Doctor of Philosophy Dissertation, Massachusetts Institute of Technology.

Shumway RH, Stoffer DS (2000) Book: Time series analysis and its applications, Springer publishing, New York, NY [Chapter 2].

Simon H (2002). Book: Adaptive Filter Theory, Prentice Hall Press, Hamilton, Ontario, Canada. [Chapter 8]

Spreafic R, Arcelli P, Frassoni C, Canetti P, Giaccone G, Rizzuti T, Mastrangelo M, Bentivoglio M (1999) Development of layer I of the human cerebral cortex after midgestation: architectonic findings, immunocytochemical identification of neurons and glia, and in situ labelling of apoptotic cells. *J Comp Neurol* 410: 126-142

Srinivasan V, Eswaran C, Sriraam N (2007) Approximate entropy-based epileptic EEG detection using artificial neural networks. *IEEE Trans Inf Technol Biomed*. 11(3): 288-295.

Stewart GW (1973) Book: Introduction to Matrix Computations, Academic Press, New York, NY. [Chapter 3]

Spencer SS (2002) Neural networks in human epilepsy: evidence and implications for treatment. *Epilepsia*. March, Vol. 43, Issue 3: 219-227.

Spencer SS, Spencer DD (1994) Entorhinal-Hippocampal interactions in medial Temporal Lobe epilepsy. *Epilepsia*. July, Vol. 35, Issue 4: 721-727.

Takens F (1981) Detecting strange attractors in turbulence. Book: Dynamical Systems and Turbulence, Lecture m in Mathematics, Springer-Verlag Publishing, Heidelberg, Germany. 898:366-381.

Thulasidas M, Guan C, Wu J (2006) Robust classification of EEG signal for brain-computer interface. *IEEE Trans Neural Syst Rehabil Eng.* 14(1):24-9.

Towne AR, Waterhouse EJ, Boggs JG, Garnett LK, Brown AJ, Smith JR, DeLorenzo RJ (2000). Prevalence of Nonconvulsive Status Epilepticus in Comatose Patients. *Neurology*. 54(2):340-345.

Whittle P (1983). Prediction and Regulation, 2nd edn., revised. University of Minnesota Press, Minneapolis. [Chapter 4]

Williamson PD, Thadani VM, Darcey TM (1992a) Occipital lobe epilepsy: clinical characteristics, seizure spread patterns and results of surgery. *Ann Neurol*. 31:3-13.

Williamson PD, Boon PA, Thadani VM (1992b) Parietal lobe epilepsy: diagnostic considerations and results of surgery. *Ann Neurol*. 31:193-201.

Wolf A, Swift JB, Swinney HL, Vastano JA (1985) Determining lyapunov exponents from a time series. *Physica D*. 16:285-317.

Worrell GA, Parish L, Cranstoun SD, Jonas R, Baltuch G, Litt B (2004) High-frequency oscillation and seizure generation in neocortical epilepsy. *Oxford Journals: Brain*. Vol. 127, Issue 7: 1496-1506.

Young LS, Rand D (1982) Book: Dynamical Systems and Turbulence, Lecture Notes in Mathematics. 898:366-381, Springer-Verlag Publishing, New York.

Zaveri HP, Pincus SM, Goncharova I, Duckrow RB, Spence DD, Spence SS (2009) Localization-related epilepsy exhibits significant connectivity away from the seizure-onset area. *Neuroreport*. June, Vol. 20, Issue 9: 891-895.

Zhang J, Xanthopoulos P, Liu CC, Bearden S, Uthman BM, Pardalos PM (2010) Real-time differentiation of nonconvulsive status epilepticus from other encephalopathies using quantitative EEG analysis: a pilot study. *Epilepsia*, February, Vol. 51, Issue 2: 243-250.

Zhang J, Xanthopoulos P, Chien JH, Tomaino V, Pardalos PM (2011) Minimum Prediction Error Models and Causal Relations between Time Series, Wiley Encyclopedia of Operations Research and Management Science, January, Vol. 5: 3271-3285, John Wiley & Sons Inc. Publishing, New York, NY.

BIOGRAPHICAL SKETCH

Jicong Zhang is currently a Ph.D. candidate in the Department of Industrial and Systems Engineering at University of Florida. He defended his doctorate dissertation on March 15 and is scheduled to graduate in 2011. He was born in the City of Wuhan in China and spent most of his early life growing up in that city. He earned his B.S. degree majoring in electronics informatics, and M.S. degree majoring in signal processing and information systems, both from the Department of Electronic Engineering at Tsinghua University, the top-one university in China. Then he joined the Ph.D. program in the Department of Industrial and Systems Engineering at University of Florida in fall-2006 semester. He has once worked on shipping problem by ships, empty container allocation problem, and perishable inventory (blood) control problem, and he earned the highest score in the Ph.D. general exam in 2007. From the second year of his Ph.D., he selected the topic, data mining and optimization in health care, under the supervision of Distinguished Professor Panos M. Pardalos. Mr. Zhang has more than ten publications in journals, books and proceedings up to date and he is the first-author in five of them. In addition, he has a lot of presentations and posters in conferences and workshops. Especially, as a Ph.D. student in engineering school, Mr. Zhang published a full-length paper as the first author in the peer-reviewed medical journal *Epilepsia*. From 2008 to 2011, he collaborated with Optima Neuroscience Inc., VA hospitals, and Cyberonics Inc. to work on data mining, machine learning, pattern recognition and prediction problems in healthcare and biomedical applications. Specifically he developed EEG quantification methods of patient classification and fast diagnosis of generalized NCSE, together with his colleagues. He also developed improved methods for seizure detection and prediction in epileptic patients. Furthermore, he has worked on biomarkers indicative of

some neurological disorders such as traumatic brain injury. There are many interesting and significant results from Mr. Zhang's work, which give strong indications or conclusions for real-world applications in biomedicine and healthcare. Mr. Zhang is very happy working with his Ph.D. academic advisor Dr. Panos M. Pardalos in the past four years. In 2004, Mr. Zhang worked full-time at Intel China Research Center for three months. In 2010, he worked in R&D department of Cyberonics Inc. on two major projects and one minor project for eight months. He is a member of IEEE and INFORMS.

Anyone interested in Mr. Zhang's CV, publication list or other information can contact him at: gatorjicong@gmail.com.